DUBLIN CITY UNIVERSITY

SCHOOL OF PHYSICAL SCIENCES

SPECTROSCOPIC CHARACTERISATION OF HIGH DIELECTRIC CONSTANT MATERIALS ON SEMICONDUCTING SURFACES

Stephen McDonnell B.Sc.

Doctor of Philosophy

January 2009

Supervised by Prof. G. Hughes

Dedication and Acknowledgements

I would like to thank my supervisor, Greg Hughes, for continually inspiring me with his endless energy and enthusiasm for research. He can at times make research seem like a full time hobby rather than a job. My thanks also to Paul Hurley and all those who worked on the ‘k-mos’ project. I would also like to give special thanks to Bob Wallace of the University of Texas at Dallas for giving me the opportunity to work with his group as well as Austin Cunningham for his part in organising that placement. That experience was one that cannot be matched and I feel it played an important part of shaping not only this thesis but also me as an individual.

My thanks to all my colleagues in DCU, especially Oisín and Ian for their guidance in my first years, Barry for keeping me focused with his continual threats to graduate before me, Paddy for doing the early shifts in Aarhus and all the others who have come and gone from the surface and interfaces group. I am very grateful to Marko, Chris and Servando from UTD for welcoming me to Dallas, sharing the heavy work load and celebrating good results with nights of American Pool. To all the ‘C.O.D.’, midnight monopoly and lunch-time soccer lads, I am eternally grateful for your part in keeping me sane. Also worth mentioning are all those musicians who have helped me chill out during stressful times.

Finally I would like to thank my immediate family, my siblings for all of their support to their ‘little’ brother and in particular to my parents, not only for their incredible financial support but also for being the main contributors to making me who I am today. My Mother, encouraging me to enjoy logic puzzles and testing me with basic algebra at a young age, most certainly shaped my future love of physics an ultimate career choice, while my Father, who always made sure that the ‘Playstation’ was turned off when I was meant to be studying, also encouraged us all to never shy away from a hard day’s work. I am forever indebted to them both for my up-bringing and I would like to dedicate this work to their belief in me.

Finally I would like to acknowledge the financial support of Science Foundation Ireland.

Declaration

I hereby certify that this material, which I now submit for assessment on the programme of study leading to the award of doctor of Philosophy is entirely my own work and has not been taken from the work of others save and to the extent that such work has been cited and acknowledged within the text of my work.

Signed:________________________(Candidate)
ID No.: 50061832
Date:_________________________

Abstract

In this work, various insulator/semiconductor interfaces on silicon, gallium arsenide (GaAs) and germanium have been studied by photoemission spectroscopy. Where possible, these interfaces were then tested electrically after the formation of capacitor structures. Each system presents its own unique challenges in the drive to the ultimate goal of developing smaller, faster and lower powered devices. On silicon substrates, an *in-situ* analysis of hafnium oxide grown by micro e-beam deposition in an oxygen atmosphere on an ultra-thin SiO_2 buffer layer was carried out using XPS and synchrotron radiation. The self-limiting growth of an interfacial hafnium silicate layer was observed and the substrate temperature during the hafnium oxide depositions was found effect the onset temperature of hafnium silicide formation during post-deposition anneals. Hafnium oxide has also been grown *ex-situ* on silicon substrates by e-beam deposition in an oxygen atmosphere. The affects of an argon plasma ion assisted deposition technique (used in the growth of optical coatings to aid in film densification) and the oxygen back pressure on the growth of an interfacial oxide region were investigated by XPS. On gallium arsenide substrates, the elimination of anomalous frequency dispersion of the accumulation capacitance of GaAs high dielectric constant (high-κ) MOS devices by the use of a passivating silicon interfacial layer has been investigated. It has typically been assumed that this affect is due to a high interface state density and associated Fermi level pinning which is avoided by utilizing a high-κ/Si interface instead of the high-κ/GaAs interface. The surface treatment prior to silicon deposition is shown here to be a critical step in reducing this effect. Samples with and without frequency dispersion of the accumulation capacitance but with equally high interface state densities are presented, indicating that interface state density may not be the sole cause of the frequency dispersion of the accumulation capacitance. On germanium substrates, the use of a GeON based high-κ dielectric was investigated, as the water soluble native oxide of germanium has been shown in many works to be stabilised by the addition of nitrogen. A preliminary characterisation study of the interfacial quality of the GeON/Ge system is presented. Hafnium germanate has shown promise on silicon and here it has been analysed, with XPS and UPS on germanium substrates with 3 interfacial layers previously reported in the literature.

Publications Resulting From This Work

- **Electrical, Structural, and chemical properties of HfO_2 films formed by electron beam evaporation**
  K. Cherkaoui, S. Monaghan, M. A. Negara, M. Modreanu, P. K. Hurley, D. O'Connell, S. McDonnell, G. Hughes, S. Wright, R. C. Barklie, P. Bailey, T. C. Q. Noakes, Journal of Applied Physics **104** (2008) 064113

- **GaAs Interfacial self-cleaning by atomic layer deposition**
  C. L. Hinkle, A. M. Sonnet, E. M. Vogel, S. McDonnell, G. J. Hughes, M. Milojevic, B. Lee, F. S. Aguirre-Tostado, K. J. Choi, H. C. Kim, J. Kim, R. M. Wallace, Appl. Phys. Lett. **92** (2008) 071901

- **Frequency dispersion reduction and bond conversion on n-type GaAs by in situ surface oxide removal and passivation**
  C. L. Hinkle, A. M. Sonnet, E. M. Vogel, S. McDonnell, G. J. Hughes, M. Milojevic, B. Lee, F. S. Aguirre-Tostado, K. J. Choi, J. Kim, R. M. Wallace, Appl. Phys. Lett. **91** (2007) 163512

- **Characterisation and passivation of interface defects in (1 0 0)-Si/SiO_2/HfO_2/TiN gate stacks**
  P. K. Hurley, K. Cherkaoui, S. McDonnell, G. Hughes, A. W. Groenland, Microelectronics Reliability **47** (2007) 1195-1201

Table of Contents

Dedication and Acknowledgements 1

Declaration 2

Abstract 3

Publications Resulting From This Work 4

Table of Contents 5

Table of Figures 8

1 Introduction 14
- 1.1 Introduction 15
- 1.2 History 15
- 1.3 Importance of the Transistor Gate Dielectric 16
- 1.4 Scaling MOSFET's 18
- 1.5 Choice of alternate high-κ dielectrics 20
- 1.6 Semiconductor substrate comparisons 23
- 1.7 Thesis Organisation 26
- 1.8 References 28

2 Principles of the experimental techniques 29
- 2.1 Photoelectron Spectroscopy 30
- 2.2 X-ray Photoelectron Spectroscopy 33
- 2.3 Ultraviolet Photoelectron Spectroscopy 48
- 2.4 Electrical Characterisation 49
- 2.5 Reference 52

3 Experimental Details 54
- 3.1 Ultra High Vacuum Chambers 55
- 3.2 Deposition Techniques 57
- 3.3 Synchrotron Radiation Sources 60
- 3.4 Surface preparation procedures 61
- 3.5 Reference 65

4 *In-Situ* analysis of the micro e-beam growth of HfO_2 on silicon(111) 67
- 4.1 Introduction 68
- 4.2 Experimental 71
  - 4.2.1 Experimental procedure and surface preparations 71
  - 4.2.2 Characterisation 72
- 4.3 Results 73
  - 4.3.1 Buffer oxide, structure and fitting 73
  - 4.3.2 Room Temperature Hafnium Oxide Deposition 77
  - 4.3.3 Elevated Temperature Hafnium Oxide Deposition 83
  - 4.3.4 Post Deposition High-Temperature Anneal 84

4.3.5 Comparisons 86
4.4 Conclusion 88
4.5 References 90

5 *Ex-situ* analysis of PIAD HfO_2 on silicon(100) 92
5.1 Introduction 93
5.2 Experimental 93
5.2.1 Samples 93
5.2.2 Characterisation 94
5.3 Results 94
5.3.1 Thick Reference Samples 94
5.3.2 Oxygen Pressure during Deposition 97
5.3.3 Argon Ion Assist 101
5.3.4 Comparisons 106
5.4 Conclusion 109
5.5 References 111

6 *In-situ* Atomic Layer Depositions of high-κ dielectric layers on GaAs(100) surfaces 113
6.1 Introduction 114
6.2 Experimental 117
6.2.1 Surface preparations 118
6.2.2 Depositions 118
6.2.3 Characterisation 119
6.3 Results 120
6.3.1 Native oxide, chemical composition and curve fitting 120
6.3.2 Surface Preparation 125
6.3.3 XPS of high-κ layers on GaAs 138
6.3.4 XPS of high-κ layers on GaAs: Effect of silicon interlayer 141
6.4 Conclusion 152
6.5 References 154

7 Characterisation of hafnium germanate dielectric films on germanium(100) substrates 158
7.1 Introduction 159
7.2 Experimental 160
7.2.1 Samples 160
7.2.2 Characterisation: 161
7.3 Results 161
7.3.1 Native oxide and fitting 161
7.3.2 Native oxide removal 163
7.3.3 Interlayers 168
7.3.4 Hafnium Germanate 174
7.4 Conclusion 178
7.5 References 179

8 Conclusions and future work 182
8.1 Conclusions 183
8.1.1 Hafnium oxide grown on silicon dioxide 183
8.1.2 High-κ dielectrics on GaAs substrates 184

8.1.3 High-κ dielectrics on germanium substrates 186
8.2 Future work 187
8.3 References 189

Table of Figures

Figure 1.1 a) The basic structure of an n-channel MOSFET and b) an n-channel device under positive gate bias 17

Figure 1.2 For thick and thin barriers a) the wavefunction of an electron as it reaches a potential barrier b) physical representation of 'a', and c) a metal-oxide-semiconductor (p-type) system biased with a positive voltage (inversion).. 19

Figure 1.3 Bandgap versus static dielectric constant for candidate gate oxides [6] 22

Figure 1.4 Energy versus momentum diagram for the electron transitions between the valence and conduction bands for direct and indirect bandgap materials................... 26

Figure 2.1 Simple XPS set-up. X-rays excite electrons which are emitted from the sample and the kinetic energies of these electrons are measured by an energy analyser. [1] 30

Figure 2.2 Typical hafnium oxide (HfO_2) survey spectrum. Electrons excited by the MgKα anode and plotted in terms of electron binding energy. 31

Figure 2.3 An energy level diagram for a sample and spectrometer in electrical contact during an XPS experiment taken from [1]... 32

Figure 2.4 IMFP with kinetic energy calculated using Tanuma, Powell and Penn for SiO_2. [4] 34

Figure 2.5 Narrow scan of the Indium 3d region.. 35

Figure 2.6 The core-level chemical shift between surface oxide and bulk silicon. 36

Figure 2.7 Hafnium oxide 4f spectra analysed with the Mg kα X-ray anode. 37

Figure 2.8 Schematic of angle resolved XPS at a) normal emission b) θ > 0 and c) an example of a SiO_2 on silicon substrate system... 39

Figure 2.9 Si 2p core-level features before and after curve fitting using the AAnalyser software[14] 47

Figure 2.10 UPS spectrum of an oxygen free Ge(100) surface taken at 45° take-off angle with a photon energy of 21.2 eV. 48

Figure 2.11 Typical C-V characteristics of 5 nm HfO_2 on p-type silicon................... 50

Figure 3.1 Ultra high vacuum chambers for a) *in-situ* hafnium deposition experiments b) *ex-situ* hafnium experiments c) *in-situ* GaAs and Ge experiments. 55

Figure 3.2 Physical set-up of the PIAD system[2] and a schematic of the densification process...58

Figure 3.3 Schematic of one ALD cycle for AL2O3 depositions using TMA and H2O as metal and oxidation precursor. 59

Figure 3.4 Diagram of the Aarhus Storage Ring in Denmark (ASTRID). 61

Figure 4.1 The Si 2p XPS spectra of the self limiting ultra-thin buffer oxide[12] taken with a range of photon energies by both soft-XPS (130 eV – 260 eV) and conventional XPS (1486.6 eV). 74

Figure 4.2 The Si 2p photoemission spectra of the ultra-thin buffer oxide[12] obtained at a) 130 eV and b) 1486.6 eV photon energy. The spectra were obtained using the parameters described in the text. a) shows the calculated CLCS's from these fits as well as values taken from Himpsel *et al.*[13]..75

Figure 4.3 The photoemission spectra after the first hafnium oxide deposition of a) Hf 4f taken at 1486.6 eV photon energy, b and c) Hf 4f and Si 2p respectively taken at 130 eV photon energy. The binding energy separation between the HfO_2 and interfacial hafnium is included in b) and the calculated thickness of the interfacial oxide is shown in c). 77

Figure 4.4 The photoemission spectra, taken sequentially after each hafnium oxide deposition, of a) and b) Hf 4f and Si 2p respectively both taken at 1486.6 eV photon energy during the conventional XPS experiment as well as c and d) Hf 4f and Si 2p respectively both taken at 130 eV photon energy during the synchrotron photoemission experiment. The spectral lines in (b-d) have been normalised to their maximum intensities to allow for easier viewing. 78

Figure 4.5 Sample of fitted spectral features of the Si 2p core-levels obtained at 130eV photon energy after each HfO2 deposition…………………………………...79

Figure 4.6 Interfacial oxide thickness versus hafnium oxide deposition time for hafnium oxide deposited at room temperature. The interfacial oxide thickness was calculated using the ratio of the overlayer to substrate signals from the Si 2p spectra obtained at different photon energies..80

Figure 4.7 The O 1s and Hf 4f XPS spectra taken sequentially with continued depositions of hafnium oxide. The binding energy separation is shown to remain constant to within 0.1 eV and the atomic concentrations of the final film are given...81

Figure 4.8 a) Valence Band spectra of the ultra-thin buffer oxide[12] and after multiple room temperature HfO_2 depositions. b) Work Function spectra continually shifting to lower kinetic energy with each room temperature HfO_2 deposition...........................82

Figure 4.9 soft x-ray photoemission spectra for sequential hafnium oxide depositions of a) Hf 4f taken at 47 eV photon energy, b) Si 2p taken at 130 eV photon energy, C) Valence Band spectra taken at 130 eV photon energy, d) Work function spectra taken at 37 eV photon energy. 83

Figure 4.10 The a) O 1s and Hf 4f, b) Si 2p XPS spectra taken at 1486.6 eV photon energy after sequential 5 min UHV anneals at temperatures range from 700-1000 °C. Included in b) is the thickness of the interfacial oxide..85

Figure 4.11 Soft x-ray photoemission spectra of the a)Hf 4f core-level and the b) Valence Band region with sequential UHV high temperature anneals........................86

Figure 4.12 Schematical representation of a) ultra-thin buffer oxide[12] on silicon, b) Early HfO_2 growth on the buffer oxide at room temperature, c) Early HfO_2 growth on the buffer oxide at ~250 °C allowing for the diffusion of hafnium to the substrate. ...87

Figure 4.13 Soft x-ray photoemission Hf 4f spectra, a) after 30sec 700 °C UHV anneal taken at 47 eV and 94 eV photon energy, b) after continued UHV 700 °C annealing up to 1200 s taken at 47 eV photon energy, c) comparison of the Hf 4f spectra after depositions at both room temperature and 250 °C degrees obtained at 130 eV. 88

Figure 5.1 a) Angle resolved X-ray photoemission spectra of O 1s and Hf 4f for 70 nm PIAD HfO_2 on silicon. b) The simulated angular dependence of the overlayer to substrate signal ratio for a theoretical overlayer where no diffusion into the underlying substrate has taken place plotted along with the same ratio measured for the hydroxide signal's angle dependence...95

Figure 5.2 Photoemission spectra of the Hf 4f core-level, a) depth profile of 70 nm HfO_2 scanned after sequential argon bombardments, b) depth profile of 6-7 nm HfO_2 scanned after sequential argon bombardments, c) example of peak fitting for 'a', d) example of peak fitting for 'b'. 96

Figure 5.3 a) X-ray Photoemission Spectra of the silicon 2p core-level for PIAD HfO_2 on silicon grown under various oxygen flow rates. b) An example of the fitting for the Si 2p core-level. 98

Figure 5.4 X-ray Photoemission Spectra of the oxygen 1s and the hafnium 4f core-level for PIAD HfO_2 on silicon grown under various oxygen flow rates 99

Figure 5.5 I-V characteristics for PIAD HfO_2 on both P and N-type silicon, grown under various oxygen flow rates 100

Figure 5.6 C-V characteristics for PIAD HfO_2, grown under various oxygen flow rates, on p-type silicon. 101

Figure 5.7 The Si 2p XPS of a HF silicon sample exposed to the predeposition PIAD stabalisation conditions and a HF silicon control sample. 102

Figure 5.8 The Si 2p XPS spectra for HfO_2 grown on silicon with varying Plasma Ion assistance..104

Figure 5.9 HRTEM of sample A-C. The thickness of the interfacial oxide is obtained using the silicon crystal lattice as a reference for scale. These images were supplied by R. Dunne and S. Cosgrove at Intel Ireland...105

Figure 5.10 a) I-V characteristics for e-beam deposited HfO_2 on both p and n-type silicon, with no Plasma Ion assistance as well as b) C-V characteristics for a p-type sample at 100 Hz and 100 KHz. 106

Figure 5.11 a) The Si 2p XPS spectra for samples 3 and A normalised to maximum signal and the silicon substrate at 99.6 eV binding Energy b) the O 1s and Hf 4f XPS spectra for samples 3 and A normalised to their maximum signal and the Binding Energy was referenced to 0 eV so that the O 1s and Hf 4f separation could be easily viewed. 107

Figure 5.12 a) The Si 2p XPS spectra for samples grown under condition D normalised to maximum signal and the silicon substrate at 99.6 eV binding Energy b) the O 1s and Hf 4f XPS spectra for the same sample normalised to their maximum signal and the binding energy was referenced to 0 eV for the Hf 4f so that the O 1s and Hf 4f binding energy separation could be easily viewed. 108

Figure 5.13 I-V and C-V characteristics for e-beam deposited HfO_2 on both p-type silicon, with no Plasma Ion assistance and no oxygen. 109

Figure 6.1 As frequency is increased, the capacitance on the accumulation side decreases from C_{max} to C_{min}. Figure taken from Hasegawa and Sawada.[2]................114

Figure 6.2 Arsenic and gallium 2p (Top) and 3d (Bottom) spectra for the native oxide on p and n type GaAs. 121

Figure 6.3 The As 3d and Ga 3d spectra for p-type (Top) and n-type (bottom) GaAs as the samples were processed from native oxide through to the final 450 °C UHV anneal. 126

Figure 6.4 The As 2p and Ga 2p spectra for p-type (Top) and n-type (Bottom) GaAs as the samples were processed from Native oxide through to the final 450 °C UHV anneal. 127

Figure 6.5 Oxygen 1s spectra for n and p type GaAs from native oxide through to 450 °C annealed sample. Peak widths were allowed to vary to accommodate a fixed ratio for the As to Ga related oxygen components. 129

Figure 6.6 Comparison of the oxide removal capabilities of the standard NH_4OH etch, the subsequent UHV anneal and the AHT on n-GaAs using a) As 2p b) Ga 2p and c) O 1s spectra. 132

Figure 6.7 As 3d and Ga 3d spectra for sequential depositions of Si on NH_4OH treated n-type GaAs. 134

Figure 6.8 Ga 3p and Si 2p spectra for sequential depositions of Si on NH_4OH treated N-type GaAs. 135

Figure 6.9 Example of the fitting for the Ga 3p and Si 2p core-levels. 136

Figure 6.10 Bonding environments on GaAs after (a) NH_4OH treatment (b) initial Si depositions (c) continued Si depositions. 138

Figure 6.11 As and Ga 2p features for *in-situ* ALD deposition of Al_2O_3 and HfO_2 onto untreated GaAs with a native oxide layer. 139

Figure 6.12 As 2p and Ga 2p features for *in-situ* ALD deposition of Al_2O_3 and HfO_2 onto NH_4OH GaAs. 140

Figure 6.13 As 2p and Ga 2p regions (Top) and As 3d and Ga 3d regions (Bottom) for both NH_4OH + Anneal and AHT starting surfaces. 142

Figure 6.14 As and Ga 3d spectra for AHT and NH4OH+Anneal treated samples after the deposition of silicon. 143

Figure 6.16 Ga 3p and Si 2p for silicon deposited on a) NH_4OH+Anneal treated and b) AHT surfaces. 145

Figure 6.16 Al 2p spectra for samples A through D. Peak positions are normalised to As 3d at 41.56 eV. Features for sample B-D have been offset on the Y-Axis. Integrated peak areas are included. 146

Figure 6.17 As and Ga 3d features for sample A-D following ALD of Al_2O_3. All curves have been normalised to maximum intensities allowing strongly attenuated signals to be seen as easily as others. 147

Figure 6.18 Ga 3p and Si 2p spectra for samples C and D after the ALD of 1 nm Al_2O_3. 149

Figure 6.19 C-V characteristics for samples A-D with capacitance given per unit area. 150

Figure 6.20 a) Nicollian and Brews[48] and b) Hasegawa and Sawada[2] models using 5 x 10^{13} cm^{-2} eV^{-1} as a parameter for interface state density. 152

Figure 7.1 The Ge 2p and Ge 3d XPS spectra for the native oxide on germanium...162

Figure 7.2 The Ge 2p, O 1s and C 1s XPS spectra for a range of surface treatments, a) untreated, b) 20secs DIW rinse, c) 10 min HF (10%) emersion, d) 400 °C flash clean, e) 20min UV/ozone exposure, f) sample e) after a 400 °C flash clean. 164

Figure 7.3 a) The deconvolved Ge 3d XPS core-level for sample b-d) along with the O 1s and C 1s core-levels. 165

Figure 7.4 a) The deconvolved Ge 3d and 2p XPS core-level for sample b) and e) along with the O 1s and C 1s core-levels of the surface before and after UV-ozone cleaning. 167

Figure 7.5 a) The deconvolved Ge 3d and 2p XPS core-level for sample e-f) as well as b) UPS spectra of the valence band structure of the same samples. 168

Figure 7.6 The Ge 2p and 3d XPS core-level spectra for a) UV/ozone treated Ge, b) UV/ozone treated germanium post nitridation and c) cleaned germanium post nitridation. 169

Figure 7.7 The cure fitted Ge 3d XPS core-level spectra of the GeON and GeN interlayers. 170

Figure 7.8 The O 1s, N 1s and C 1s XPS core-level spectra for a) UV/ozone treated Ge, b) UV/ozone treated germanium post nitridation and c) cleaned germanium post nitridation. 171

Figure 7.9 The Ge 3d XPS for clean germanium and silicon deposited on clean germanium. The binding energies have not been altered from the raw data. 173

Figure 7.10 The Ge 2p, O 1s and Hf 4f XPS core-levels for 7 nm HfGeO films grown on a silicon substrate. 174

Figure 7.11 The O 1s XPS spectra for HGO on GeN and GeON interlayers. a) shows the attempt to fit the spectra with only 2 components. b) shows the better fits obtained with a 3rd GeON component. 175

Figure 7.12 The Si 2p XPS core-level spectra before and after HGO depositions on the Si interlayer. 176

Figure 7.13 The O 1s core-level spectra of HGO/GeON/Ge before and after a Post deposition anneal..177

1 Introduction

1.1 Introduction

This introduction will discuss the importance of the transistor gate dielectric layer in metal oxide semiconductor field effect transistors (MOSFET's) which is the focus of this thesis. The challenges faced in maintaining the material properties of this layer with the continued scaling of device size will be discussed following a brief history of the semiconductor industry and the original choice of the SiO_2/Si system.

1.2 History

Many people believe that the invention of the transistor will be remembered in the centuries to come alongside the printing press and the steam engine as one of the technological achievements that allowed for the dramatic advancement of the human race. Of course semiconductor devices had been used long before the invention of the transistor. The work of Braun as early as 1874 observed 'the asymmetric nature of the electrical conduction between metal contacts and semiconductors' which led to the use of semiconductors as radio detectors.[1] Both Julius Edgar Lilienfield and Oskar Heil had US and British patents grants for the solid state amplifier and the field effect transistor (FET) respectively in 1930 and 1934.[2] While the eventual invention of the transistor at Bell Laboratories in 1947 and the integrated circuit (IC) in 1958 relied on those earlier works, it was these two technological advances which led to the development of the semiconductor industry, heralding the arrival of the "information age".

It is hard to discuss the semiconductor industry without mentioning the famous observation by Gordon Moore when he was asked to write about any trends that he felt would be important to the future of the semiconductor industry for the 35th edition of 'Electronics Magazine'. He observed that 'the level of chip complexity that could be manufactured at minimal cost is an exponential function that doubles in a given period of time' (originally this time period was observed as being 1 year)[2] and also, that the cost of making an integrated circuit was observed to halve in the same period of time. These two observations implied that the cost of producing integrated circuits with optimal transistor densities would remain constant with time.[3] Ten years

later the ‘period of time’ was reviewed by Gordon Moore and observed to be 1½ years and he then predicted that it would continue at a rate of approximately 2 years. The industry has endeavoured to follow this trend, calling it ‘Moore’s law’, with a ‘time period’ of two years. An important point from an economic as well as a technological standpoint is that the Intel Corporation gained an early advantage in the production of memory by implementing a new generation of technology every second time period (3-4 years) by increasing the memory by a factor of 4 instead of 2 and allowing programmers time to fully utilise the new technology before changing it. The application of Moore’s law has varied from following the trend of the number of transistors per unit area, to the number of bits in memory and finally to the speed (performance) of microprocessors after the implementation of complementary MOSFETs (CMOS) structures.[2]

Both silicon and germanium were in use during the early days of transistor fabrication. The first IC, demonstrated by Jack Kilby at Texas Instruments, was a flip-flop made by connecting two germanium die, while the first mass production of ICs was implemented by Fairchild on silicon. The eventual choice of silicon over germanium as the primary substrate for the semiconductor industry was most likely the stability of a thermally grown SiO_2 layer on silicon in comparison to the unstable GeO_2/Ge system. This allowed for a high quality channel/insulator interface to be obtained without developing repeatable gate oxide deposition techniques. SiO_2 would be used as a gate dielectric layer in metal oxide semiconductor field effect transistors (MOSFET’s) for the years to come.

1.3 Importance of the Transistor Gate Dielectric

An example of a typical n-channel MOSFET (NMOS device) is shown in figure 1.1a. Fundamentally, a transistor’s function in a digital circuit is to act as an electronic switch. In a MOSFET, the transistor is ‘On’ when a current flows between the source and drain. The source and drain regions (n-type in this example) are separated by a layer of oppositely doped semiconductor which inhibits conduction when no external voltage is applied. Switching action is induced when a bias (positive for n-channel) is applied to the gate. The majority carriers (electrons) are pushed away

from the gate oxide by the positive bias on the gate. This effectively inverts the majority charge carrier in the channel region for as long as the bias is applied, as illustrated in figure 1.1b. This electrically induced change of majority carriers in the channel is called 'inversion' and allows a current to flow between the source and drain.

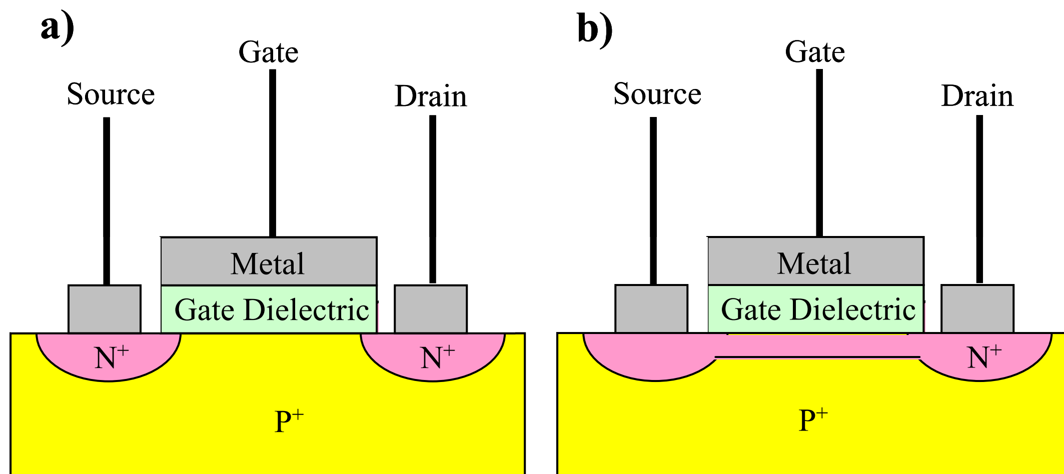

Figure 1.1 a) The basic structure of an n-channel MOSFET and b) an n-channel device under positive gate bias

A critical factor in the performance of a MOSFET is the thickness of the gate dielectric. As the size of the individual transistors is reduced, the capacitance would decrease unless the thickness of the dielectric layer was correspondingly reduced, as the capacitance across the dielectric can be related to its thickness by

$$C = \frac{\varepsilon_0 \kappa A}{t} \tag{1.1}$$

Where, C is capacitance, ε_0 is the permittivity of free space, κ is the dielectric constant of the material, A is the area of the capacitor (gate) and t is the dielectric thickness. As 'Moore's Law' continued to drive the semiconductor industry, the area of the gate decreased to allow more transistors per unit area. The thickness of this gate dielectric was eventually reduced to less that 2 nm as the number of transistors on a microprocessor reached hundreds of millions. This reduction in device size is often referred as the 'scaling of device dimensions'. These ultrathin dielectrics suffer

heavily from reliability and high power consumption issues caused in part by charge trapping,[2] and quantum tunnelling through the dielectric which manifests itself as leakage current. Devices with high leakage currents are unsuitable for hand-held portable device applications due to their high power consumption which lowers battery lifetimes and their high operating temperatures which could make devices uncomfortable to hold. As the number of atomic layers in the gate dielectric approached single digits it became obvious that a move away from SiO_2 would eventually be required if continued scaling of the MOSFET dimensions was to continue.

This thesis sets out to investigate a number of aspects relating to the potential use of new dielectric materials on both silicon and alternative high mobility substrates using a range of characterisation techniques. In particular the interfacial chemistry of the insulator/semiconductor interfaces and the resultant electrical properties are analysed and correlated.

1.4 Scaling MOSFET's

With the growing technological literacy of the average consumer continually on the rise, the demand for faster computing power, larger storage capacities and smaller, more portable devices has insured that with the release of each new generation of memories and microprocessors the semiconductor industry continually adheres Moore's Law.[3] The two main challenges in meeting consumer demands are increasing device performance and lowering power consumption. The increased performance allows smaller, portable devices to match the capabilities of a previous generation desktop computer, while lowering power consumption insures that battery-powered devices can be operated with reasonable battery lifetimes.

As the gate dielectric is reduced to below 5 nm, direct quantum tunnelling through the dielectric layer becomes a major problem with respect to power consumption. This direct tunnelling mechanism which is schematically displayed in figure 1.2 does not require high gate voltages.

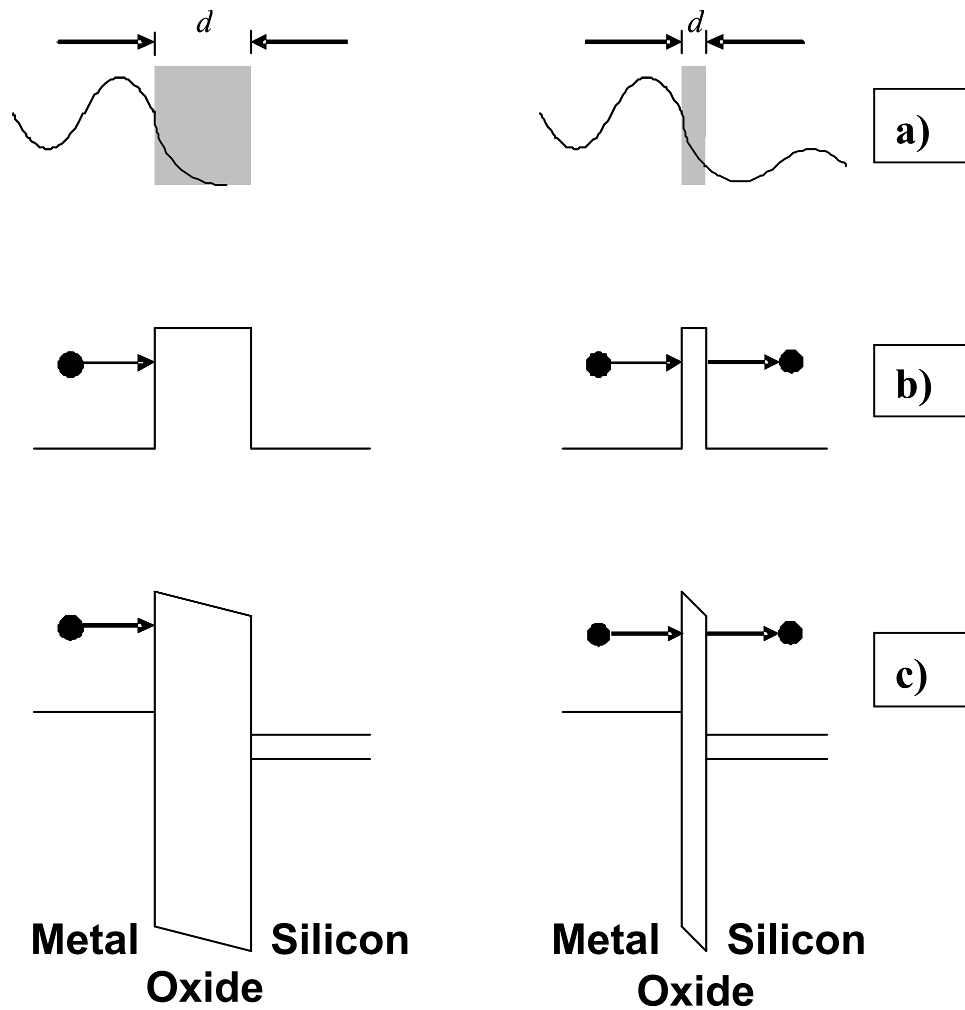

Figure 1.2 For thick and thin barriers a) the wavefunction of an electron as it reaches a potential barrier b) physical representation of 'a', and c) a metal-oxide-semiconductor (p-type) system biased with a positive voltage (inversion).

The expression for the tunnelling probability[1]

$$T \cong 16\left(\frac{E}{V_0}\right)\left(1-\frac{E}{V_0}\right)\exp\left(-2\left[\sqrt{\frac{2m\left(V_0-E\right)}{\hbar}}\right]d\right) \tag{1.2}$$

is seen to be dependent on both the barrier height (V_0) and the barrier thickness (d) which, for gate insulators, are the band-gap offsets with silicon and physical thickness of the gate oxide respectively. In Equation 1.2 'm' is the mass of the electron and 'E' is its energy.

The use of higher dielectric constant materials as a replacement for the SiO_2 dielectric layer reduces the problems caused by quantum tunnelling through the gate by increasing the physical thickness of the layer while maintaining the capacitance of a thinner SiO_2 layer. Because SiO_2 has been used for many decades, it is common for researchers to reference the dielectric properties of a new material to those of SiO_2. When discussing high-κ dielectric layers, the equivalent oxide thickness[4] (EOT) is often quoted rather than the physical thickness of an oxide layer. This is the thickness of SiO_2 that would result in the same capacitance that is achieved by a particular thickness of high-κ dielectric. The EOT can be expressed as

$$EOT = \left(\frac{\kappa_{SiO_2}}{\kappa} \right) t_{physical} \tag{1.3}$$

where κ and κ_{SiO2} are the dielectric constants of the new material and SiO_2 respectively and $t_{physical}$ is the physical thickness of the oxide.

1.5 Choice of alternate high-κ dielectrics

The International Technology Roadmap for Semiconductors (ITRS) continually updates the future technological requirements for semiconductor devices. The 2007 report[5] predicted that the 45 nm node (which is actually now in production) would be in the manufacturing stages by 2010 and that the physical channel length would be 18 nm. To obtain the required capacitance density for these transistors to achieve carrier accumulation and inversion would require an electrically equivalent oxide thickness of 1 nm.[2,5] With a physical thicknesses of 1 nm, quantum mechanical tunnelling would allow gate leakage currents higher than the proposed limits[5] of 1.11×10^3 A/cm^2.

While finding materials with a dielectric constant greater than SiO_2 (~3.9) is not difficult, the number of potential candidates are reduced by other selection criteria. The six criteria listed below are taken from Robertson.[4]

1. The κ value must be high to be used for a reasonable number of years of device dimension scaling.
2. The oxide is in direct contact with the Si channel, so it must form a thermodynamically stable interface.
3. It must be kinetically stable and be compatible with processing at 1000 °C for 5 seconds as in present process flows.
4. It must act as an insulator, by having band offsets with Si of over 1 eV to minimise carrier injection into its bands.
5. It must form a good electrical interface with silicon.
6. It must have few bulk electrically active defects.

1. The first requirement, that the replacement dielectric must be scalable, is driven by economics. The cost of implementing a new technology that would only last one generation (remember that a 'generation' in Moore's law is only 3-4 years) would not be tolerated as anything other than a last resort. This unfortunately rules out otherwise promising mid-κ dielectrics such as Al_2O_3.

2. The new dielectric material must not react with the underlying silicon to form SiO_2 or a silicide. An SiO_2 layer, even only 0.3 nm to 0.5 nm, would take up a large portion of the 1 nm EOT 'budget' and a silicide could effectively short-circuit the source and drain regions of the transistor.

3. The activation of the implanted source and drain dopants requires a high temperature (1000 °C) rapid thermal anneal (RTA). The new dielectric material must be stable while in contact with silicon up to these temperatures, although possible production tricks such as a 'Gate Last' process using a dummy gate which is removed and replaced with the high-κ layer after the RTA may provide a way around this restriction. The fact that the replacement dielectric must act as an insulator to prevent large gate leakage currents is what rules out many of the high-κ materials. Robertson[6] reports that, in general, the bandgap of materials decrease as the dielectric constant increases as shown in figure 1.3.

4. The quantum mechanical tunnelling through a material is strongly dependant on its physical thickness as discussed earlier, however, the height of the

barrier is also important. The increased physical thickness of the gate insulator layer allowed by the used of high-κ materials would be nullified if the trade-off was a substantial reduction in the band-offsets with silicon which would result in comparable or worse gate leakage currents. It is estimated that the band offsets must be greater than 1 eV and since, in practice, the conduction band (CB) offset is less than the valence band (VB) offset,[4] it is the CB band offset which is monitored as a figure of merit in researching new high-κ materials.

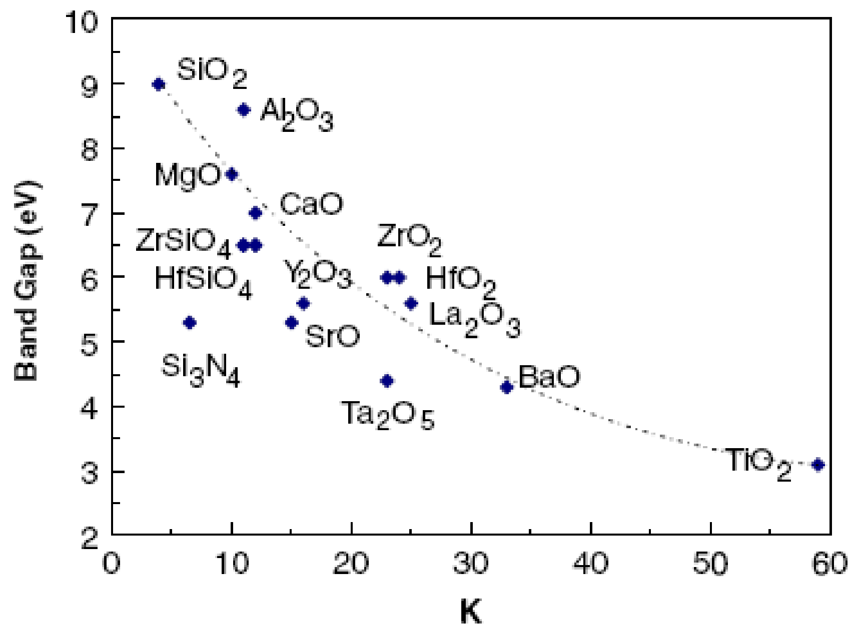

Figure 1.3 Bandgap versus static dielectric constant for candidate gate oxides [6]

5. In order to obtain a good electrical interface with the underlying silicon, the interface should be atomically smooth and the density of interface defects must be low.[1] On an atomically clean unreconstructed silicon (100) surface the surface atoms have two unsatisfied bonds, labelled as 'dangling bonds' which have a density of approximately 10^{15} cm^{-2}. These bonds can give rise to states within the bandgap of the semiconductor.[2] At the Si/SiO_2 interface, the bonding to oxygen ties up many of the dangling bonds, which electrically passivates them. Post deposition anneals in forming gas allow many more of these dangling bonds to be electrically passivated by hydrogen. Failure to passivate such bonds can lead to trapped charge at the interface which can result in Fermi-level pinning. This shall be discussed in chapter 2.4 in more detail.

6. The sixth criteria list by Robertson is a low concentration of bulk defects. In particular this applies to bulk defects that give rise to states in the bandgap. These states trap charge which may act as starting points for dielectric breakdowns. Even before a breakdown occurs, trapped charges cause problems such as trap assisted tunnelling and threshold voltage shifts, which alter the voltage at which a transistor turns on. Trapped charge can also scatter carriers in the channel region which effectively lowers mobility.[4]

After an excellent review by Wilk *et al*[7] which discussed the wide range of high-κ dielectrics that were being study, much of the focus turned to the promising zirconium and hafnium silicates. The advantage of silicates over higher dielectric constant pure metal oxides is that they are thermodynamically stable on silicon while still having a reasonably high dielectric constant. With hafnium silicates already being introduced into the latest generation of Intel microprocessors, hafnium oxide and in particular the thermal instability of this dielectric on silicon was chosen as one of the focuses for this thesis.

1.6 Semiconductor substrate comparisons

A semiconducting material can be thought of as a material with a bandgap lower than a typical insulator. The term bandgap refers to the energy difference between the highest available energy state in the valence band and the lowest energy state in the conduction band. For insulators, a large bandgap inhibits electrons gaining enough thermal energy to be promoted to the conduction band even under very high temperature conditions. Liu[8] states that insulators generally have a bandgap of 8 eV or higher, however many of the high dielectric constant materials under investigation have bandgaps of ~5 eV and are still considered to be insulators. Metals can be thought of as either having no bandgap or having a Fermi level in the conduction band. In either case there are electrons free in the conduction band to conduct current under the application of an applied electric field.

Semiconductors have a lower bandgap than insulators, 1.11 eV for silicon, 1.43 eV for gallium arsenide and 0.67 eV for germanium. Generally these bandgaps would

still be large enough to prevent electron excitation to the conduction band at normal temperatures since the thermal energy supplied is approximately equal to kT where k is the Boltzman's constant and T is the temperature in Kelvin. This would result in available thermal energies of 0.025 eV at room temperature and 0.034 eV at 100 °C (typical high performance microprocessors operating temperature). The electrons that are excited to the conduction band are called charge carriers and the typical concentration of these charge carriers generated by thermal excitation are on the order of 10^6 – 10^{10} cm^{-3} in comparison to the atom concentration of 10^{23} cm^{-3}. Since the generation of a liberated electron results in the generation of a hole, the two 'intrinsic' carrier concentrations are equal.

The electronic properties of semiconductor materials can, however, be altered by adding specific impurity atoms. In the case of silicon, the addition of group III or group V atoms would provide additional holes or electrons respectively. When the impurities cause the addition of holes, the material is referred to as p-type, the addition of electrons results in n-type semiconductor material. P-type and n-type silicon are commonly fabricated by adding boron and phosphorous impurities respectively. For GaAs, silicon can be used as an n-type or p-type dopant depending on the growth conditions but its use as an n-type dopant is more common.[8] Beryllium can also be used as a p-type dopant. From an energy band point of view, p-type dopants work by adding an empty energy level just above the valence band edge. The electrons in the valence band can be promoted into this level with thermal energy resulting in hole formation in the valence band. For n-type dopants the additional electrons exist at an energy level just slightly below the conduction band. These electrons can be promoted into the conduction band with available thermal energy where they are free to conduct.

The experiments in this thesis utilise silicon, gallium arsenide and germanium semiconductor substrates. Both germanium and silicon are group IV semiconductor materials while GaAs is commonly referred to as a III-V semiconductor material. The electronic properties of silicon, germanium and gallium arsenide differ by more than just their bandgaps. The electron and hole mobilities, μ_n and μ_p respectively, are different for each material and this directly affects their conduction properties in a

MOSFET channel. Table 1.1 shows a breakdown of some of the important properties of these semiconductor materials where E_g is the bandgap of the material.

	E_g (eV)	μ_n (cm^2/V-s)	μ_p (cm^2/V-s)
Si	1.11	1350	480
GaAs	1.43	8500	400
Ge	0.67	3900	1900

Table 1.1 Important electronic properties of semiconductor materials relevant to this thesis [9].

One of the main advantages that silicon substrates have over the other higher mobility substrates is the excellent qualities of its native oxide. Silicon dioxide's high bandgap of 8.8 eV makes it an excellent insulator which is important to stop current leakage through the gate dielectric. There is also a low density of interface states at the Si/SiO_2 interface which improves the electrical performance of device.[2] In contrast, the native oxides of GaAs have poor electrical properties.[10,11] This fact makes even the use of high-κ materials difficult since many deposition methods result in at least some interfacial oxides. This particular problem will be discussed in detail in chapter 6. The native germanium oxide is water soluble and so is unstable in atmospheric conditions. Germanium's lower bandgap may make its use problematic if the operating temperature of microprocessors continues to rise, since the amount of thermally generated charge carriers would be significantly higher than for silicon devices and therefore make a transistor more difficult to turn off.

GaAs has a 'direct bandgap' while silicon and germanium both have indirect bandgaps. A direct bandgap means that the minimum energy in the conduction band is at the same crystal momentum **k** as maximum in the valence band and this is shown graphically in figure 1.4. A direct bandgap directly facilitates efficient optical transitions between the two bands. For an indirect bandgap, the minimum of the conduction band and the maximum of the valence band do not occur at the same value of **k**. An electron transition between the two bands is therefore not direct and requires a change in momentum. Indirect transitions are less likely to emit a photon, thus giving GaAs a major advantage over silicon and germanium devices in optoelectronic devices.[9]

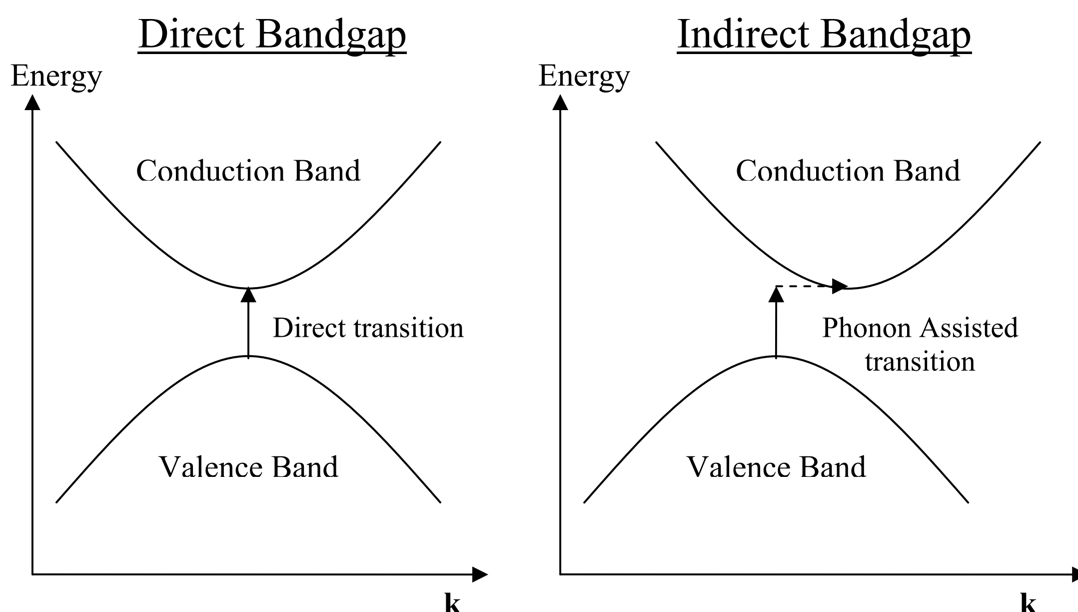

Figure 1.4 Energy versus momentum diagram for the electron transitions between the valence and conduction bands for direct and indirect bandgap materials.

1.7 Thesis Organisation

In chapter 2 there will be a detailed discussion of the primary characterisation techniques used in these studies. These techniques include ultra-violet, x-ray and soft x-ray photoelectron spectroscopy's as well as electrical analysis using a probe station.

Chapter 3 will describe in detail the three ultra high vacuum (UHV) systems, deposition techniques and surface preparations used throughout these studies. Two of these systems were situated in Dublin City University while the third was at the University of Texas at Dallas. The deposition techniques used were e-beam deposition, atomic layer deposition and sputter deposition. Surface preparations include chemical treatments such as hydrofluoric acid (HF) and ammonium hydroxide (NH_4OH) as well as ultra-violet oxidation, atomic hydrogen exposures and nitridation.

Chapter 4 details the results of a study of hafnium oxide (HfO_2) on silicon. This study was performed *in-situ* so that details of the interfacial chemistry during the initial deposition stages of HfO_2 could be investigated. Samples were deposited on flash cleaned silicon and some were annealed in UHV to temperatures of 1000 °C to

study the thermodynamic stability of these films' at the temperatures used during current industry processes.

Chapter 5 presents the chemical and electrical characterisation study of (HfO_2) films deposited by e-beam deposition on chemically cleaned HF-last silicon substrates. Attempts were made to characterise a modified e-beam deposition process that is designed to produce more dense dielectric films. The effects of an oxygen backing pressure on the hafnium oxide films chemical state was also studied.

Chapter 6 deals with gallium arsenide as an alternative substrate to silicon. Surface treatments are studied, along with the effects of silicon interlayer and high-κ depositions onto the GaAs substrate. The electrical benefits resulting from the insertion of a silicon interlayer between the high-κ layer and the GaAs substrate are correlated with detailed studies of the interfacial chemistry.

Chapter 7 looks at germanium as a high mobility substrate. Surface preparations are studied by x-ray photoelectron spectroscopy and the *in-situ* characterisation of hafnium germanate films on germanium with germanium oxynitride, germanium nitride and silicon interlayers is presented. Like chapter 4 this work is a purely physical characterisation study of both the high-κ films and the interfacial chemistry of these films on germanium.

1.8 References

[1] D. A. Neamen *Semiconductor Physics and Devices: Basic Principles* 2nd edition Irwin Book Team (1997)

[2] H. R. Huff, D. C. Gilmer *High Dielectric Constant Material: VLSI MOSFET Applications* Springer series in Advanced Microelectronics **16** (2005)

[3] G. E. Moore *Cramming more components onto integrated circuits* Electronics **38(8)** (1965) 114

[4] J. Robertson, Rep. Prog. Phys. **69** (2006) 327-396

[5] S.I. Association, *The International Technology Roadmap for Semiconductors* (2007)

[6] J. Robertson J. Vac. Sci. Technol. B **18** (2004) 1785

[7] G. D. Wilk, R. M. Wallace, J. M. Anthony, J. App. Phys. **89(10)** (2001) 5243-5275

[8] W. Liu, *Fundamentals of III-V devices: HBTs, MESFETs, and HFETs/ HEMTs* John Wiley and Sons, Inc. (1999)

[9] B. G. Streetman, *Solid State Electronic Devices 4th edition,* Prentice-Hall Inc. (1995)

[10] W.E. Spicer, I. Lindau, P.E. Gregory. C.M. Garner, P. Pianetta and P.W. Chye, J. Vac. Sci. Technol. **13** (1976) 780

[11] M. J. Hale, S. I. Yi, J. Z. Sexton, A. C. Kummel, and M. Passlack, J. Chem. Phys. **119** (2003) 6719

2 Principles of the experimental techniques

2.1 Photoelectron Spectroscopy

Photoelectron spectroscopy is the kinetic energy analysis of electrons which are emitted from a material following the incidence of a photon beam. In practise the surface of a sample is irradiated by mono-energetic photons, typically with photon energies ranging from 21.2 eV (ultraviolet spectroscopy) to 1486.6 eV (Al Kα X-ray spectroscopy). These photon energies are normally sufficient to excite electrons from the atoms near the surface of the sample, through the photoelectric effect, and the kinetic energies of these emitted electrons are analysed via a set-up similar to the one shown in figure 2.1.

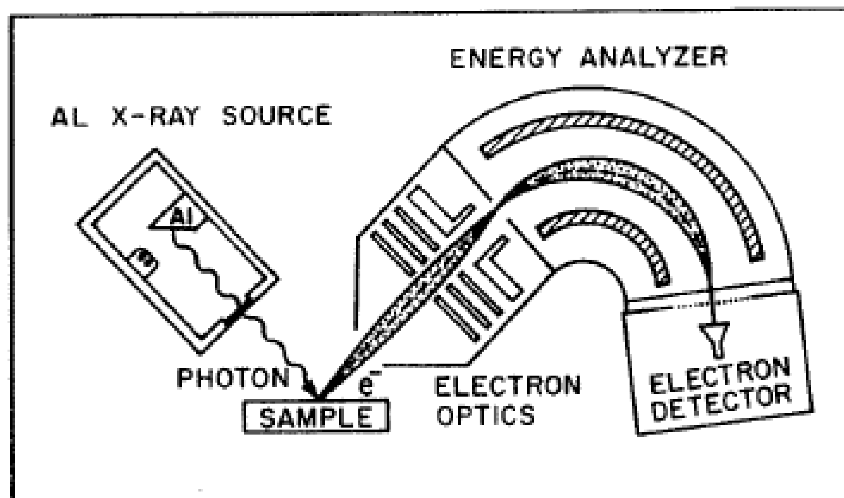

Figure 2.1 Simple XPS set-up. X-rays excite electrons which are emitted from the sample and the kinetic energies of these electrons are measured by an energy analyser. [1]

From the Einstein equation[2]

$$E_B = hv - KE \tag{2.1}$$

one can see that when a photon excites an electron, the binding energy (E_B) of that electron, measured with respect to the vacuum level, is related to the incident photon energy (hv) and the kinetic energy (KE) of the excited electron. In photoemission spectroscopy, the photon energy is known and the kinetic energy of the emitted electrons is analysed. Since every element has a unique electron configuration, the

elemental composition of a sample can be determined once the recorded binding energies of the emitted electrons are compared to known values.

An electron which reaches the analyser without suffering any collisions or phonon interactions should have a kinetic energy unique to electrons emitted from the same core-level of the same element. Electrons which do suffer collisions should have random kinetic energies and simply add to the background signal when a wide range of electron energies are analysed. Figure 2.2 shows a survey scan of a hafnium oxide sample. It can be seen that the Mg Kα x-rays excite electrons from many hafnium core-levels which are readily identifiable when compared to reference spectra.[3]

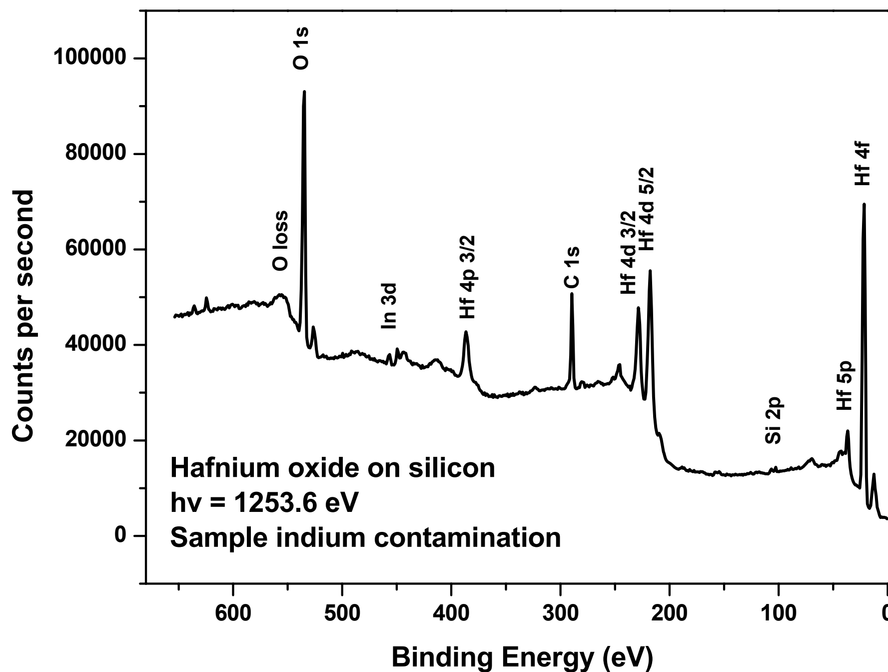

Figure 2.2 Typical hafnium oxide (HfO_2) survey spectrum. Electrons excited by the MgKα anode and plotted in terms of electron binding energy.

Since only electrons which reach the analyser without suffering collisions have kinetic energies that are related to their original binding energies, useful information can only be obtained from the first 5-10 nm of the surface even though the penetration depth of the incident X-rays is on the order of 1-10 μm. The probability that an emitted electron will escape the sample without suffering collisions

decays exponential with the distance from the sample surface. It is this fact that makes XPS a highly surface sensitive technique.

Figure 2.3 shows an energy level diagram for the full photoemission and analysis process. From this it is clear that the sum of the electrons initial binding energy with respect to the Fermi level E_B^F and its kinetic energy E_{kin}^1 after being emitted does not equal the photon energy of the impinging x-rays.

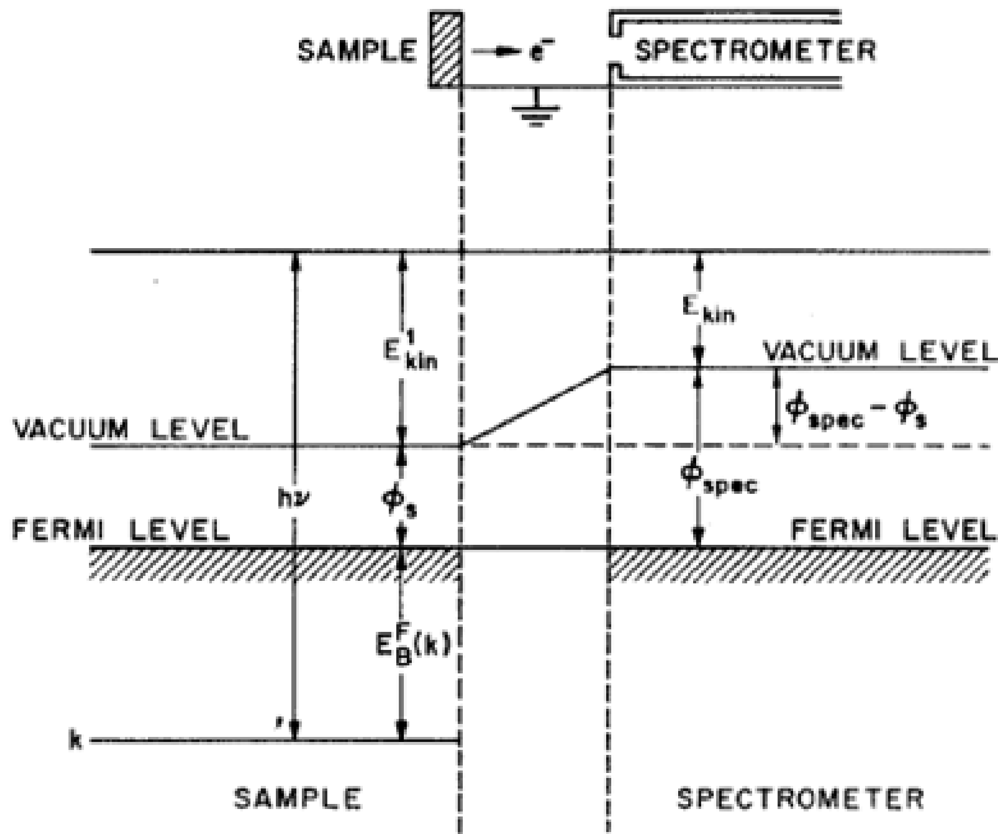

Figure 2.3 An energy level diagram for a sample and spectrometer in electrical contact during an XPS experiment taken from [1]

When referencing the binding energy of an electron to the Fermi level, the workfunction of the sample Φ_s, defined as the deference between the vacuum level and the Fermi level $E_{vac} - E_f$, must be considered when determining the actual kinetic energies of the emitted electrons and an expression for the photon energy can be written as

$$hv = E_B^F + E_{kin}^1 + \phi_s \tag{2.2}$$

In figure 2.3 it is assumed that the sample and spectrometer are in electrical contact. Feldman and Mayer[1] explain how an electron passing from the sample to the spectrometer experiences a potential difference equal to the difference in the sample and spectrometer workfunctions, Φ_s and Φ_{spec} respectively. They define the measured kinetic energy E_{kin} as

$$E_{kin} = E_{kin}^{1} + \left(\phi_s - \phi_{spec}\right) \tag{2.3}$$

This can be substituted into equation 2.2 to give the expression

$$h\nu = E_B^F + E_{kin} + \phi_{spec} \tag{2.4}$$

allowing for the extraction of the initial binding energy of an electron from knowing the incident photon energy ($h\nu$), the measured kinetic energy E_{kin} and the workfunction of the spectrometer (Φ_{spec}). The workfunction of the sample has no effect on the measured kinetic energy of the emitted electrons. The workfunction of the spectrometer can be determined using a reference sample such as gold and the recorded spectrum is normally shifted by that value to compensate.

2.2 X-ray Photoelectron Spectroscopy

X-ray photoelectron spectroscopy (XPS) is a photoemission process that uses monochromatic X-rays as the incident photons. A conventional X-ray source consists of twin magnesium and aluminium anodes generating x-rays which have photon energies of 1253.6 eV (Mg Kα) or 1486.6 eV (Al Kα) respectively. Photons with these energies provide sufficient energy to excite the core-level electrons from atoms. The effective sampling depth of any photoemission technique is dependant on the exponential decay of a signal with depth into the sample which results in 95% of the analysed spectra coming from a thickness equal to 3 times the inelastic mean-free path (IMFP) of an electron in the sample material. The IMFP is dependant on the kinetic energy of the electrons as shown in figure 2.4 and so can actually be different for electrons excited from different core-levels within the same atom.

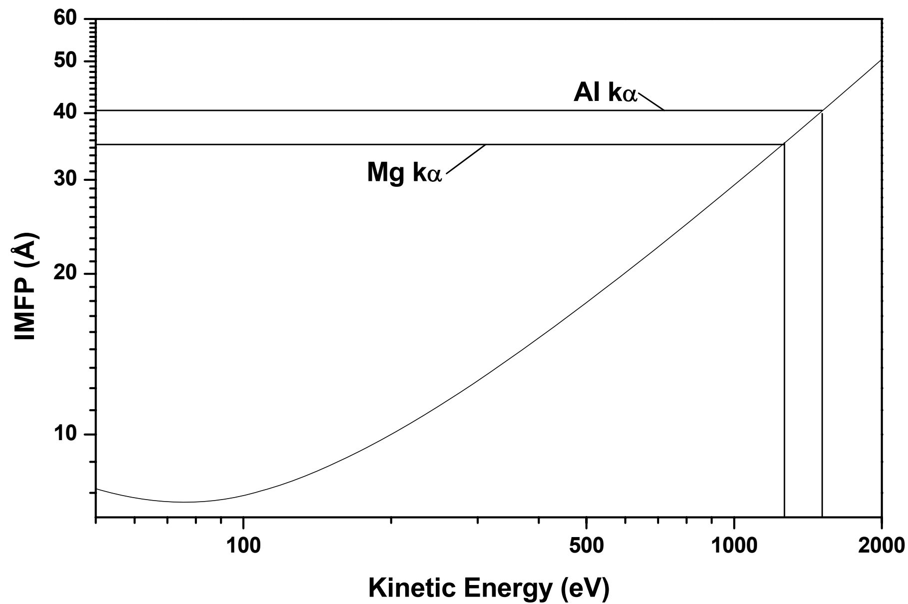

Figure 2.4 IMFP with kinetic energy calculated using Tanuma, Powell and Penn for SiO_2. [4]

Element identification

Figure 2.2 showed a typical survey scan of a material (in that case hafnium oxide). Elements that are present in the sample in atomic concentration greater than 0.1-1% can normally be identified by their strongest core-level feature. While not all binding energies are unique to a specific element, positive identification can usually be made by either having prior knowledge of the expected elemental composition (i.e. knowing what the sample is made of) or by utilizing the presence of the secondary core-level spectral features. For example, the hafnium survey spectrum contains sharp features due to the 4d and 4p core-levels as well as the hafnium 4f. Knowledge of the expected core-levels allows a positive identification to be made since the combination of all expected core-levels will be unique for a given element.

Elements present in low concentrations can be harder to positively identify. Using figure 2.2 as an example, the presence of indium at a binding energy of 445 eV could be overlooked as background noise on the wide range scan. Knowing that an indium source was located near the hafnium source when this sample was grown meant that the presence of indium contamination was being actively looked for.

Figure 2.5 shows a narrow window scan of the indium 3d region and the feature can be seen as clearly rising above the background signal. In these situations the detection of less intense secondary core-level features may not be possible due to the low concentration of the material. It can be possible to tentatively assign a feature to a given contaminant based on both its binding energy and its 'spin-orbit splitting'. The spin-orbit splitting is the energy separation between the two features generated by electrons originating from the same core-level but with different spin-orbit coupling. In the case of the In 3d core-level, this energy separation is known to be 7.54 eV and observing a value close to this value is a very strong indication that the element has been correctly identified.

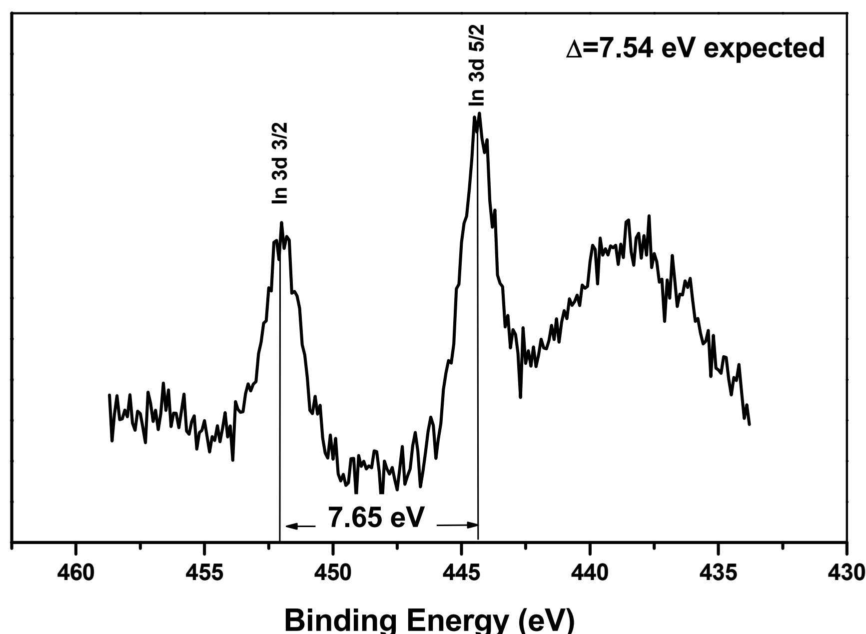

Figure 2.5 Narrow scan of the Indium 3d region.

Chemical Shift

An equally important capability of XPS is its ability to distinguish between the same element in different chemical environments. This is possible because the binding energy of an electron in an atom is sensitive to the changes in charge density around that atom caused by the formation of a chemical bond. Conventional XPS can

be sensitive to core-level shifts greater than 0.1eV. To describe this phenomenon, the simple system of silicon and silicon dioxide will be used as an example.

Figure 2.6 shows an XPS spectrum of the Si 2p core-level for an ultra-thin silicon dioxide layer grown on a silicon substrate. It is clear that the silicon bonded to oxygen appears at a higher binding energy than the silicon bonded to silicon in the substrate. This is because of the differences in the electronic structure of the two systems. In the silicon-silicon covalent bonds, the valence electrons are shared equally between the silicon atoms involved in the bonding. The silicon-oxygen bonds are more ionic in that the more electronegative oxygen takes more of the overall negative charge and forms a dipole. Electrons excited from these silicon atoms will be leaving a slightly positively charged atom which will reduce their kinetic energy. This is apparent from an increase in binding energy of approximately 4 eV relative to the substrate silicon signal.

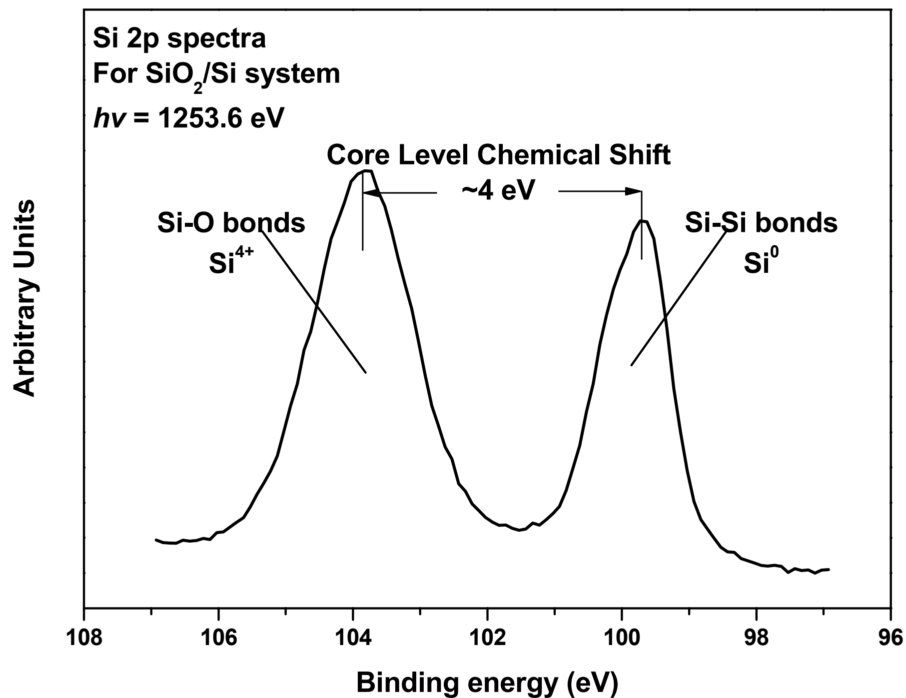

Figure 2.6 The core-level chemical shift between surface oxide and bulk silicon.

When analysing known native oxides, the core-level chemical shift (CLCS) of the oxide related peak to the substrate peak can be referenced to known values and give important information on the oxidation state of the sample.

Quantification

Analysis of the relative intensity of strong core-level features from the different elements present in a sample can yield semi-quantitative information on the relative atomic concentrations in the film. Figure 2.7 shows a narrow range scan of the hafnium 4f core-level region. Electrons excited from this core-level can have two slightly different kinetic energies dependant on their spin-orbit coupling. An expression explaining the integrated intensity of this peak contains four main contributions. The first is the atomic concentration of the element being analysed assuming a uniform homogenous compound. The second is the sampling depth of electrons being emitted from that core-level which is dependant on the electrons kinetic energy. The third contribution is the photo-ionisation cross-section of that specific core-level which is the probability that an electron of that core-level will be excited and finally the transmission function of the analyser which determines the sensitivity of the analyser to electrons of that kinetic energy.

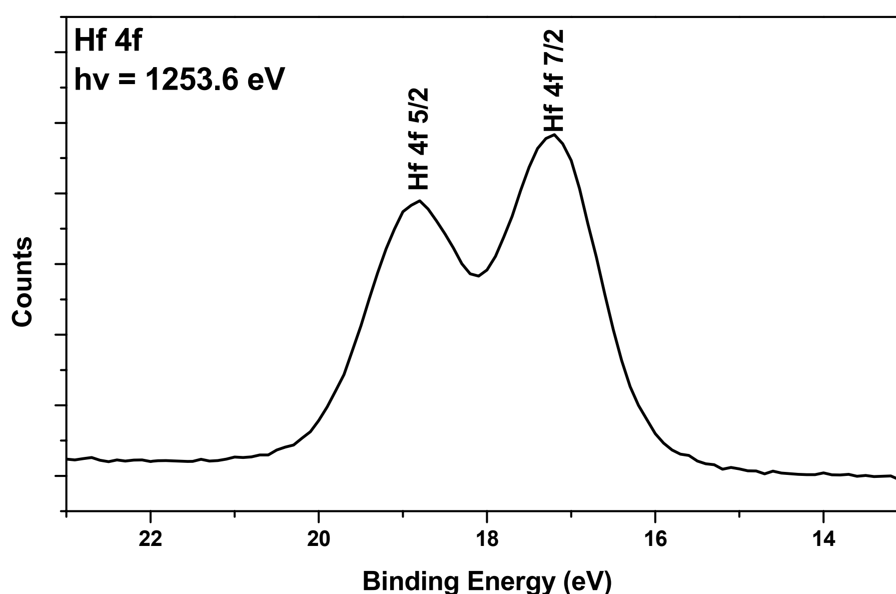

Figure 2.7 Hafnium oxide 4f spectra analysed with the Mg kα X-ray anode.

Using these four contributions it is possible to determine relative sensitivity factors (RSF's) for each core-level associated with each element present and from these it is possible to determine the relative atomic concentrations in a material. Published values for these RSF's are available from XPS reference manuals and the

use of these factors is what can yield the semi-quantative analysis. The strongest core-level spectra from each detected element is ‘normalised’ by dividing the integrated intensity by the relevant RSF. The total sum of all normalised peak areas is then defined as 100% and the atomic percentages can be easily calculated.

Care must be taken when drawing conclusions from such results because factors other than those listed above can affect the results. Firstly, such analysis assumes that all elements in the compound are distributed uniformly throughout the material. A layered system, where elemental ‘A’ was situated on top of elemental ‘B’ would result in a greater attenuation of elemental B and so drawing conclusions about the materials stoichiometry from the simple application of RSF’s to the integrated intensities of the relevant core-level would be inaccurate. Surface contamination will attenuate electrons with lower kinetic energies to a greater degree than electrons with higher kinetic energies. Ultra-thin films with a thickness less than the inelastic mean free path will be subject to the compensations made by the RSF’s for differences in each electron’s sampling depth due to their respective kinetic energies which, in the case of ultra-thin films, have effectively all been made equal.

Depth Profiling

Despite being sensitive to only the top few nanometres of a sample, XPS can still be used to develop depth profiles of the chemical composition through thicker films from the surface right down to the substrate. To achieve this, the surface material must be removed, which then allows analysis of the underlying material. If the amount of material being removed can be controlled then it is possible to determine an accurate chemical composition (%) versus depth (m) profile.

Argon bombardment is an example of such an *in-situ* depth profiling technique. Here, the surface material can be removed in a controlled manner by bombarding the sample with energetic argon ions. By measuring the ion current at the sample, due to the incident charged ions, and knowing the sputter rate, which is dependant on the material, it is possible to know how much of the material has been removed for a sputter of a given duration. Sequential XPS scans as a function of sputter time allow for a chemical depth profile to be acquired.

A non-destructive depth profiling technique that is useful to analyse the surface localised chemical composition is angle resolved XPS (ARXPS). All of the previous discussion of the sampling depth for photoemission experiments assumes that the excited electrons leave the sample by the shortest possible path which is the path perpendicular to the surface. These electrons from any given depth beneath the surface will have the highest probability of escaping the sample without being involved in any collisions.

Figure 2.8 shows the standard XPS setup with the analyser collecting electrons that leave the sample perpendicular to the surface and a setup where the analyser is collecting electrons leaving the sample at an angle θ with respect to the surface normal. The former setup analyses electrons from sampling depth d while the latter analyses electrons that are emerging from a smaller sampling depth d' because the probability that a photoemitted electron will reach the analyser without undergoing any collisions decays exponentially as the physical distance of the point of origin moves deeper into the sample. Plotting the relative intensities of different photoemission peaks as a function of the emission angle allows for a depth profile of

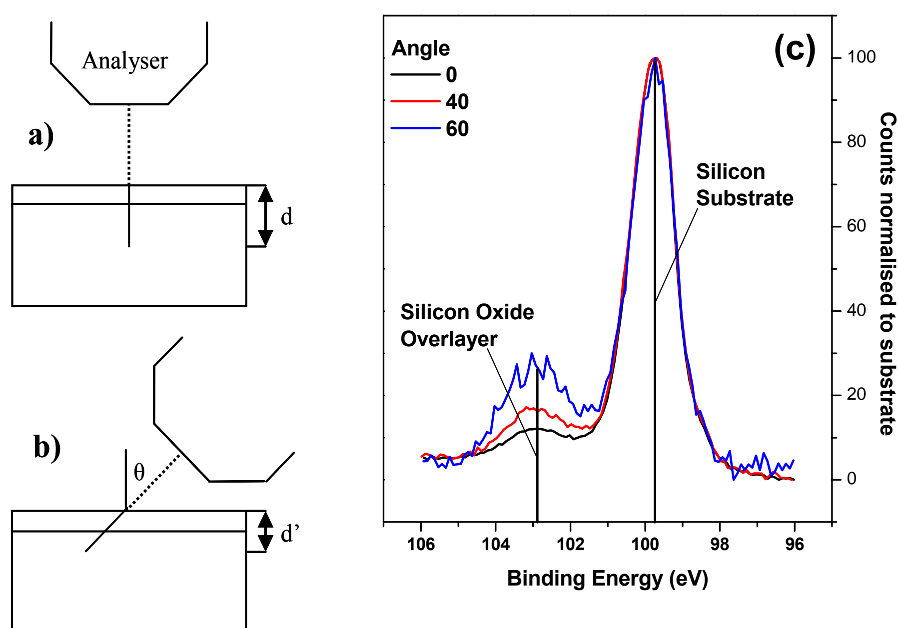

Figure 2.8 Schematic of angle resolved XPS at a) normal emission b) θ > 0 and c) an example of a SiO_2 on silicon substrate system.

a region equal to the maximum sampling depth for that material. An example of a SiO_2 film on silicon analysed at a range of angles in figure 2.8c shows an increase in the intensity of the overlayer SiO_2 signal as the detector angle with respect to the surface normal is increased.

Thickness Calculations

XPS can be a useful tool for calculating the approximate thickness of thin films which are less than 10 nm by comparing intensity of a core-level feature from an element within the film to the intensity of a core-level feature from an elemental present in the underlying substrate. An expression for the integrated intensity of a given photoemission peak I_A obtained from an infinitely thick layer (A) can shown as

$$I_A \sim n_A \sigma_A \int_0^\infty \exp[\frac{-z}{l_{A,A}(\cos\theta)}]dz \tag{2.5}$$

where θ is the photoelectron take-off angle with respect to the surface normal as shown earlier in figure 2.8 and both n_A and σ_A are known values for the atomic density of the given element A in the sample (n_A), and the atomic photoionisation cross-section (σ_A).[5,6] l is the effective attenuation length (EAL) of a photoelectron. In this chapter l is frequently shown with 2 subscripts x and y (e.g. $l_{x,y}$). In these situations x is the location of the atom from which the photoelectron is emitted, either the overlayer (A) or substrate (S) and y is the material the photoelectron is travelling through and being attenuated by, either the overlayer (A) or substrate (S). The effective attenuation length is known to differ from the inelastic mean free path (IMFP) due to elastic-scattering which causes the photoelectrons signal to decay in a non-exponential manner[7]. This variation from the IMFP value is dependant on the composition of the sample but, in general, changes in physical properties such as an increased density will result in a reduction of the EAL.

If layer A is not infinitely thick but instead a finite thickness d, an expression for the photoemission signal from a layer A is seen to depend on its thickness d

$$I_A = n_A \sigma_A l_{A,A} \{1 - \exp[\frac{-d}{l_{A,A}(\cos\theta)}]\} \tag{2.6}$$

An expression for the intensity of the underlying substrate signal I_S is seen to depend on the same thickness d as shown by[5]

$$I_S \sim n_S \sigma_S \exp[\frac{-d}{l_{S,A}(\cos\theta)}] \int_0^{\infty} \exp[\frac{-z'}{l_{S,S}(\cos\theta)}] dz \tag{2.7}$$

$$I_S = n_S \sigma_S l_{S,S} \exp[\frac{-d}{l_{S,A}(\cos\theta)}] \tag{2.8}$$

A ratio of the experimentally measured overlayer and substrate integrated intensities I_A and I_S respectively should yield a value d from the expression

$$\frac{I_A}{I_S} = \frac{n_A \sigma_A l_{A,A} \{1 - \exp[\frac{-d}{l_{A,A}(\cos\theta)}]\}}{n_S \sigma_S l_{S,S} \exp[\frac{-d}{l_{S,A}(\cos\theta)}]} \tag{2.9}$$

The values for $n_A\ \sigma_A l_A$ and $n_S\ \sigma_S l_S$ are often experimentally determined from infinitely thick overlayer and substrate samples and given as I_A^{∞} and I_S^{∞} respectively which changes Equation 2.9 to

$$\frac{I_A}{I_S} = \frac{I_A^{\infty}}{I_S^{\infty}} \frac{\{1 - \exp[\frac{-d}{l_{A,A}(\cos\theta)}]\}}{\exp[\frac{-d}{l_{S,A}(\cos\theta)}]} \tag{2.10}$$

This ratio $\frac{I_A^{\infty}}{I_S^{\infty}}$ is sometimes referred to as R_0[6,8] or 1/K.[5,9,10] It has been noted by Seah and Spencer[6] that the average of experimentally determined values of R_0 for the SiO_2/Si system varies substantially (40%) from the theoretically determined value as well as varying, to a lesser degree, from one XPS system to another.

Experimentally determining this ratio is quite difficult since it requires not only perfectly clean reference samples of SiO_2 and Si but these samples must also be analysed under identical conditions. The presence of surface carbon attenuates

underlying signals and its concentration will generally vary from one sample to another. Removing the carbon by gentle Ar ion bombardment is possible but introduces other inaccuracies due to surface roughening.[6]

In this study, with the exception of the well studied SiO_2/Si system, the value of R_0 was theoretically calculated. Values for n_A and n_S were calculated from published values for the bulk densities ρ_A and ρ_S and the molecular or atomic masses M_A and M_S.[11,12] Where thickness measurements are presented, the relevant constants will be stated in the text. For conventional un-monochromated XPS the value of R_0, for the SiO_2/Si system, quoted by Himpsel *et al*[5] of 0.82 for an Al Kα source was used, while 0.75 was used for monochromated XPS. These values fall within the range of 0.67-0.94 quoted by Seah and Spencer.[6]

In situations where the electrons emitted from the substrate and overlayer have comparable kinetic energies (e.g. SiO_2 on Si) a simplified expression can be obtained

$$\frac{I_A}{I_s} = R_0\{\exp[\frac{+d}{l(\cos\theta)}]-1\} \tag{2.11}$$

Rearranging this equation in terms of *d*

$$d = l\cos\theta\ln[1+\frac{R_{\exp}}{R_0}] \tag{2.12}$$

results in the commonly used expression for the approximate thickness of native oxides. Since electrons from the oxides will normally be within 5 eV of the kinetic energy of electrons from the substrate they will have an almost identical EAL and the subscripts for *l* can be dropped.

R_{exp} is the experimentally determined oxide to substrate ratio $\frac{I_A}{I_S}$. Angular resolved XPS (ARXPS) is a method often used to experimentally obtain R_{exp} for a

range of θ which allows the value of d to be obtained from the resultant slope of a $\ln\left[1+\frac{R_{\exp}}{R_0}\right]$ vs $\sec\theta$ plot.[9]

Novel thickness measurements

Thickness calculations using two core-levels with significantly different kinetic energy:

In most cases there will be more than one core-level from a particular element available for analysis in a sample. Once the appropriate EAL for any given core-level is used, thickness calculations should be possible using any of the available core-levels and a common value for R_0. In situations where two core-levels have significantly different kinetic energies their respective EAL's and R_{exp} should also be substantially different. By manipulating the equation 2.11 so that it is in terms of $\frac{1}{R_0}$ the expressions for two widely separated core-levels can then be set as equal.[13]

$$\frac{I_{S,HKE}}{I_{A,HKE}}\left[\exp[\frac{+d}{l_{HKE}(\cos\theta)}]-1\right]=\frac{I_{S,LKE}}{I_{A,LKE}}\left[\exp[\frac{+d}{l_{LKE}(\cos\theta)}]-1\right] \qquad (2.13)$$

In the above expression $I_{S,HKE}$, $I_{A,HKE}$, are the intensities for the substrate and overlayer respectively, l_{HKE} is the EAL of the high kinetic energy (HKE) core-level in the overlayer while $I_{S,LKE}$, $I_{A,LKE}$, l_{LKE} are the same parameters for the lower kinetic energy (LKE) core-level. The value of d can then be extracted without knowing the values for the constant R_0 which is required for the standard method of thickness determination (equation 2.12) and should therefore have a greater accuracy. The value of d depends heavily on changes in the value of l. As such, taking values for the EAL of the high and low kinetic energy levels from the same source or perhaps using software such as NIST Electron EAL Database[4] is required to ensure accurate measurements.

Multiple Layers:

Separating equation 2.10 into expressions for I_A and I_S makes it easy to expand them to account for an additional overlayer B which has been deposited on top as shown in expression 2.14 and 2.15 for the layer A and the substrate respectively.

$$I_A = I_\infty \left\{ 1 - \exp[\frac{-d_A}{l_{A,A}(\cos\theta)}] \right\} \exp[\frac{-d_B}{l_{A,B}(\cos\theta)}] \quad (2.14)$$

$$I_S = I_o \exp[\frac{-d_A}{l_{S,A}(\cos\theta)}] \exp[\frac{-d_B}{l_{S,B}(\cos\theta)}] \quad (2.15)$$

In situations where I_A and I_S are measured at similar kinetic energies, $l_{A,B}$ and $l_{S,B}$ are approximately equal. Since the attenuation is the same for both I_A and I_S these terms will cancel out when measuring the ratio R_{exp} and so the thickness of I_A can be determined as normal without considering layer B.

In the case of N layers where layer N-1 lies above layer N, 1 is the uppermost layer and i is the layer to be measured, general expressions for I_i and I_S can be shown as

$$I_i = I_i^\infty \left\{ 1 - \exp[\frac{-d_i}{l_{i,i}(\cos\theta)}] \right\} \exp\left[\frac{-1}{\cos\theta} \left(\sum_{j=1}^{j=i-1} \frac{d_j}{\lambda_{ij}} \right) \right] \quad (2.16)$$

$$I_s = I_s^\infty \exp\left[\frac{-1}{\cos\theta} \left(\sum_{j=1}^{j=n} \frac{d_j}{\lambda_{sj}} \right) \right] \quad (2.17)$$

When the ratio of I_i to I_S is taken, these expressions take the form as shown by Vitchev *et al*:[9]

$$\frac{I_i}{I_s} = \frac{I_i^\infty}{I_s^\infty} \left[1 - \exp\left(\frac{-d_i}{\lambda_{ii}\cos\theta} \right) \right] \exp\left[\frac{1}{\cos\theta} \left(\sum_{j=1}^{j=n} \frac{d_j}{\lambda_{sj}} - \sum_{j=1}^{j=i-1} \frac{d_j}{\lambda_{ij}} \right) \right] \quad (2.18)$$

The thickness of layer n can be determined without knowing the thickness of layers n-1 to 1. Each layer can therefore be measured in turn, with its thickness then allowing for the thickness of the layer above to be calculated.

Compound overlayers:

For compound semiconductors, such as GaAs, the native oxide contains more than one oxidised element. The substrate will therefore be attenuated by all of the oxide components and so a general expression such as equation 2.10 can be used to describe its signal.

For the purpose of this study it was assumed that the various oxides in a compound native oxide are homogenously mixed together in the overlayer rather than being stacked. Based on this assumption one oxide signal would not be attenuated by the other. Since thickness measurements are generally conducted using the ratio of substrate Y and oxide Y taken from a single spectrum, such ratios are skewed by the attenuation of the signal from substrate Y by oxide X not seen at that binding energy.

Here it is proposed for a binary compound that the equivalent thickness of oxide X and oxide Y can be determined from their respective oxide/substrate intensity ratios as shown in equations 2.19 and 2.20

$$\frac{I_x}{I_S} = \frac{I_x^\infty}{I_S^\infty}\left[\frac{\{1-\exp[\frac{-d_x}{l_{x,x}(\cos\theta)}]\}}{\exp[\frac{-d_x}{l_{S,x}(\cos\theta)}+\frac{-d_y}{l_{S,y}(\cos\theta)}]}\right] \tag{2.19}$$

$$\frac{I_y}{I_S} = \frac{I_y^\infty}{I_S^\infty}\left[\frac{\{1-\exp[\frac{-d_y}{l_{y,y}(\cos\theta)}]\}}{\exp[\frac{-d_y}{l_{S,y}(\cos\theta)}+\frac{-d_x}{l_{S,x}(\cos\theta)}]}\right] \tag{2.20}$$

Starting with an educated guess for the value of either d_x or d_y, the total thickness $d = d_x + d_y$ can be determined after calculating d_x and d_y using an iterative

process. This can easily be expanded to *n* overlayer components by adding extra attenuation terms to the expression for the substrate signal as needed.

Spectral Analysis

The important information to be obtained from a core-level feature such as binding energy position, peak width and intensity can be easily extracted from the core-level features of an element that is present in only one chemical state within the sample. It is quite common, however, for an elemental to exist in more than one state within the sampling depth of XPS. Typically the binding energy position of a given core-level for an element is 2 different chemical states with not vary by more than 5 eV and as such there can be consider intermixing within the feature observed by XPS.[5]

In order to obtain all of the relevant information from each observed chemical state of an element, curve fitting of the raw core-level feature is regularly performed. In this thesis, the software AAnalyser[14] was utilised for this purposed. Known core-level parameters are required as a starting point for a realistic fit to be obtained. For example, in the case of silicon dioxide, the Si 2p core-level has a known spin orbit splitting of 0.61 eV, and an intensity ratio of 2:1 for the 3/2 feature with respect to the 1/2 feature. These parameters are independent of chemical state and so can be fixed when curve fitting. The full width half maximum (FWHM) of a core-level contains two components. One component is the Lorentzian line width which is intrinsic to the particular core-level and is independent of chemical state. The second component is the Gaussian line width which is due largely to instrumental peak broadening but can also increase as the sample becomes amorphous. This is because the charge distribution around an atom can be affected by atoms other than its first neighbours and so will become more random for amorphous samples in comparison to well ordered crystals. Also variations in bond angles between two otherwise identical molecules will cause slight variations in the calculated binding energy. Both of these affects with be small and as such a Gaussian distribution around the average value will be seen.

Figure 2.9 shows an example of an SiO_2 layer grown on an Si(111) surface. The figure shows both the raw data and the analysed spectra which allows for the extraction of each chemical states binding energy position, Gaussian line width and integrated intensity. The binding energy position can then be used to positively

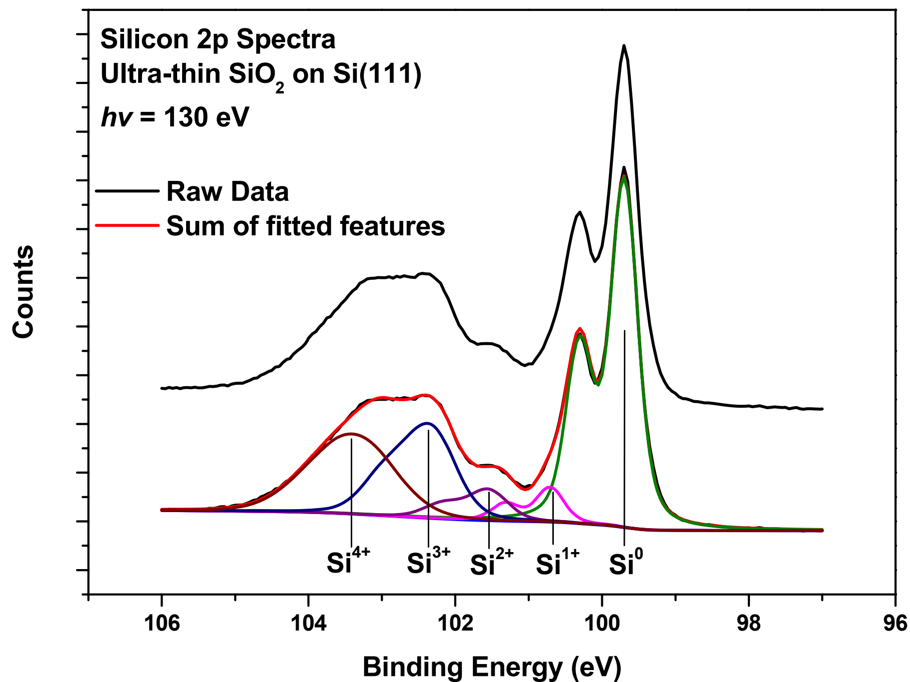

Figure 2.9 Si 2p core-level features before and after curve fitting using the AAnalyser software[14]

identify each feature, while the integrated area is used to establish either atomic concentration in a sample or film thickness when these intensities are compared to that of the substrate features. The Gaussian line width serves a check when curve fitting since an excessively large peak width often indicates that another chemical state is present and should be included. The identifying labels attached to each feature in this case correspond to the oxidation states of silicon. The indices denotes the charge on the atom due to electron charge transfer to the element bonded oxygen atoms. As such it is clear that Si^{4+} corresponds to SiO_2, while Si^{3+} corresponds to Si_2O_3 which is one the interfacial oxide in a SiO_2/Si interface. Similarly Si^{2+}, Si^{1+} and Si^0 correspond to SiO, Si_2O and Si respectively.

2.3 Ultraviolet Photoelectron Spectroscopy

Another photoemission technique is ultra-violet photoemission spectroscopy (UPS). Instead of generating photons with energies > 1 keV, using an X-ray source, UPS uses much lower energy photons, typically in the range of 10-45 eV. The vacuum ultra violet (VUV) source used in this work was a helium discharge lamp which generates photons with an energy of 21.2 eV. An example of a UPS spectrum taken of oxide free germanium is shown in figure 2.10.

Because of the much lower photon energy used with respect to XPS, the energy is not typically sufficient to excite electrons from the deeper lying core-levels of atoms. Instead it is electrons emitted from the valence bands of the material that are analysed with respect to the Fermi level and this provides useful information on the electronic properties of the sample including the valence band offsets. In sequential deposition experiments, the valence band offset between the overlayer and substrate can be measured, which is of great importance when characterising potential high-κ replacements for SiO_2. As mentioned previously, the conduction band offsets are

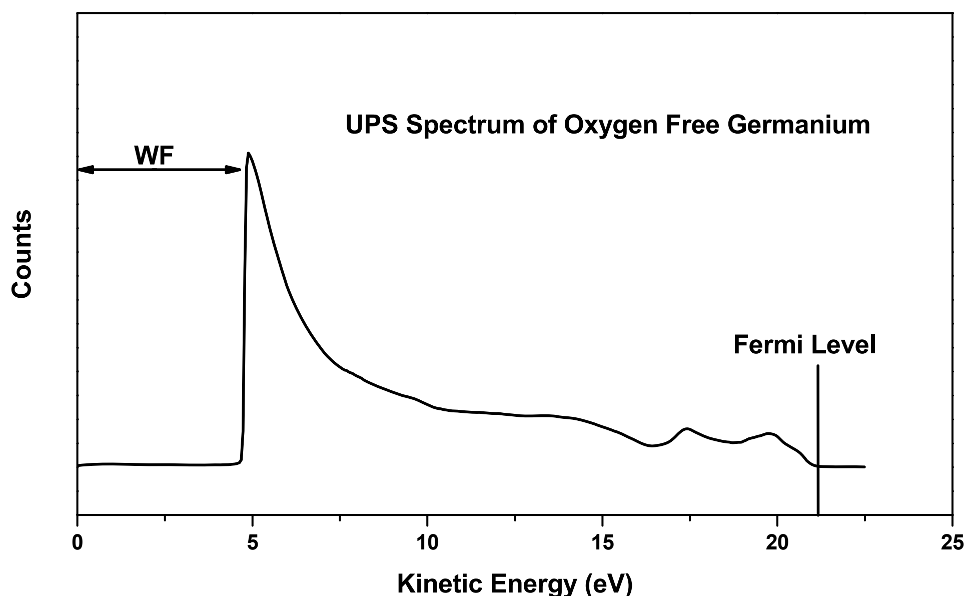

Figure 2.10 UPS spectrum of an oxygen free Ge(100) surface taken at 45° take-off angle with a photon energy of 21.2 eV.

typically smaller and while these can not be measured directly by UPS, they can be inferred if the bandgap of the overlayer material and the substrate are well known. Changes in the workfunction of the sample can be monitored since the photon energy is well known. Since the workfunction of the spectrometer is corrected for, no electrons with kinetic energies less than the value of the workfunction of the sample will be measured. The workfuntion of the material can therefore be determined from the low energy cut off in the signal as seen in figure 2.10.

2.4 Electrical Characterisation

The two electrical characterisation techniques used in this study are current-voltage (I-V) and capacitance-voltage (C-V) measurements. Both of these require the formation of capacitor structures on the high-κ material which in this work is normally achieved by the deposition of an appropriate metal onto the high-κ film through a shadow mask. The resultant gate electrodes will therefore have known dimensions. An electrical probe is brought into contact with a metal gate while the back of the sample is in electrical contact with the 'chuck' of the probe station. An applied voltage is then ramped in a controlled manner across an appropriate range and either the current through the gate dielectric (leakage current) or the capacitance of the gate dielectric is recorded.

The gate leakage current is due to direct electron tunnelling through the gate dielectric and as such is strongly affected by the physical thickness of the gate dielectric, due to the exponential dependency of an electron's tunnelling probability on the thickness of the potential barrier. Since the tunnelling probability is also dependent on the barrier height the gate leakage current is also affected by the valence band and conduction band offsets with silicon. Therefore, the I-V characteristics of a film give information about the insulating properties of the dielectric.

Figure 2.11 shows an example of a C-V sweep for HfO_2 grown on a p-type silicon substrate. When plotting capacitance versus voltage, the capacitance measured on different sized devices can be normalised once the area of the device size is known and quoted as capacitance per unit area. By drawing majority carriers to the

semiconductor/insulator interface, the capacitor structure is brought into 'accumulation' and the maximum measured capacitance is achieved due to their being the lowest possible physical distance between the charges across the dielectric material. By pushing the majority carriers away from the interface the channel region

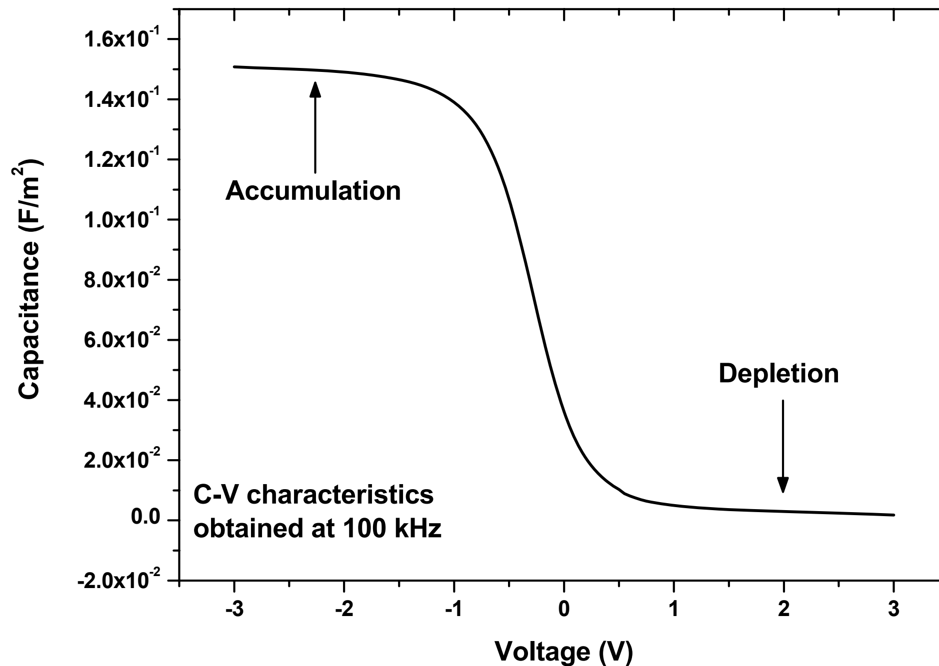

Figure 2.11 Typical C-V characteristics of 5 nm HfO_2 on p-type silicon.

is said to be in 'depletion' and the capacitance drops to a minimum due to the larger distance between the "plates" of the capacitor. The capacitance is measured using an impedance meter (Agilent 4284A LCR meter). In order to get the capacitance, the instrument applies an ac voltage of low amplitude (25mV typically), the resulting displacement current is then measured. The instrument calculates the ratio V/I to get the impedance (z) and measures the phase angle (θ) between V and I. From z and θ and a model (here the model was capacitance in parallel with a conductance Cp-G) a value for capacitance can be extracted.

Non-ideal C-V characteristics can be caused by many things. In particular, and most relevant to the work in this thesis, the trapping of charge at the interface can compensate for the applied electric field which reduces the effect of the applied gate voltage on the semiconductor surface potential. If there is sufficient surface charge

present then it may not be possible to invert the channel region and this eventuality is called Fermi-level pinning.[15]

2.5 Reference

[1] L. C. Feldman, J. W. Mayer, Fundamentals of surface and thin film analysis, Elsevier Science Publishing Co., Inc. (1986)

[2] J. C. Vickerman, Surface Analysis – The Principal Techniques, J. Wiley and Sons, (1997)

[3] J. F. Moulder, W. F. Stickle, P. E. Sobol, K. D. Bomben, *Handbook of X-ray Photoelectron Spectroscopy* Perkin-Elmer Corporation, Physical Electronics Division (1992)

[4] Electron inelastic-mean-free-path database version 1.1 provided by the National Institute of Standards and Technology, NIST

[5] F. J. Himpsel, F.R. McFreely, A. Taleb-Ibrahimi, J.A. Yarmoff and G. Hollinger, Phys. Rev. B **38**, (1988) 6084

[6] M.P. Seah and S. J. Spencer, Surf. Interface Anal. **33** (2002) 640

[7] A. Jablonski, C.J. Powell, Surface Science Reports **47** (2002) 33

[8] K.J. Kim, K. T. Park, J. W. Lee, Thin Solid Films **500** (2006) 359

[9] R.G. Vitchev, J.J. Pireaux, T. Conard, H. Bender, J. Wolstenholme, Chr. Defranoux, Applied Surface Science **235** (2004) 21–25

[10] R.G. Vitchev , Chr. Defranoux , J. Wolstenholme, T. Conard, H. Bender, J.J. Pireaux, Journal of Electron Spectroscopy and Related Phenomena **149** (2005) 37–44

[11] G.W.C. Kaye, T.H. Laby *Tables of Physical and Chemical Constants* (16th edition) Longman: Harlow (1995)

[12] D.R. Lide, *CRC Handbook of Chemistry and Physics* (88th edition) CRC Pres: Boca Raton, FL, (2000)

[13] T. Deegan, G. Hughes, Applied Surface Science **123/124** (1998) 66

[14] A. Herrera-Gómez, *et. al.*, Physical Review B 61 (2000) 12988-12991

[15] H. R. Huff, D. C. Gilmer *High Dielectric Constant Material: VLSI MOSFET Applications* Springer series in Advanced Microelectronics **16** (2005)

3 Experimental Details

3.1 Ultra High Vacuum Chambers

During these studies XPS was conducted in three separate ultra-high-vacuum (UHV) systems which are shown as figure 3.1. System A as used for *in-situ* studies, where hafnium oxide was grown from a micro e-beam evaporator on silicon and analysed without breaking vacuum as will be described in chapter 4. System B was used primarily to analyse samples prepared *ex-situ* such as the sample sets which will be presented in chapter 5. System C was attached to many other deposition chambers and allowed for the analysis of both samples grown *in-situ* and samples prepared *ex-situ*. This system was used exclusively for obtaining the data presented on gallium arsenide and germanium substrates which will be presented in chapters 6 and 7 respectively.

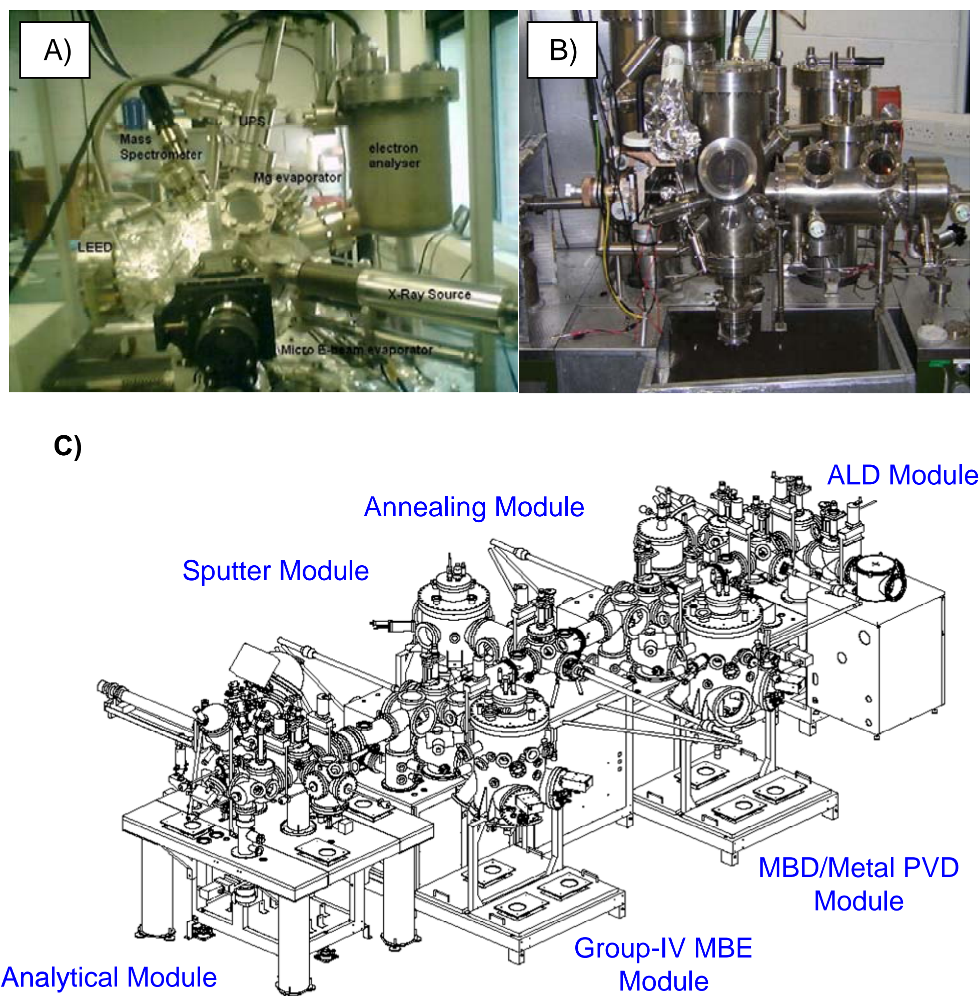

Figure 3.1 Ultra high vacuum chambers for a) *in-situ* hafnium deposition experiments b) *ex-situ* hafnium experiments c) *in-situ* GaAs and Ge experiments.

System A is used primarily for *in-situ* experiments although it can easily be modified to allow analysis of samples prepared *ex-situ*. The analysis chamber is pumped by a turbo molecular pump and a base pressure of 10^{-10} mbar is routinely achieved with a bake-out procedure. The chamber has an electron energy analyser and both a dual anode (Mg and Al) x-ray source and an ultra-violet spectroscopy (UPS) source. This chamber also has an e-beam evaporator containing a magnesium source and a micro e-beam evaporator with a hafnium wire source. Low resistivity silicon substrates could be heated via direct current heating to > 1000 °C enabling atomically clean surfaces to be prepared. This heating mechanism also allowed depositions at elevated temperatures and post deposition anneals to be carried out. Temperatures above 500 °C were monitored by an infrared pyrometer.

System B consisted of three chambers. The first is a fast entry loadlock that is pumped by a roughing pump to approximately 10^{-2} mbar. The second chamber is pumped by a diffusion pump and is held at better than 10^{-6} mbar. The analysis chamber which is also pumped by a diffusion pump is maintained at 10^{-10} mbar or better. It has a dual anode (Mg and Al) x-ray source as well as an electron energy analyser and is used exclusively as an XPS chamber. Argon bombarding capabilities are available and the sample can be rotated with respect to the analyser to allow for angular resolved XPS.

System C, which is located in National Science and Engineering Research Laboratory (NSERL) at the University of Texas at Dallas (UTD), consisted of an analysis chamber containing an electron energy analyser, a monochromated aluminium x-ray source, a UPS source, argon bombardment and ion scattering spectroscopy (ISS) capabilities. Samples prepared *ex-situ* could be annealed to approximately 500 °C. *In-situ* depositions and anneals could also be carried out on 4 inch wafers in the adjoining deposition and annealing chambers without removing the samples from vacuum.

3.2 Deposition Techniques

E-beam

Electron beam (e-beam) deposition is a physical vapour deposition technique. A target, e.g. hafnium oxide pellets, can be used as a source material which is evaporated by thermally heating the material with an incident high energy (3-4 kW) electron beam. The film condenses on a substrate which is in the line of sight of the evaporation source. The technique is housed in a vacuum chamber which facilitates the deposition of films which have minimum levels of contamination. An alternative e-beam configuration for metal oxide deposition used in the experiments discussed in chapter 4 of this thesis is micro e-beam deposition. This involved the evaporation of the metal in an oxygen back pressure. In practise a backing pressure of oxygen is normally used even in conjunction with metal oxide sources to help ensure the deposition of a fully oxidised film.

A variation on conventional e-beam deposition, which was used for some depositions of hafnium oxide discussed in this thesis, is plasma ion assisted deposition (PIAD). For these depositions the metal oxide is still evaporated by an e-beam but an argon plasma is also struck in the deposition chamber as shown in figure 3.2. There is a self induced potential difference (~70 V) that lightly accelerates the argon ions towards the surface of the substrate. Like ion beam assisted deposition (IBAD)[1] this light bombardment is meant to increase the density of the deposited film by gently bombarding the layer during depositions as schematically shown in figure 3.2. This technique is commonly used for the deposition of optical coatings[2] but was used here with a view to ensuring the highest possible dielectric constant for a deposited material by reducing the amount of voids or vacancies in the material.

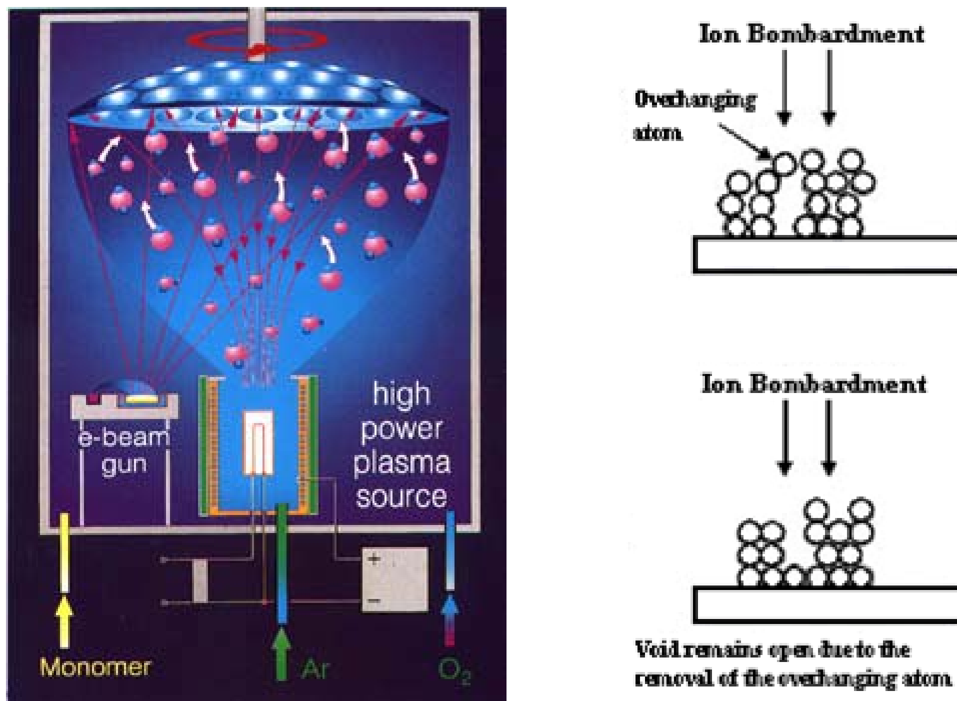

Figure 3.2 Physical set-up of the PIAD system[2] and a schematic of the densification process.

Atomic Layer Deposition

Atomic layer deposition (ALD) is a modified chemical vapour deposition (CVD) technique. Unlike conventional CVD, where gaseous precursors are mixed over, and condense onto, a heated substrate, in ALD the precursors for deposition are pulsed sequentially. For metal oxides, H_2O is often chosen as the oxidising precursor. A metalorganic precursor for the metal component should react with water to form the metal oxide of interest and a volatile component that leaves the heated substrate. Intermittent pulses of an inert gas like nitrogen are used to purge the deposition chamber of these volatile compounds between deposition cycles.

In ALD growth of metal oxide dielectrics on silicon, it is common to use the H_2O pulse before the metallisation pulse so that the metal will be reacting with a partially oxidised surface and not reacting with the silicon. In this thesis, ALD was the deposition technique used for dielectrics on GaAs substrates. In order to minimise interfacial oxide growth the first pulse in the growth sequence was always the metalorganic precursor.

Figure 3.3 shows a schematic representation of Al_2O_3 deposition taken from the Picosun website.[3] During the first pulse, the trimethyl-aluminium (TMA) reacts with hydroxyls on the substrate in one of two ways. The aluminium can bond to one oxygen atom and remain bonded to two CH_3 groups liberating one hydrogen atom from the hydroxyl and one CH_3 which forms methane (CH_4). Alternatively, the aluminium can also bond to two oxygen atoms and remain bonded to only one CH_3 group. This liberates two hydrogen atoms and two CH_3 groups which form two methane molecules. Any surplus TMA along with the methane is then purged by nitrogen and the oxidising water pulse is injected. During this pulse, the water reacts with any CH_3 groups that are still bonded to aluminium resulting in the formation of Al-O bonds with the released hydrogen bonding to CH_3 resulting in the formation of methane which is then removed along with any surplus water by another nitrogen pulse. This complete sequence is referred to as one ALD cycle.

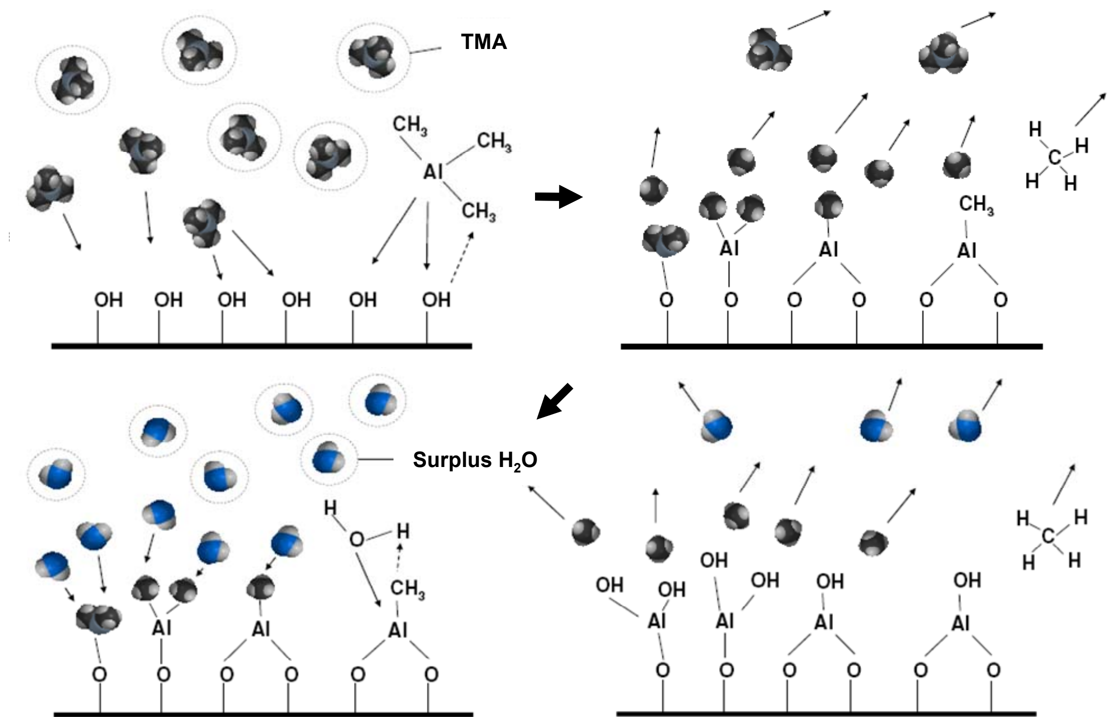

Figure 3.3 Schematic of one ALD cycle for AL2O3 depositions using TMA and H2O as metal and oxidation precursor.

Reactive Sputtering Deposition

Reactive sputtering of a metal oxide consists of bombarding a metal oxide target with an inert plasma or bombarding a metal target in an oxygen atmosphere. In this study reactive sputtering was used to co-deposit $HfGeO_x$ films onto germanium substrates by simultaneously bombarding a Ge and HfO_2 target in an Ar/O plasma. The oxygen was required to ensure the full oxidation of the germanium but would often be used even when depositing HfO_2 from the metal oxide target to ensure the deposition of a fully oxidised dielectric film.

3.3 Synchrotron Radiation Sources

Charged particles, such as electrons, emit radiation when they are accelerated. At synchrotron radiation sources, the broadband spectrum of radiation emitted by electrons as their path is bent by bending magnets can be used as a photon source for photoemission experiments as shown in figure 3.4. The use of mono-chromators allows for the selection of a desired photon energies. The use of a mono-chromator generally results in a higher resolution capability than a conventional XPS source. The advantage of being able to select the appropriate photon energy to optimise the surface sensitivity of the measurements is an important feature of synchrotron based photoemission experiments.

At the ASTRID synchrotron in Aarhus, Denmark, using the SGM1 beamline, photon energies from 30-650 eV could be selected which allowed for core-level experiments to be conducted at a range of surface sensitivities along with valence band and workfunction measurements similar to those obtained by UPS. Photoemission spectroscopy conducted using low photon energies is often referred to as soft x-ray photoelectron spectroscopy.

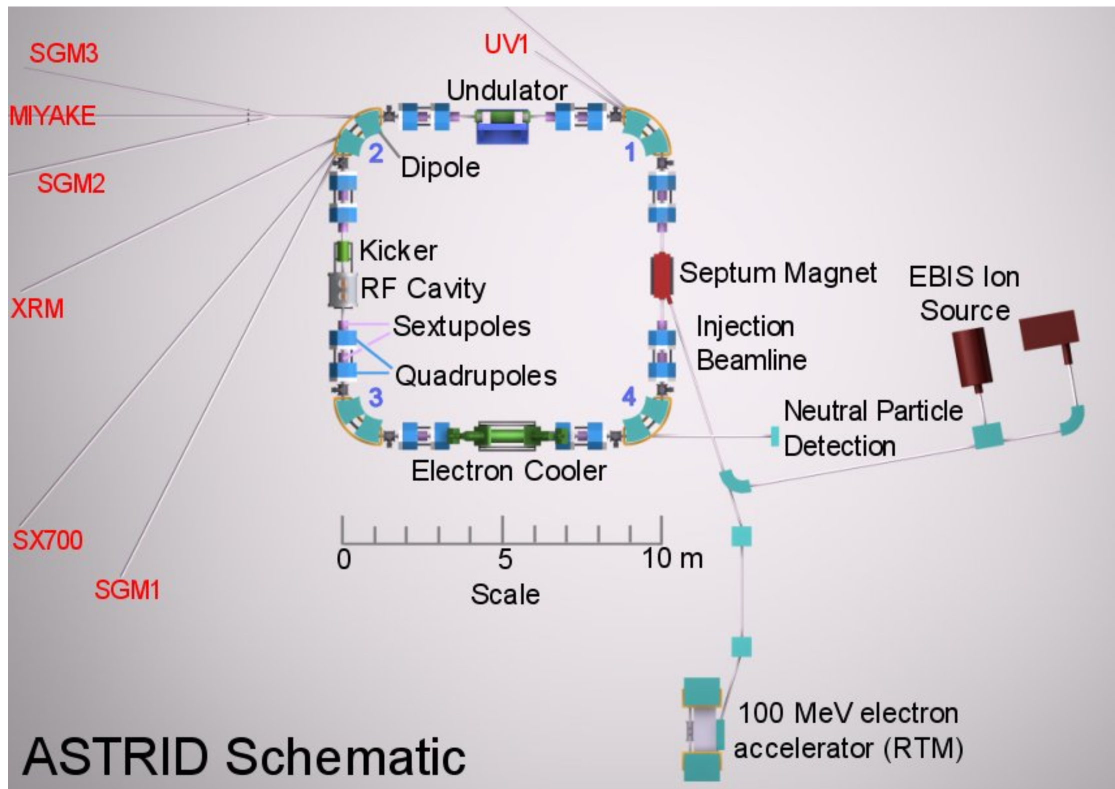

Figure 3.4 Diagram of the Aarhus Storage Ring in Denmark (ASTRID).

3.4 Surface preparation procedures

Hydrogen passivation of silicon using hydrofluoric acid

Since the quality of the interface between the gate dielectric insulator and the silicon substrate is of critical importance, ensuring that the insulator layer is grown on a clean silicon substrate is vital. The silicon substrate is typically covered by a chemical oxide which protects the underlying silicon from contamination. This oxide can be removed by thermal annealing to temperatures greater than 1000 °C in ultra-high vacuum (UHV),[4-6] however, this leaves highly reactive surface dangling bonds and as such this oxide removal method is only suitable for *in-situ* UHV experiments on silicon. The removal of the protective SiO_2 by etching the surface with dilute hydrofluoric acid (HF), results in a silicon surface that is passivated by hydrogen. This surface termination allows the silicon to be exposed to air for a period of time (typically less than 30 minutes) without any significant oxidation occurring.

Kang *et al*[7] studied the etching mechanism of dilute HF on SiO_2. They suggest that water plays an active role in the etching process by reducing the barriers to the required chemical reactions. It is a hydrogen atom from the H_2O molecule that breaks the Si-OH bond and forms another H_2O molecule. The fluorine from the HF can then bond to the silicon atom in place of the OH while the hydrogen from the HF replenishes the hydrogen donated by the original H_2O molecule to reform H_2O. This is explained by the reaction shown below.

$$\text{Si-OH} + \text{HF} + \text{H}_2\text{O} \rightarrow \text{Si-F} + 2\text{H}_2\text{O}$$

The resultant Si-F bonded silicon atom will still be bonded to one OH group and two oxygen atoms that are back bonded to the underlying silicon atoms. The remaining Si-OH bond is broken in a manner identical to the first, while the back-bonded Si-O bonds are broken by a slightly varied interaction. A hydrogen from the H_2O still breaks the Si-O bond, however, this results in an OH group bonded to the underlying silicon rather than a H_2O molecule. The original silicon atom still bonds to a fluorine from the HF and the hydrogen from the HF replenishes the hydrogen donated by the original H_2O molecule to reform H_2O. The final bond is broken, in an identical fashion to the third, resulting in SiF_4 (which is no longer bonded to the SiO_2 layer) and an OH terminated SiO_2 surface ready for continued etching. Once the oxide has been successfully removed, the silicon substrate is passivated with fluorine atoms.[8] The HF then attacks the Si-Si back-bonds which results in SiF_4 (which is no longer bonded to the silicon substrate) and a hydrogen passivated silicon surface is formed.

Native oxide reduction for GaAs wafers using ammonium hydroxide

In the high-κ dielectric on GaAs studies presented in chapter 6 of this thesis, all of the high-κ dielectric depositions were conducted by atomic layer deposition (ALD) which was described in section 3.2. The chemical reactions required to dissociate the TMA into aluminium bonded to the surface and volatile methane require the presence of OH groups on the semiconductor substrate. As such, ammonium hydroxide (NH_4OH) is often used as it is known to leave hydroxides on the surface. Lebedev *et al*[10] studied the affect of NH_4OH etching of the native GaAs oxides using soft x-ray photoemission. The etching was conducted in a nitrogen

atmosphere preparation chamber attached to the UHV system loadlock that allowed the affect of NH_4OH etching to be studied without the sample being exposed to air between etching and analysis. This study confirmed that the NH_4OH removes the bulk of the native oxides and leave arsenic hydroxides, gallium sub-oxides and elemental arsenic on the surface.

Native oxide removal for GaAs wafers by exposure to atomic hydrogen

High temperature exposure of oxidised GaAs to atomic hydrogen is known to form volatile surface oxides.[11-14] GaAs cleaning with a hydrogen cracker cell as a source for atomic hydrogen has been performed by other groups for the purposes of wafer bonding.[11] Detailed temperature programmed desorption (TPD) studies have been carried out which explain the oxide desorption mechanics.[12-14] In this study, the temperature of 430 °C was chosen which is greater than the values of 400 °C[11] and 350-400 °C[12-14] given in literature. At this temperature the desorption of arsenic oxides and Ga_2O can be expected, however, the removal of Ga_2O_3 without atomic hydrogen exposure would require temperatures closer to 500 °C.[12] Removing the native oxide at the lowest possible temperature is preferential because it minimises the loss of arsenic from the GaAs substrate. Where H* denotes atomic hydrogen, the exposure of Ga_2O_3 to atomic hydrogen at 430 °C results in the successful desorption of the remaining oxide through the reaction

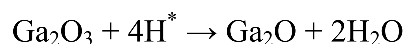

$$Ga_2O_3 + 4H^* \rightarrow Ga_2O + 2H_2O$$

Carbon removal from Ge by UV ozone exposure

Ultra-violet/ozone cleaning to remove carbon contamination is a common technique used for treating germanium substrates.[15-17] The exposure of carbon to the highly reactive O_3 results in the formation of low molecular weight species such as carbon dioxide and water.[17] This was performed *in-situ* by illuminating the germanium samples with a UV lamp while under atmospheric pressure of O_2 for 20 minutes. This forms the O_3 which can react with any carbon present near the samples surface.

Plasma nitridation of Ge and GeO_x

To nitride germanium oxide and germanium surfaces, they were exposed to a nitrogen plasma. This plasma was formed in the sputter deposition chamber. Normal sputter depositions would be carried out with an argon plasma, however, the use of nitrogen was possible. A nitrogen plasma would be struck over the HfO_2 sputter target at a very low power (approximately 10 W) which was sufficient to maintain the nitrogen plasma but not sufficient to deposit HfO_2. Exposing the samples to this nitrogen plasma resulted in the successful incorporation of nitrogen into the surface region of the samples.

3.5 Reference

[1] H. R. Huff, D. C. Gilmer *High Dielectric Constant Material: VLSI MOSFET Applications* Springer series in Advanced Microelectronics **16** (2005)

[2] S. Pongratz, A. Zöller, J. Vac. Sci. Technol. A **10(4)** (1992) 1897

[3] http://www.picosun.com/files/Picosun_ALD_031007.pdf

[4] P. Morgen, A. Bahari, U. Robenhagen, J. F. Anderson, J. –K. Hansen, K. Pedersen, M. G. Rao, Z. S. Li, J. Vac. Sci. Technol. A **23(1)** (2005) 201

[5] F. J. Himpsel, F.R. McFreely, A. Taleb-Ibrahimi, J.A. Yarmoff and G. Hollinger, Phys. Rev. B **38**, (1988) 6084

[6] I. Jiménez, J. L. Sacedón, Surface Science **482-485** (2001) 272-278

[7] J. K. Kang, C. B. Musgrave, Journal of Chemical Physics **116(1)** (2002) 275-280

[8] G. W. Trucks, K. Raghavachari, G. S. Higashi, Y. J. Chabal, Phys. Rev. Lett. **65(4)** (1990) 504-507

[9] Y. Xuan, H.C. Lin and P. D. Ye, IEEE Trans. Electron Devices **54** (2007) 1811

[10] M. V. Lebedev, D. Ensling, R. Hunger, T. Mayer and W. Jaegermann, Applied Surface Science **229** (2004) 226

[11] T. Akatsu, A. Plößl, H. Stenzel, U. Gösele, J. Appl. Phys. **86(12)** (1999) 7146

[12] Y. Ide, M. Yamada, JVST A (**12)4** (1994) 1858

[13] M. Yamada, Y. Ide, Jpn. J. Appl. Phys. **33** (1994) L671

[14] M. Yamada, Y. Ide, K. Tone, Jpn. J. Appl. Phys. **31** (1992) L1157

[15] J. S. Hovis, R. J. Hamers, C. M. Greenlief, Surface Science **440** (1999) L815-819

[16] X. –J. Zhang, G. Xue, A. Agarwal, R. Tsu, M, -A. Hasan, J. E. Greene, A. Rockett, J. Vac. Sci. Technol. A. **11** (1993) 2553

[17] M. Ouyang, C. Yuan, R. J. Muisener, A. Boulares, J. T. Koberstein Chem. Mater. **12(6)** (2000) 1591-1596

4 *In-Situ* analysis of the micro e-beam growth of HfO_2 on silicon(111)

4.1 Introduction

High-κ dielectrics on Silicon

The MOSFET has been an ever improving technology based on the continued scaling of the transistor to smaller dimensions which has often required refinements in device fabrication process.[1] The implementation of entirely new processes, whether they be for lithography or film growth, has always been more difficult to achieve because of the inherent uncertainties that they brought to the fabrication process. A new process would have to be extensively researched to eliminate potential problems and demonstrate enhanced performance before being introduced. The addition of new materials into the fabrication process has always been approached in a very cautious manner; for example, the change from aluminium to copper as the metal of choice for interconnects took many years to perfect before implementation.

The continued publication of experiments explaining the SiO_2/Si interface after 30 years of its use in industry serves as evidence of how much is still not understood about this well studied and important interface. Because of this, the shift to another, less studied, dielectric material is understandably a difficult step for industry to make. Still, the introduction of copper as a replacement to aluminium and the use of germanium in silicon to strain the transistor channel proves that if a new material can provide significant advantages and also provide reasonable scalability then it will be adopted.

The shift to high-κ dielectrics has become generally accepted as an inevitable step[2], although the use of SiON and now $HfSiO_x$ in the last two generations of MOSFET's at Intel show that the removal of silicon oxide as a component in the dielectric has still not been completely achieved. The primary reason for this is that the SiO_2/Si interface works well and is very well understood. Problems such as thermodynamic stability, interface quality and process compatibility[2,3] make the introduction of a silicon free high-κ dielectric problematic.

As the physical thickness limit of the SiO_2/Si system drew closer, the development of silicon based dielectric replacements such as high dielectric constant silicates was undertaken by industry and these are currently being integrated into commercial production. It has been suggested that the scaling of such silicates could result in their use as a high-κ interfacial layer between silicon and another high-κ material.[3] As such, the focus of the research community shifted to non-silicon high-κ dielectrics, such as the promising HfO_2 and ZrO_2 as well as the more exotic La_2O_3. The mid-κ dielectric Al_2O_3 has remained the focus for many studies and this is most likely due its thermodynamic stability on silicon[3] and also because it serves as a baseline for the study of the more complicated aluminates.

In this and the following chapter, the HfO_2 on silicon interface will be discussed. Hafnium oxide was chosen for being one of the most promising of the possible high-κ dielectric materials in terms of electrical reliability.[3] With a reported dielectric constant of 25 and a bandgap of 5.8 eV it should allow for a significant increase in the physical thickness of a gate dielectric without losing EOT while still having sufficient band offsets with silicon to act as an insulating layer.[2] Extensive research has been carried out on both the chemical and electrical properties HfO_2 on silicon. Early works by Kang *et al*[4] on the reliability properties of HfO_2 on silicon showed that for a HfO_2 layer with an EOT of 13.5 Å, the leakage currents were four times lower than SiO_2 of the same EOT and also that the time-dependant dielectric breakdown (TDDB) characteristics showed more than a 10 year life span. The same group also published promising thermal stability characteristics after rapid thermal annealing (RTA) of the dielectric layers up to 900 °C in N_2 and O_2 ambients.[5]

Early works on HfO_2 were for the purpose of dynamic random access memory (DRAM) applications and optical coatings.[3,6] The renewed interest in this material in the last 10 years revitalised the study of its physical properties. Soft x-ray photoemission studies of the oxidation of hafnium metal by Suzer *et al*[7] provides a high resolution reference to the oxidation states of hafnium. XPS studies of the HfO_2 interface by Renault[8] and Xie *et al*[9] utilise the capability of XPS to calculate the thickness of interfacial oxide under thin high-κ layers.

The aforementioned studies served as motivation for the HfO_2 on silicon substrate studies that will be presented in this and the following chapter. Particular mention should be made of the works by Zeman *et al* [10] and Fulton *et al*[11] discussing the thermal stability of ZrO_2, TiO_2 and HfO_2 on silicon[10] at temperature greater than 600 °C as well as the more focused x-ray photoemission study on the thermal stability of ZrO_2[11] which inspired the detailed *in-situ* high temperature annealing studies of the HfO_2/Si system which will be discussed in this chapter.

In this chapter, results of an *in-situ* characterisation study of hafnium oxide growth on silicon (111) substrates are presented. The effects of UHV post-deposition anneals are also studied and the hafnium oxide was grown at two different substrate temperatures. A critical factor in the use of high-κ dielectrics on silicon is the suppression of interfacial SiO_x formation which will have a lower dielectric constant and increase the equivalent oxide thickness of the combined oxide layer. Unfortunately, interfacial oxide growth appears to be an inherent by-product of most metal oxide depositions and is generally very difficult to control.[3]

In this study an ultra-thin self limiting SiO_2 layer, previously reported by Morgan *et al*,[12] was grown as an interfacial buffer layer on an atomically clean silicon substrate. This approach was adopted in an attempt to control interface formation and to ensure a better quality SiO_2/Si interface following the deposition of HfO_2. While testing the electrical quality of this interface was beyond the scope of this study, it was hoped to determine whether or not the catalytic growth of an SiO_2 interfacial layer commonly seen in HfO_2 depositions would result in the formation of an interfacial oxide thickness which would be too great for reasonable device applications.

4.2 Experimental

4.2.1 Experimental procedure and surface preparations

In these experiments, an ultrathin SiO_2 layer was grown on an oxide free silicon surface in UHV. The sample would then be analysed by XPS without breaking vacuum before the growth of a HfO_2 layer. XPS analysis would be conducted after each subsequent deposition of HfO_2 until a thickness was reached where the substrate signal was completely suppressed. For experiments carried out using conventional XPS, the analysis UHV chamber also served as the deposition chamber. For the experiments carried out using synchrotron radiation, the analysis chamber could be sealed off from the deposition chamber so that O_2 never contaminated the analysis chamber. Transferring the sample between the analysis chamber and the deposition chamber was possible without breaking UHV and typically took 10 minutes.

The samples in this study were typical 1 cm x 2 cm and underwent no *ex-situ* preparation. They were cleaved from a boron doped 4 inch p-type Si(111) wafer of resistivity 1-3 mΩ-cm (doping concentration 2-5 x 10^{19} cm^{-3}). The native SiO_2 was removed by *in-situ* direct current flash heating of the silicon sample to greater than 1100 °C which results in the desorption of the SiO_2 from the surface leaving an oxygen free surface.[12-14] Oxide desorptions at lower temperatures would have required the use of a silicon flux in order to maintain a smooth surface.[15] The SiO_2 buffer layer was grown following the procedures reported by Morgan *et al*.[12] The sample was heated to 600 °C by direct current heating and the chamber was back-filled to a pressure of 1 x 10^{-7} mbar of O_2 for 30 minutes. The buffer oxide would then be analysed by photoemission.

For the experiment carried out using conventional XPS the deposition of the HfO_2 layer was performed using the micro e-beam evaporator described in Chapter 3. The hafnium wire had a purity of 97%, the 3% contamination was primarily zirconium and depositions were conducted with the UHV chamber back-filled to 5 x 10^{-7} mbar of oxygen. The depositions of HfO_2 were conducted at room temperature and photoemission spectra were obtained after each deposition. After the growth of

the HfO_2 layer the sample was annealed at increasingly high temperatures through direct current heating to temperatures up to 1000°C to determine the thermal stability of the interface at high temperature.

For the experiment carried out using synchrotron radiation the deposition of the HfO_2 layer was performed with the same micro e-beam evaporator and with the same hafnium wire with the same partial pressure of oxygen. This experiment was conducted twice, for the first experiment the sample was at room temperature while for the second experiment the sample was heated by direct current heating to 200-250 °C during deposition. This second sample was also annealed at increasingly high temperatures through direct current heating to temperatures up to 1000°C to determine the thermal stability of the interface at high temperature.

4.2.2 Characterisation

In the two separate experiments the samples were analysed by either *in-situ* conventional XPS or soft x-ray photoemission after the growth of the SiO_2 buffer layer. Core-level spectra from the samples were also obtained after each HfO_2 deposition to allow for a detailed analysis of the $HfO_2/SiO_x/Si$ interface regions to be conducted. For the conventional XPS experiments all spectra were acquired using the Al Kα x-ray line of 1486.6 eV, in the vacuum system A described in chapter 3. For the experiments carried out using synchrotron radiation the SGM1 beamline in Astrid at the University of Aarhus also described in chapter 3 was used. Although the growth of the SiO_2 buffer layer and the deposition conditions of the hafnium dioxide excluding the substrate temperature were the same for both experiments, the deposition rate of hafnium oxide could not be kept identical. The deposition rate was different due to the different geometries of the UHV chapters which resulted in a different distance between the evaporator and the sample. This could not have been avoided and since the deposition rates in both cases were slow (approximately 0.2 Å/min) it was thought to have a negligible affect on results.

4.3 Results

4.3.1 Buffer oxide, structure and fitting

The growth of an ultra-thin SiO_2 layer on a 'flash cleaned' silicon substrate has been demonstrated by Morgen *et al.*[12] That study demonstrated that the growth of this oxide was self limiting and longer exposures to 1 x 10^{-7} mbar of O_2 at a substrate temperature of 600 °C did not result in any noticeable increase in the SiO_2 film thickness. Here, a similar SiO_2 layer was grown as a 'buffer layer' before the deposition of HfO_2. In comparison to the unintentionally grown SiO_x interfacial layers that will be discussed in chapter 5, it was presumed that a deliberately grown SiO_2 layer would provide a higher quality interface. Although this experiment was conducted in UHV, the buffer oxide was grown within 30 minutes of flash cleaning to minimise contamination of the silicon surface.

The buffer SiO_2 layer was analysed both by synchrotron radiation at a range of photon energies including 130 eV, 160 eV, 200 eV and 260 eV photon energy as well as by conventional XPS at 1486.6 eV. Valence band and work-function spectra were also taken at the SGM1 beamline and will be discussed separately. Figure 4.1 shows the differences in the profile of the Si 2p spectral region for the different photon energies. The increase in sampling depth with increased photon energy is clear from the diminishing oxide peak with respect to the substrate. At a photon energy of 1486.6 eV the surface oxide is not readily visible and is only detectable upon close inspection. Also obvious, from the Si 2p substrate peak, is the difference in binding energy resolution between a monochromated synchrotron source and an un-monochromated x-ray source which is unable to resolve the spin-orbit splitting of 0.61 eV in the Si 2p core-level.

The time taken for each analysis step was typically between 2-3 hours and so it can been assumed that there was at least this time between the growth of the SiO_2 buffer layer and the growth of the first hafnium oxide layer. Similar time periods would separate each hafnium deposition and the sample was again analysed. It should be noted that overnight break caused 12-14 hour breaks between depositions as the

experiment took place over 3-4 days. At all times the same was held in UHV. The hafnium oxide was intentionally grown at a low deposition rate and in small increments so that the first reactions between the hafnium oxide and underlying SiO_2 could be investigated.

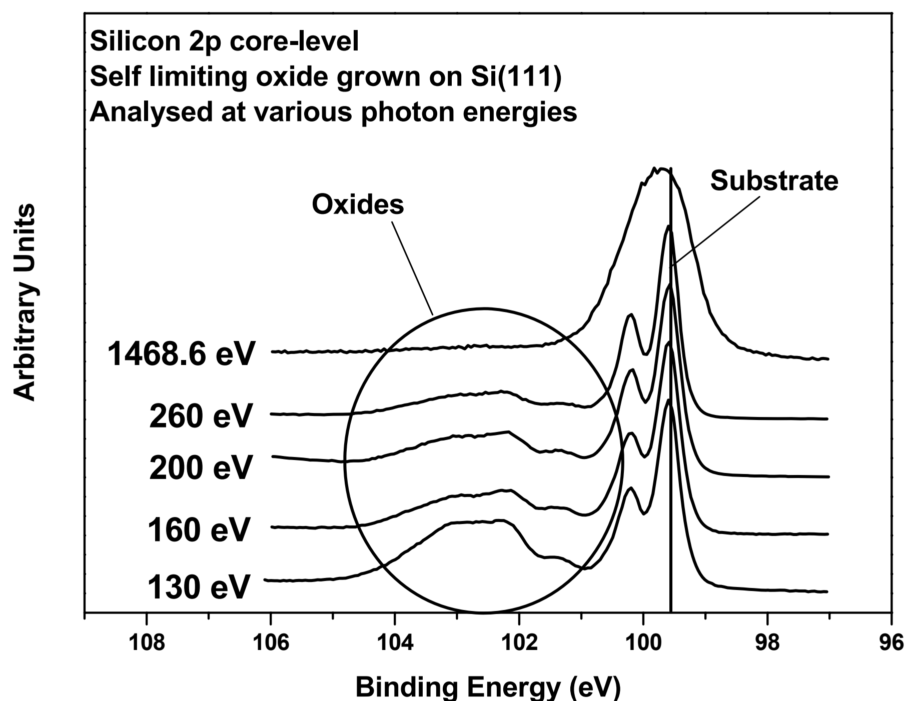

Figure 4.1 The Si 2p XPS spectra of the self limiting ultra-thin buffer oxide[12] taken with a range of photon energies by both soft-XPS (130 eV – 260 eV) and conventional XPS (1486.6 eV).

Figure 4.2 shows the spectral analysis of the SiO_2 layer analysed at 130 eV photon energy as well as an identically grown layer scanned by conventional XPS. For the 130 eV spectra, the fitting parameters given by Himpsel *et al*[13] were used as a starting point. The core-level chemical shifts (CLCS's) for the various Si oxidation states were not fixed but are seen to agree reasonably well with the reported values and are shown in table 4.1. The value of R_{exp} that would be used for thickness calculations is the sum of the area under the four oxide features Si^{1+}, Si^{2+}, Si^{3+} and Si^{4+} divided by the area under the substrate feature Si^0. These values are also included in Table 4.1. It is possible to fit the spectra obtained by conventional XPS using identical parameters to those obtained from the 130 eV spectra with the exception of

the Gaussian contribution to the full width half maximum (FWHM), since this contribution is due in part to the instrumental broadening. This approach, however, would imply a resolution greater than can be obtained by XPS and so for this study fitting was performed using a single bulk oxide and single interfacial oxide peak.

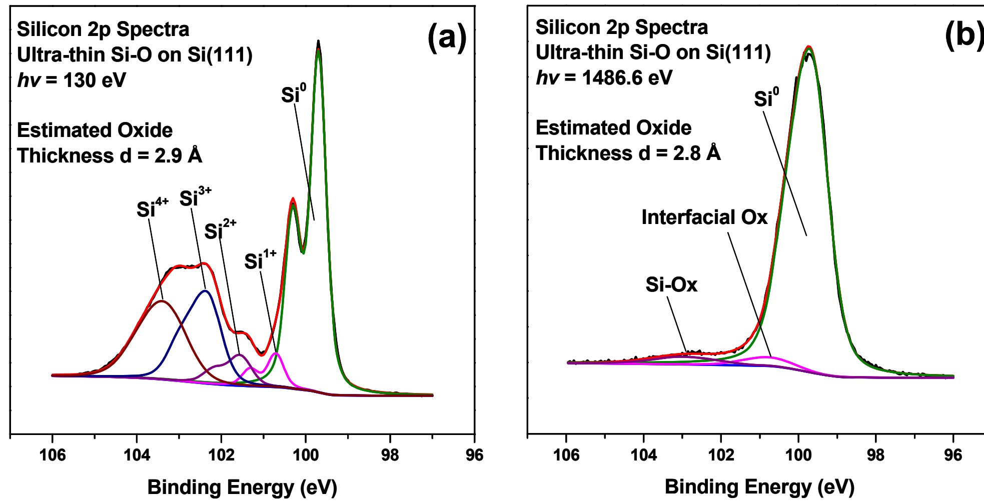

Figure 4.2 The Si 2p photoemission spectra of the ultra-thin buffer oxide[12] obtained at a) 130 eV and b) 1486.6 eV photon energy. The spectra were obtained using the parameters described in the text. a) shows the calculated CLCS's from these fits as well as values taken from Himpsel *et al.*[13]

	Si^{0}	Si^{1+}	Si^{2+}	Si^{3+}	Si^{4+}
Area	77.2	7.7	9.2	31.3	33.5
Gaussian (eV)	0.33	0.33	0.52	0.67	1.04
CLCS (eV)	0	+ 1.01	+ 1.85	+ 2.62	+ 3.54

Table 4.1 Extracted parameters for the spectral analysis shown in figure 4.2. Lorentzian peak width was fixed at 1.7

The thickness measurement techniques described by Himpsel *et al*[13] and explained in chapter 2 were used to both measure the thickness of the starting SiO_2 layer and also monitor any change in thickness caused by subsequent high-κ depositions. The expression

$$d = l \cos\theta \ln[1 + \frac{R_{exp}}{R_0}] \quad (4.1)$$

contains the constants l, R_0 and θ. These constants were described in detail in chapter 2.1 pages (39, 41 and 42) as being the electron attenuation length (l), the theoretical ratio of and infinitely thick overlayer signal to an infinitely thick and clean substrate signal (R_0) and the electron take-off angle with respect to the surface normal (θ). Values of 7.1 Å and 2.1 for l and R_0 were taken from Himpsel *et al*[13] and used to calculate the SiO_2 layer thickness from the spectra obtained at 130 eV. These same constants were taken as 34.48 Å and 0.82 from Seah and Spencer[16] and Himpsel *et al*[13] respectively for the spectra obtained at 1486.6 eV. To obtain these same values for the photon energies of 160 eV, 200 eV and 260eV, the value of l was assumed to change linearly with photon energy. By fixing the SiO_2 layer thickness to 2.9 Å, the value for R_0 for each of these photon energies could be extracted. These values would then be fixed for all future measurements of SiO_x interlayer thickness so that independently calculated values could be obtained for a film of any given thickness. Table 4.2 shows the values for these constants that were extracted equation 4.1 once the values of R_{exp} were obtained from the spectral analysis of the raw data shown in figure 4.1. All measurements were taken at $\theta = 0$.

Hv	R_{exp}	l (Å)	R_0	θ	d (Å)
130	1.06	7.1	2.1	0°	2.9
160	0.65	7.7	1.42	0°	2.9
200	0.53	8.5	1.31	0°	2.9
260	0.4	9.7	1.14	0°	2.9
1486.6	0.07	34.48	0.82	0°	2.8

Table 4.2 Extrapolated and extracted values for l and R_0 from the analysis of the Si 2p core-level features taken at 130 eV, 160 eV, 200 eV, 260 eV and 1486.6 eV as shown in figure 4.1

It can be seen from the estimated thicknesses of the oxides shown in figure 4.2 that the original SiO_2 layer can be thought of as simply one-two monolayers of SiO_2. The individual oxidation states can be clearly resolved in the spectra acquired at the synchrotron due to inherently higher energy resolution and increased surface sensitivity at 130 eV photon energy.

4.3.2 Room Temperature Hafnium Oxide Deposition

Once the buffer oxide was grown and analysed, hafnium oxide was incrementally grown on to the ultra-thin SiO_2 layer. The first deposition of hafnium oxide onto the pre-grown silicon oxide surface shows two distinct bonding environments for the hafnium 4f core-level as shown in figure 4.3a obtained at 1486.6 eV during the experiment conducted at DCU and figure 4.3b obtained at 130 eV during the identical experiment conducted at synchrotron light source in Aarhus university. The lower binding energy component is not at a sufficiently low energy to be attributed to hafnium in a metallic or silicide state which would be shifted by more 3 eV to the lower binding energy side of the fully oxidised hafnium feature[10] and instead is attributed to interfacial sub-stiochiometric hafnium in agreement with Xu *et al*.[17] The increase in the silicon oxide signals with respect to the silicon substrate signal shown in figure 4.3c results in an increase in the ratio R_{exp} from 1.06 to 1.24 which indicates a growth of the interfacial oxide region from 2.9 Å to 3.3 Å. This would most likely be due to the metal atom catalytic affect which allows oxidation due to the dissociation of molecular O_2 in the presence of hafnium into atomic oxygen.[17-19] This thickness was calculated using the same constants for l, R_0 and θ as when calculating the thickness of the original buffer oxide.

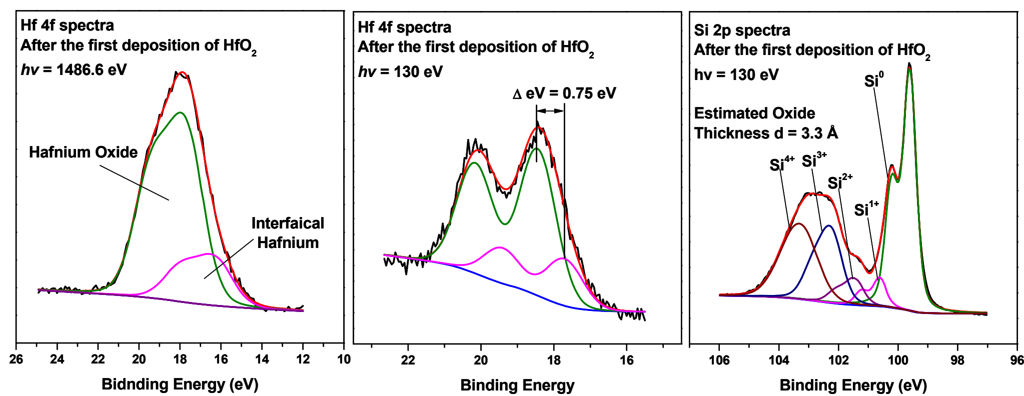

Figure 4.3 The photoemission spectra after the first hafnium oxide deposition of a) Hf 4f taken at 1486.6 eV photon energy, b and c) Hf 4f and Si 2p respectively taken at 130 eV photon energy. The binding energy separation between the HfO_2 and interfacial hafnium is included in b) and the calculated thickness of the interfacial oxide is shown in c).

The growth of the interfacial layer's thickness was monitored throughout the depositions until the substrate signal became suppressed. Figure 4.4 shows the Hf 4f and Si 2p regions throughout the film growth process for both the experiment monitored with conventional XPS at 1486.6 eV photon energy (a and b) and the experiment monitored with synchrotron radiation at 130 eV photon energy (c and d). It is clear that the increased surface sensitivity at 130 eV allows us to see the growth of the interfacial oxide which remains at the limit of detection when using a conventional x-ray source. The growth of the Hf 4f feature is still evident due to the decrease in signal to noise with increased deposition time, just as the increased signal to noise ratio in the Si 2p spectral features corresponds to the increased attenuation in the substrate signals as the overlayer film thickness increases.

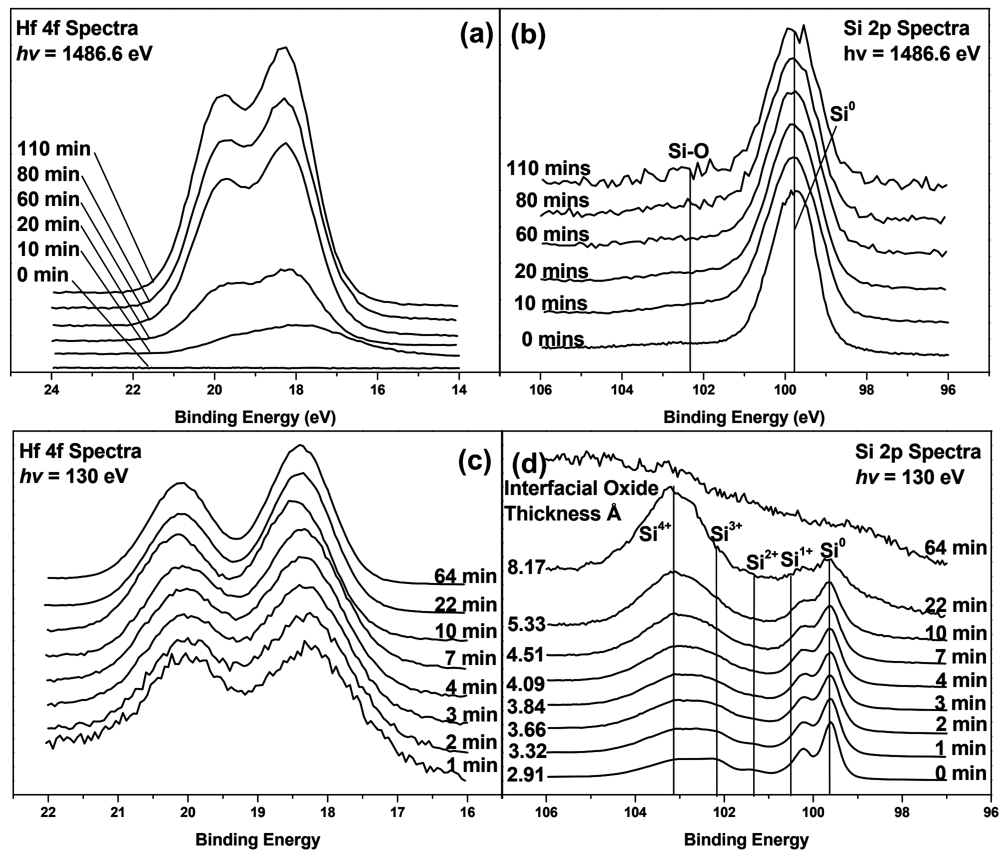

Figure 4.4 The photoemission spectra, taken sequentially after each hafnium oxide deposition, of a) and b) Hf 4f and Si 2p respectively both taken at 1486.6 eV photon energy during the conventional XPS experiment as well as c and d) Hf 4f and Si 2p respectively both taken at 130 eV photon energy during the synchrotron photoemission experiment. The spectral lines in (b-d) have been normalised to their maximum intensities to allow for easier viewing.

Figure 4.4a and figure 4.4c shows that the Hf 4f core-level for the HfO_2 film is seen at 18.4 eV. Figure 4.4d includes the thickness of the interfacial oxide calculated using the ratio of the substrate to overlayer signals (R_{exp}). Figure 4.5 shows selected examples of the fits used to obtain these ratios. There is a clear emergence of a spectral feature, labelled here as Si*, positioned 0.65 eV to lower binding energy than the substrate feature as the HfO_2 is deposited. This is a similar binding energy position to that of surface states seen on atomically clean silicon[13] and so could indicate the presence of silicon without a full arrangement of four silicon neighbours. This suggests that the underlying silicon is disturbed by the deposition of HfO_2. Such disruption of the silicon immediately below the SiO_2/Si interface could have a detrimental effect on the mobility of charge carriers in the channel of a MOSFET. Also, there is a steady reduction in the core-level shift between the Si^{4+} core-level feature and the substrate feature from 3.55 eV to 3.3 eV with each hafnium oxide deposition which is consistent with a shift from SiO_2 to $HfSiO_x$.[20] The thickness calculations were also carried out using the Si 2p spectra acquired at higher photon energies. Figure 4.6 shows these trends where the value for *l* was assumed to change linearly between the values known for 130 eV and 1486.6 eV photon energies and this assumption could be responsible for the variation between the thicknesses calculated from the 130 eV photon energy spectra and the 160 eV, 200 eV and 260 eV photon energy spectra. Also spectral features obtained at increased photon energies are more bulk sensitive and as such it is harder to clearly identify each of the four oxidation

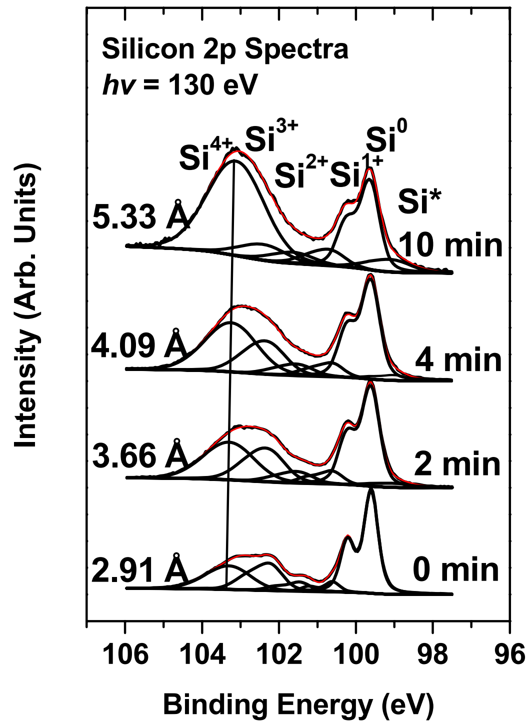

Figure 4.5 Sample of fitted spectral features of the Si 2p core-levels obtained at 130eV photon energy after each HfO_2 deposition.

states accurately which could result in the photoemission signal from the lower oxidation states being suppressed by the increased bulk silicon feature.

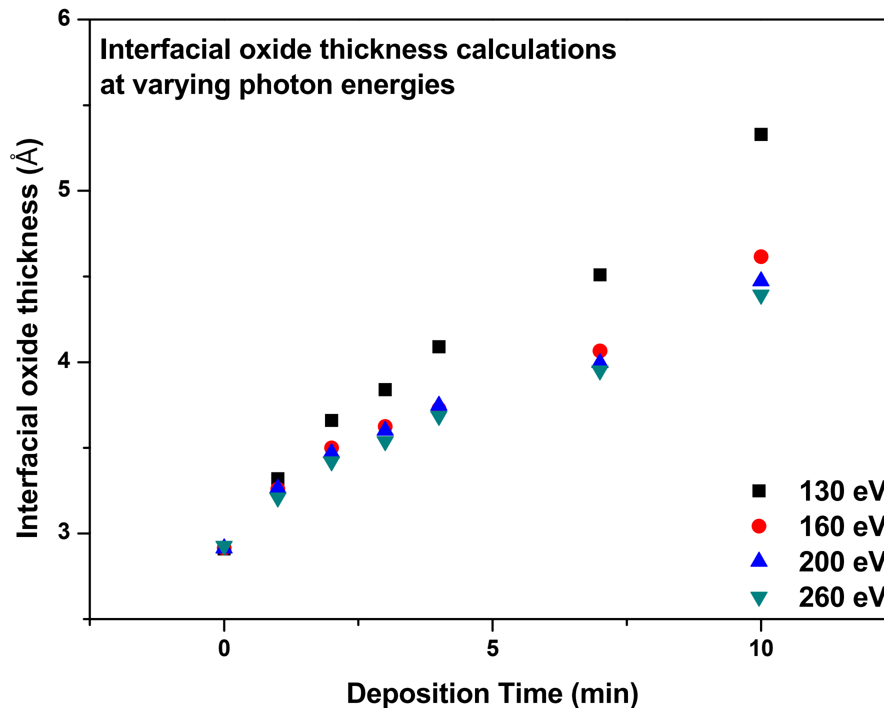

Figure 4.6 Interfacial oxide thickness versus hafnium oxide deposition time for hafnium oxide deposited at room temperature. The interfacial oxide thickness was calculated using the ratio of the overlayer to substrate signals from the Si 2p spectra obtained at different photon energies.

After the final deposition the stoichiometry of the hafnium oxide layer was calculated from the relative intensities of the Hf 4f and O 1s core-levels normalised by their relative sensitivity factors (RSF's) as described in section 2.2 and found to be 69% oxygen 31% hafnium. For thinner films with thicknesses less than the inelastic mean free path (IMFP) in the material, such calculations would tend to result in an oxygen rich ratio because of the O 1s core-level's lower kinetic energy with respect to the Hf 4f. The reasons for this, discussed in more detail in section 2.2, are that the RSFs contain a factor to compensate for the different sampling depths, in an infinitely thick film, of electrons with different kinetic energies. When the film is thin enough that electrons from the full depth of the film are easily sampled then the use of this compensation term becomes inaccurate. An alternative way to check the chemical state of the film, which is useful for ultra-thin films, is to monitor the binding energy

separation between the Hf 4f and O 1s core-levels throughout the experiment. Conventional XPS can be sensitive to core-level shifts as small as 0.1 eV. In figure 4.7, it can be seen that with the exception of the first ten minute room temperature deposition of HfO_2 the core-level shift remains constant at 514.36 ± 0.06 eV. The wider core-level separation for the first 10 minute deposition is not unexpected since the spectral analysis of this data, shown earlier in figure 4.3a, indicated that this first deposition contained a noticeable sub-stoichiometric hafnium oxide signal.

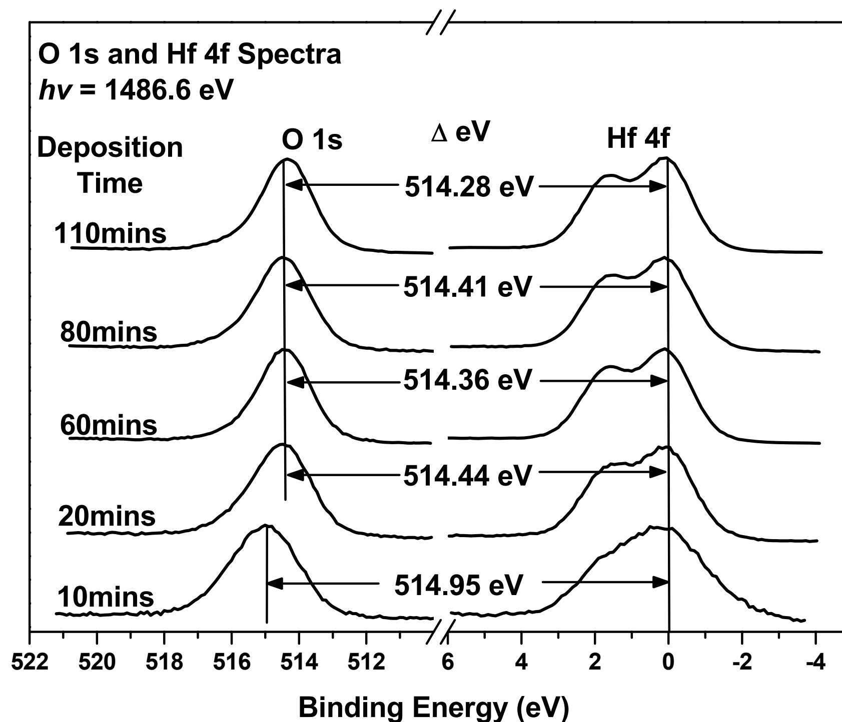

Figure 4.7 The O 1s and Hf 4f XPS spectra taken sequentially with continued depositions of hafnium oxide. The binding energy separation is shown to remain constant to within 0.1 eV and the atomic concentrations of the final film are given.

For the gate dielectric to function as an effective insulator between the silicon substrate and the gate electrode the valence band (VB) and conduction band (CB) offsets must typically be greater than 1 eV. For most dielectrics the VB offset is greater than the CB offset and so the CB offset is seen as a figure of merit.[2] In UPS and soft x-ray photoemission, the CB offset can be inferred by experimentally determining the VB offset and using known values for the bandgaps of the substrate and the insulator. The change in the valence band offset was monitored at 130 eV

photon energy until the underlying silicon layer was undetectable. Shown in figure 4.8a is the valence band offset between the HfO_2 overlayer and the silicon which is seen to saturate at 3.6 eV before the underlying silicon signal is lost. Assuming a bandgap[2] for HfO_2 of 5.8 eV this result implies a conduction band offset of 1.1 eV which should be sufficient for the HfO_2 layer to function as an insulator between the transistor gate and the conduction channel.

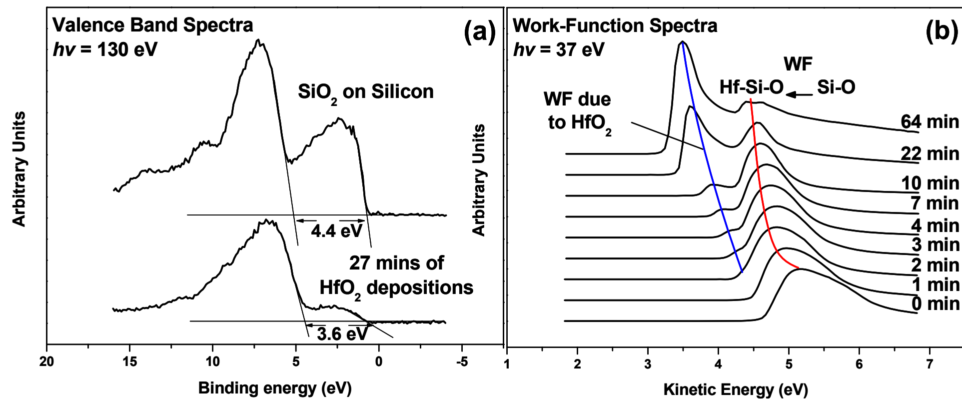

Figure 4.8 a) Valence Band spectra of the ultra-thin buffer oxide[12] and after multiple room temperature HfO_2 depositions. b) Work Function spectra continually shifting to lower kinetic energy with each room temperature HfO_2 deposition.

The workfunction of the sample was monitored during the deposition process with a photon energy of 37 eV and is shown in figure 4.8b. It can be seen that the workfunction, after the deposition of hafnium oxide, has two components implying that the sample has two workfunctions. To explain this, it has been assumed that the room temperature deposition of the hafnium oxide films at these low coverages results in non-uniform growth. This should result in electrons leaving the sample from an area with no HfO_2 coverage having to overcome the workfunction of silicon dioxide in order to reach the vacuum level while electrons coming from an area with HfO_2 islands would have to overcome the workfunction of HfO_2 on silicon. It is possible that the silicon dioxide areas do gradually form thin hafnium silicate which would account for the shift and saturation of the higher kinetic energy work function signal. This result inspired further studies of hafnium oxide films grown at higher substrate temperatures.

4.3.3 Elevated Temperature Hafnium Oxide Deposition

On a separate silicon sample prepared in the same way as the previous experiments by flash cleaning and buffer oxide growth as described in section 4.3.1, HfO_2 was deposited at an elevated substrate temperature with the UHV chamber back-filled to 5 x 10^{-7} mbar of oxygen. The silicon wafer was heated by direct current heating to ~ 250 °C and the current was kept constant throughout each deposition. Depositions were typically started within 2 minutes of heating the sample. The sample would then be allowed to cool for at least one hour before synchrotron based photoemission analysis. Figure 4.9a shows that the HfO_2 core-level feature is positioned at 18.4 eV binding energy which indicates that the hafnium is in the same chemical states as the HfO_2 deposited at room temperature. The interfacial reactions seen in figure 4.9b are similar to those of room temperature growth. The interfacial oxide thickness increases during the first depositions as can be seen by the changing oxide to substrate ratio in the Si 2p spectrum. The valence band spectra in figure 4.9c

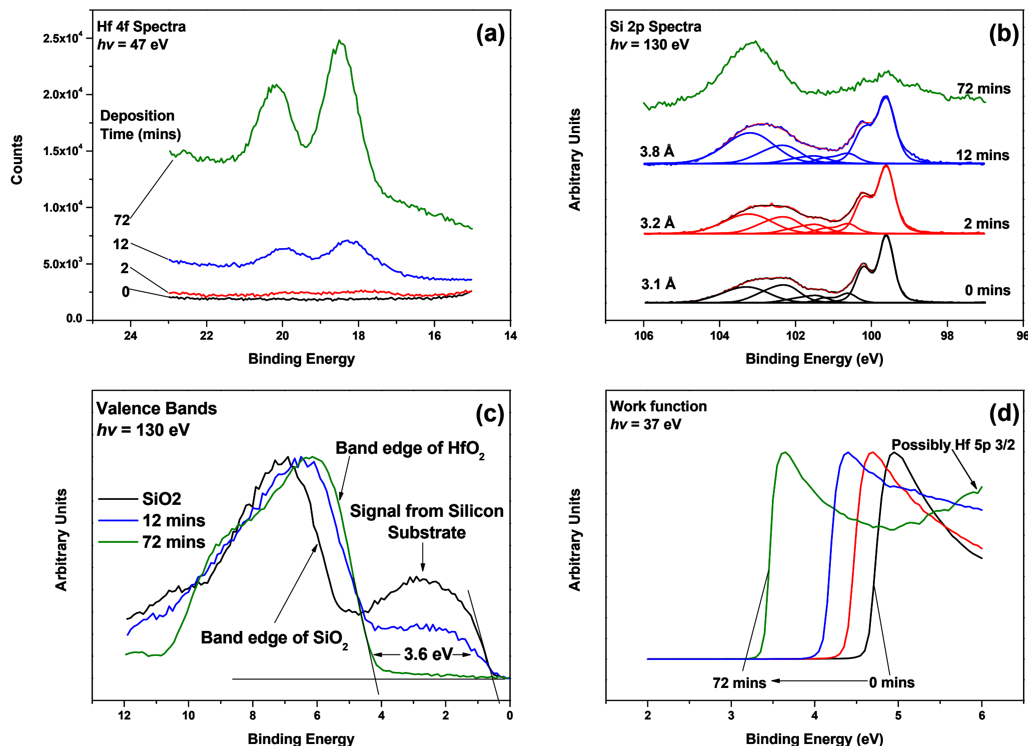

Figure 4.9 soft x-ray photoemission spectra for sequential hafnium oxide depositions of a) Hf 4f taken at 47 eV photon energy, b) Si 2p taken at 130 eV photon energy, C) Valence Band spectra taken at 130 eV photon energy, d) Work function spectra taken at 37 eV photon energy.

shows that the valence band offset appears to limit at 3.7 eV which is approximately equal to the value of 3.6 eV obtained for the HfO_2 grown at room temperature. Figure 4.9d shows that there is only a single work function which suggests that the deposition of hafnium oxide on silicon in an oxygen ambient at 250 °C results in 2D growth.

4.3.4 Post Deposition High-Temperature Anneal

It is very important for any potential high-κ material to be thermodynamically stable on silicon at temperatures used in device processing.[2] After the deposition of hafnium oxide layers on oxidised silicon described in the previous sections, the sample was heated by direct current heating at temperatures ranging from 700 °C to 1000 °C in steps of 100 °C for 5 minute durations. The chemistry of the film and interface was monitored using conventional XPS and also, for a sample grown at ~ 250 °C substrate temperature, using synchrotron radiation.

Similar annealing experiments have been reported by Zeman *et al*[10] on TiO_2, ZrO_2 and HfO_2 using ultra-violet photoelectron emission microscopy to monitor the films. The same group reported a more detailed study of the ZrO_2 system[11] using XPS to monitor the films. In both studies the high-κ layers were grown, at room temperature, by e-beam deposition on oxidised silicon and so provide a good comparison for this study. They found that the HfO_2 did not decompose and form $HfSi_x$ until 1000 °C. Xu *et al*,[17] however, report silicide formation at temperatures as low as 700 °C when HfO_2 is grown directly onto clean silicon without the use of a buffer layer.

From analysing both the relative peak areas as well as the binding energy separation of the Hf 4f and O 1s core-levels as a function of annealing temperature as shown in figure 4.10a it is clear that 5 minute anneals at temperatures up to 900 °C have no affect on the chemical composition of the hafnium oxide films. The shift in both the O 1s and Hf 4f features to lower binding energies suggests a reduction in surface charging which could indicate a decrease in the insulating properties of this film. Following a 5 minute anneal at 1000 °C there is a clear feature on the lower

binding energy side of the Hf 4f oxide feature. This feature can be identified as Hf-Si bonds from literature.[21] The ratio of the hafnium oxide feature (higher binding energy Hf 4f component) to the O 1s feature still remains constant indicating that any hafnium which has not become involved in forming hafnium silicide remains fully oxidised.

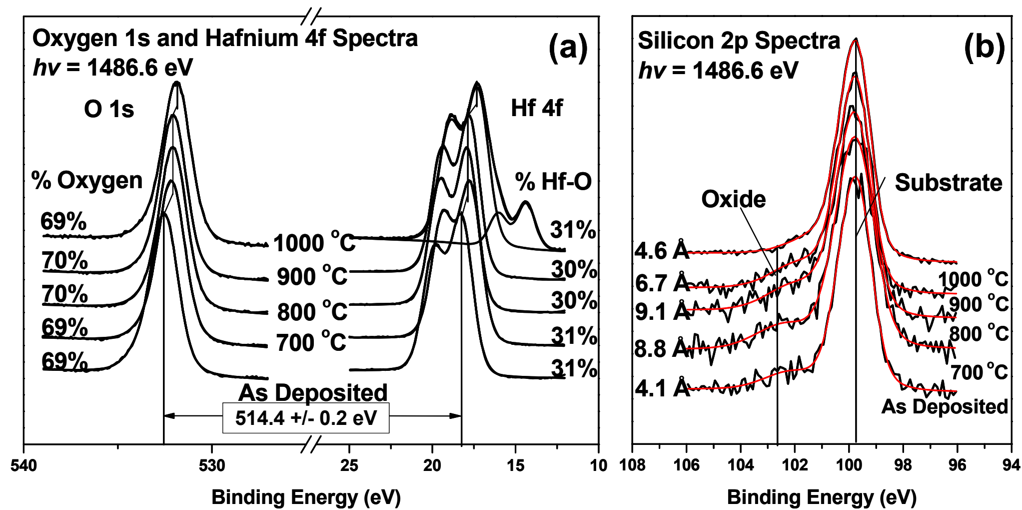

Figure 4.10 The a) O 1s and Hf 4f, b) Si 2p XPS spectra taken at 1486.6 eV photon energy after sequential 5 min UHV anneals at temperatures range from 700-1000 °C. Included in b) is the thickness of the interfacial oxide.

The Si 2p spectra taken during these annealing experiments are displayed in figure 4.10b. It is apparent that there is an increase in the interfacial oxide thickness as a function of annealing temperature. Since the stoichiometry of the hafnium oxide layer is not seen to change, the silicon is most likely oxidised by excess oxygen in the hafnium oxide layer. The decomposition of the hafnium oxide layer coincides with the reduction in the Si-O feature from the Si 2p spectra as can be seen in figure 4.10b. This is in agreement with the thermal annealing reports by Zeman *et al*[10] that suggest, for the $HfO_2/SiO_2/Si$ system with SiO_2 interlayers of less than 3 nm, the SiO_2 layer interacts with the underlying silicon to form SiO which desorbs through the hafnium oxide layer and allows for an interaction between the hafnium oxide and silicon substrate through the following reactions.

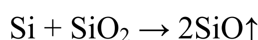

$$Si + SiO_2 \rightarrow 2SiO\uparrow$$

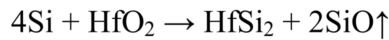

$$4Si + HfO_2 \rightarrow HfSi_2 + 2SiO\uparrow$$

Synchrotron radiation based high temperature anneals of hafnium films grown on pre-oxidised silicon at ~ 250 °C substrate temperature yield different results. Figure 4.11a shows that the Hf 4f region monitored at 47 eV shows the presence of a hafnium silicide signal after anneals at 700 °C which increases in intensity at higher temperatures. It is clear from the valence band spectra in figure 4.11a that the valence band offset is reduced to zero after anneals to temperatures greater than 900 °C which is consistent with the formation of an interfacial hafnium silicide which would be metallic in nature and therefore emit electrons with energies up to the Fermi level. The early evidence of this signal emerging can be seen by the rising background between 0 eV and 4 eV (in the bandgap) indicating a low concentration of electrons that must originate from a more metallic source than HfO_2.

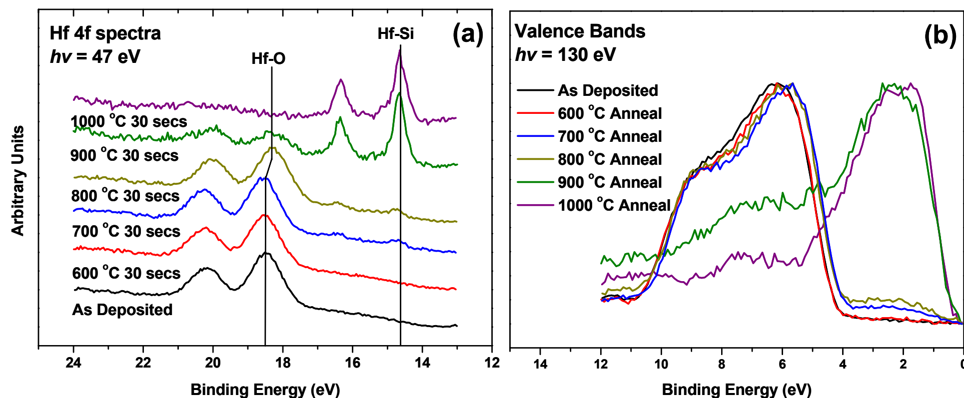

Figure 4.11 Soft x-ray photoemission spectra of the a)Hf 4f core-level and the b) Valence Band region with sequential UHV high temperature anneals.

4.3.5 Comparisons

The different hafnium silicide formation temperatures, for hafnium oxide films grown on silicon at room temperature and at 250 °C, require explanation. It is likely that during the early depositions at 250 °C, the hafnium oxide molecules have a higher probability of diffusing through what is no more than two monolayers of SiO_2 due to the higher available thermal energy. This results in the hafnium oxide being in

direct contact with unoxidised silicon as schematically shown in figure 4.12. The required temperature for the reaction

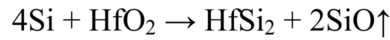

$$4Si + HfO_2 \rightarrow HfSi_2 + 2SiO\uparrow$$

is not known, but in situations where the HfO_2 is separated from the silicon substrate by an interfacial oxide layer, the desorption of this interfacial layer (at 1000 °C) is required before the silicide forming reaction can take place.[10,11] Therefore, if the hafnium oxide has diffused below the interfacial oxide layer, it may be expected that this hafnium could bond to silicon at high temperatures of 700 °C as reported by Xu *et al*[17] for hafnium oxide grown directly on silicon substrates without the use of a buffer layer. This comparison is logical since the decomposition of the intentionally pre-grown SiO_2 would no longer be required for the hafnium species which had diffused through the buffer layer due to the substrate being heated to 250 °C.

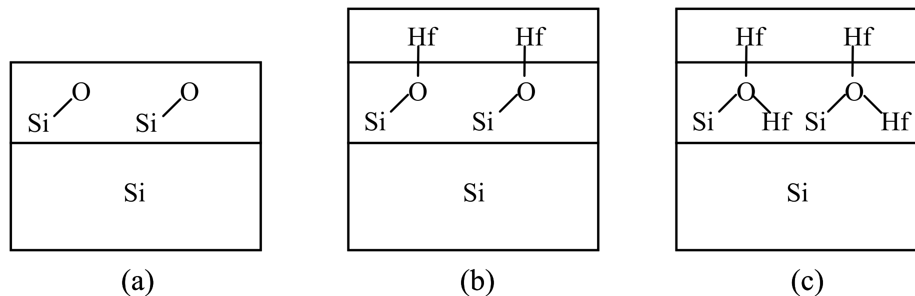

Figure 4.12 Schematical representation of a) ultra-thin buffer oxide[12] on silicon, b) early HfO_2 growth on the buffer oxide at room temperature, c) early HfO_2 growth on the buffer oxide at ~250 °C allowing for the diffusion of hafnium to the substrate.

This type of silicide formation should be limited to the hafnium that has diffused through the interfacial oxide. This can be confirmed by the combined evidence drawn from the three spectra in figure 4.13. Figure 4.13a shows that, when analysed at higher photon energies, the hafnium silicide component in the Hf 4f signal, after the 700 °C anneal, increases with respect to the hafnium oxide signal which suggests that the hafnium silicide component comes from below the hafnium oxide as the higher photon energy has a higher sampling depth into the material. Also figure 4.13b shows that extended anneals at 700 °C show no increase in the hafnium

silicide signal, indicating that further silicide formation requires the decomposition of the interfacial layer to bring more hafnium oxide into contact with the underlying silicon. Figure 4.13c shows a comparison of the Hf 4f core-level for samples grown at room temperature and elevated temperature. While no clear evidence of Hf-Si bonds exists, the increased background in the region corresponding to Hf-Si bonds means that the Hf-Si concentration before high-temperature anneals may in fact be on the limit of XPS detection, which would be expected if some HfO_2 is assumed to be in direct contact with Si.

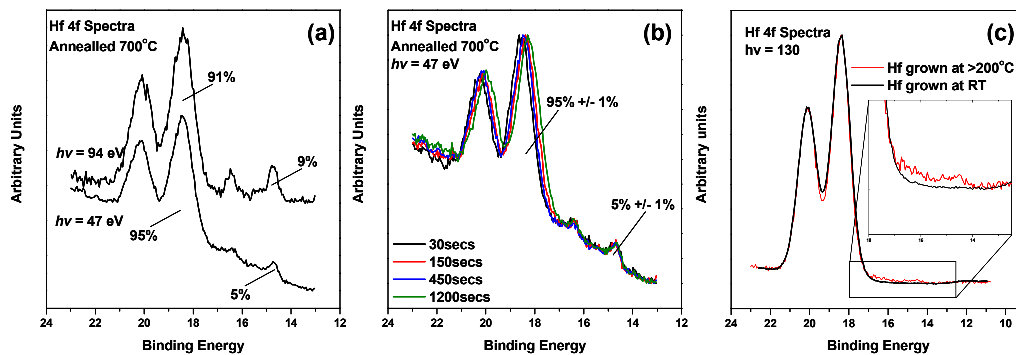

Figure 4.13 Soft x-ray photoemission Hf 4f spectra, a) after 30sec 700 °C UHV anneal taken at 47 eV and 94 eV photon energy, b) after continued UHV 700 °C annealing up to 1200 s taken at 47 eV photon energy, c) comparison of the Hf 4f spectra after depositions at both room temperature and 250 °C degrees obtained at 130 eV.

4.4 Conclusion

Ultrathin silicon dioxide layers were grown on flash cleaned silicon (111) substrates at 600 °C in $1x10^{-7}$ mbar of oxygen. These layers appeared to be one monolayer thick as measured by XPS. Hafnium oxide was deposited from a hafnium wire source in $5x10^{-7}$ mbar of oxygen at both room temperature and 250 °C on these substrates.

The room temperature depositions showed an increase in the interfacial oxide layer and it has been suggested here that this layer become more hafnium silicate-like with each HfO_2 deposition. The evidence for this is the shift in the Si^{4+} core-level feature to a lower binding energy which indicates a shift from SiO_2 to $HfSiO_x$. These

films appeared to be thermodynamically stable up to temperatures of 900 °C with no evidence of any change in the chemical state of the HfO_2 as seen by monitoring the core-level binding energy separation between the Hf 4f and O 1s core-levels. After an anneal at 1000 °C a clear hafnium silicide feature was seen in the Hf 4f core-level spectrum. These results agreed with a photoelectron emission microscopy study by Zeman *et al*[10] which had been conducted on $HfO_2/SiO_2/Si$ sample grown under similar conditions to those used in this work. That work suggested that the formation of hafnium silicide first required with breakdown of the deliberately grown buffer oxide layer.

The workfunction measurements of the films grown at room temperature implied that the films grew in islands. The depositions of HfO_2 on identically prepared ultra-thin SiO_2 on silicon(111) surfaces at an elevated temperature of 250 °C also showed an increase in the interfacial oxide layer's thickness. This interfacial oxide was also assumed, from Si 2p core-level spectra, to be silicate like. These films were seen to being forming hafnium silicide at 700 °C. This is shown to most likely be because of the diffusion of hafnium through the monolayer of silicon oxide during the deposition at 250 °C which allowed for the formation of a layer of silicides at 700 °C without the breakdown of the silicon oxide interfacial layer. This is consistant with reports by Xu *et al*[17] that hafnium silicide forms at 700 °C when hafnium is grown directly onto silicon without the use of a deliberately grown buffer oxide. It has been shown clearly in this study that the deposition temperature of hafnium oxide layers on identically prepared samples affects the subsequent thermodynamic stability of the films.

The spectral analysis of the Si 2p core-level features after the deposition of HfO_2 revealed a core-level feature positioned 0.6 eV to lower binding energy than the Si 2p substrate feature. The similar binding energy position of this feature to the known surface states[13] of the atomically clean Si(111) suggests that this feature could be due to substrate silicon atoms without a full arrangement of silicon neighbours. Such a situation could easily arise as silicon from the substrate is incorporated into the interfacial oxide layer. The resulting disruption to the substrate immediately below the interfacial layer could reduce the mobility of the charge carriers in the channel region.

4.5 References

[1] H. R. Huff, D. C. Gilmer *High Dielectric Constant Material: VLSI MOSFET Applications* Springer series in Advanced Microelectronics **16** (2005)

[2] J. Robertson, Rep. Prog. Phys. **69** (2006) 327-396

[3] G. D. Wilk, R. M. Wallace, J. M. Anthony, J. App. Phys. **89(10)** (2001) 5243-5275

[4] L. Kang, B. H. Lee, W. -J. Qi, Y. Jeon, R. Nieh, S. Gopalan, K. Onishi and J. C. Lee, IEEE Elec. Dev. Lett. **21(4)** (2000) 181-183

[5] B. H. Lee, L. Kang, R. Nieh, W. -J. Qi, J. C. Lee, Appl. Phys. Lett. **76(14)** (2000) 1926-1928

[6] S. Pongratz, A. Zöller, J. Vac. Sci. Technol. A **10(4)** (1992) 1897

[7] S. Suzer, S. Sayan, M. M. Banaszak Holl, E. Garfunkel, Z. Hussain, N. M. Hamden, J. Vac. Sci. Tech A **21(1)** (2003) 106

[8] O. Renault, D. Samour, D. Rouchon, P. Holliger, A. -M. Papon, D. Blin, S. Marthon, Thin Solid Films **428** (2003) 190-194

[9] L. Xie, Y. Zhao, M. H. White, Solid-State Electronics **48** (2004) 2071-2077

[10] M. C. Zeman, C. C. Fulton, G. Lucovsky, R. J. Nemanich, W. -C. Yang, J. Appl. Phys. **99** (2006) 023519

[11] C. C. Fulton, T. E. Cook, G. Lucovsky, R. J. Nemanich, J. Appl. Phys. **99(5)** (2004) 2665-2673

[12] P. Morgen, A. Bahari, U. Robenhagen, J. F. Anderson, J. –K. Hansen, K. Pedersen, M. G. Rao, Z. S. Li, J. Vac. Sci. Technol. A **23(1)** (2005) 201

[13] F. J. Himpsel, F.R. McFreely, A. Taleb-Ibrahimi, J.A. Yarmoff and G. Hollinger, Phys. Rev. B **38**, (1988) 6084

[14] I. Jiménez, J. L. Sacedón, Surface Science **482-485** (2001) 272-278

[15] G. D. Wilk, Yi Wei, Hal Edwards, R. M. Wallace, Appl. Phys. Lett. **70(17)** (1997) 2288

[16] M.P. Seah and S. J. Spencer, Surf. Interface Anal. **33** (2002) 640

[17] R. Xu, Z. J. Yan, S. Chen, Y. L. Fan, X. M. Ding, Z. M. Jiang, Z. S. Li, Surface Science 581 (2005) 236-240

[18] K. Choi, H. Temkin, H. Harris, S. Gangopadhyay, L. Xie, M. White Appl. Phys. Lett. 82 (2004) 215

[19] B. W. Busch, W. H. Schulte, E. Garfunkel, T. Gustafsson, W. Qi, R. Nieh, J. Lee, Phys. Rev. B 62 (2000) R 13290

[20] A. Ogawa, K. Iwamoto, H. Ota, Y. Morita, M. Ikeda, T. Nabatame, A. Toriumi Microelectronic Engineering **84** (2007) 1861

[21] Y. Lebedinskii, A. Zenkevich, J. Vac. Sci. Technol. A **22(6)** (2004) 2261

5 *Ex-situ* analysis of PIAD HfO_2 on silicon(100)

5.1 Introduction

In this chapter the physical characterisation of hafnium oxide (HfO_2) films grown by plasma ion-assisted electron beam (e-beam) deposition (PIAD) from monoclinic HfO_2 source material on hydrofluoric acid (HF) cleaned silicon (100) 4-inch wafers is presented. While growth techniques such as atomic layer deposition (ALD) can yield high quality films,[1] e-beam deposition can be a cost effective way of investigating the basic chemical and electrical properties of these films as well as providing the potential to screen a wide range of potential dielectric materials.[2]

The results will be presented in two sections. Firstly, the effects of the oxygen flow rate during depositions will be studied and secondly the effects of the argon plasma assist that is used to densify films in optical coatings[3] will be discussed. A denser film is desirable because of its potential to increase the dielectric constant. The current-voltage (I-V) and capacitance-voltage (C-V) characteristics of these films were examined and attempts were made to minimise the interfacial (Si-O) oxide thickness. The interfacial oxide thickness was monitored by XPS and correlated with the C-V measurements. A selection of samples were analysed with high resolution transmission electron microscopy (HRTEM) and the interfacial oxide thickness measurements made were compared to those obtained from the XPS analysis.

5.2 Experimental

5.2.1 Samples

Both n and p type 4-inch Si(100) wafers with resistivity's of 2-4 Ω cm and 10-20 Ω cm respectively were used for these experiments. The wafers were RCA cleaned in a clean room environment and a HF etch was performed immediately prior to placing the wafer into the e-beam deposition chamber. The substrate temperature during deposition was kept constant at 150 °C and the target material was hafnium oxide pellets (Umicore 99.9% purity). The oxygen partial pressure during deposition was kept constant by controlling the flow of oxygen into the deposition chamber with

mass flow controllers. When the argon ion assist was in use there was a period of 2-3 minutes during which the wafer was kept at 150 °C and both oxygen and argon flows were allowed to stabilise before the shutter was removed from in front of the hafnium oxide source. It was possible to deposited on multiple wafers at the same time and so n and p type samples labelled as have the same growth condition were in fact grown at the same time so as to insure identical conditions. 55 x 55 μm nickel contacts were deposited *ex-situ* by e-beam metallisation to form metal-oxide-semiconductor structures for electrical characterisation.

5.2.2 Characterisation

The chemical characterisation was carried out using X-ray Photoelectron Spectroscopy (XPS) in system 'B' described in chapter 3. The samples were transported in air and the earliest characterisations were conducted within 2 days of the samples being fabricated. Longer exposures to air resulted in a higher concentration of surface carbon contamination but no other detectable changes in the films. This suggests that any atmospheric effects, on the bulk hafnium oxide layers, self limited within a few days of air exposure.

5.3 Results

5.3.1 Thick Reference Samples

In order to have confidence in the fitting procedures used for the thin films in this study, an approximately 70 nm thick HfO_2 film (measured by ellipsometry), grown by PIAD, was analysed first. This thickness is effectively infinite with respect to XPS analysis which has a sampling depth of approximately 6-7 nm in HfO_2. Figure 5.1a shows angle resolved XPS (ARXPS) of the oxygen 1s and hafnium 4f core-levels for the 70 nm HfO_2 sample. In order to determine the concentration of oxygen bonded to hafnium, the oxygen 1s spectrum must be deconvolved into oxygen two peaks. One is identified as oxygen in a Hf-O environment and the other is identified as oxygen related to the adsorption of surface hydroxyls.[4]

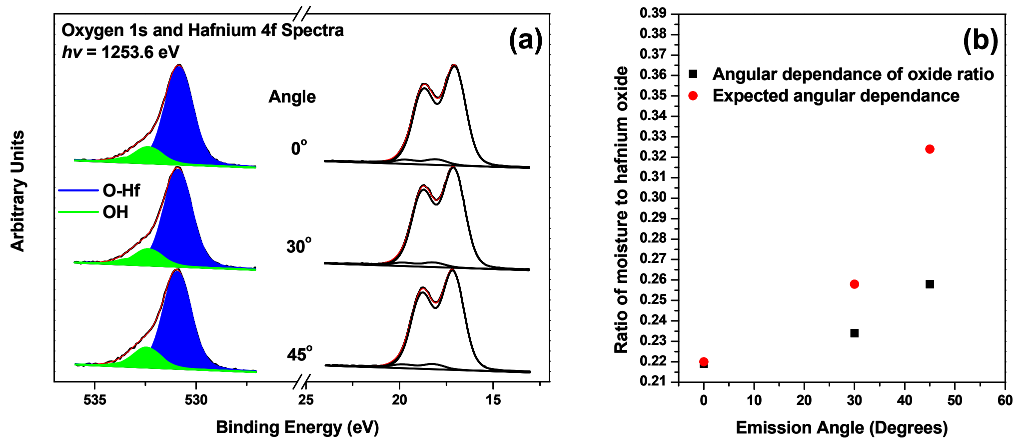

Figure 5.1 a) Angle resolved X-ray photoemission spectra of O 1s and Hf 4f for 70 nm PIAD HfO_2 on silicon. b) The simulated angular dependence of the overlayer to substrate signal ratio for a theoretical overlayer where no diffusion into the underlying substrate has taken place plotted along with the same ratio measured for the hydroxide signal's angle dependence.

The presence of this higher binding energy component that has been assigned to absorbed moisture is common in *ex-situ* XPS of metal oxides.[4,5] The use of ARXPS shows that this component is predominantly localised at the surface as illustrated in figure 5.1b. The ratio of the signal from a surface localised component to the signal from an underlayer is known to increase as the emission angle is increased from the surface normal as described in section 2.2 by the expression

$$\frac{I_A}{I_s} = R_0\{\exp[\frac{+d}{l(\cos\theta)}]-1\} \qquad (5.1)$$

which predicts the change in this ratio in situations were the surface component is completely localised on the surface of a sample and d, l and R_0 are all constant. In this example of absorbed moisture on the surface the ratios dependence on angle is lower than expected which implies that the moisture is at least partially absorbed into the sample. Successful curve fitting of the Hf 4f feature also requires a higher binding energy component which could be assigned to hafnium hydroxides which, if similar to magnesium hydroxides,[6] are expected to be at a higher binding energy to the hafnium oxide component.

Calculating the ratio of oxygen to hafnium using the integrated intensities of the O 1s and Hf 4f core-levels normalised with their relative sensitivity factors[7] is hampered by the presence of surface carbon. The presence of this overlayer attenuates the O 1s signal to a greater extent than the Hf 4f due to the very different kinetic energies of the electrons excited from these core-levels. In many *ex-situ* XPS experiments, argon ion bombardment is used to remove the surface contamination and allow for analysis of the material of interest.[8,9] Figure 5.2 shows why this approach cannot be applied to HfO_2 films. Figure 5.2a shows an attempted depth profile of a 70 nm thick HfO_2 film. The Hf 4f core-level was obtained by conventional XPS after each 60 s argon bombardment. There is a clear presence of a large lower binding energy shoulder after argon etching that can be resolved as shown by the spectral analysis in figure 5.2c into a sub-stoihiometric hafnium oxide peak and a metallic hafnium peak. This is caused by the preferential removal of oxygen from the HfO_2

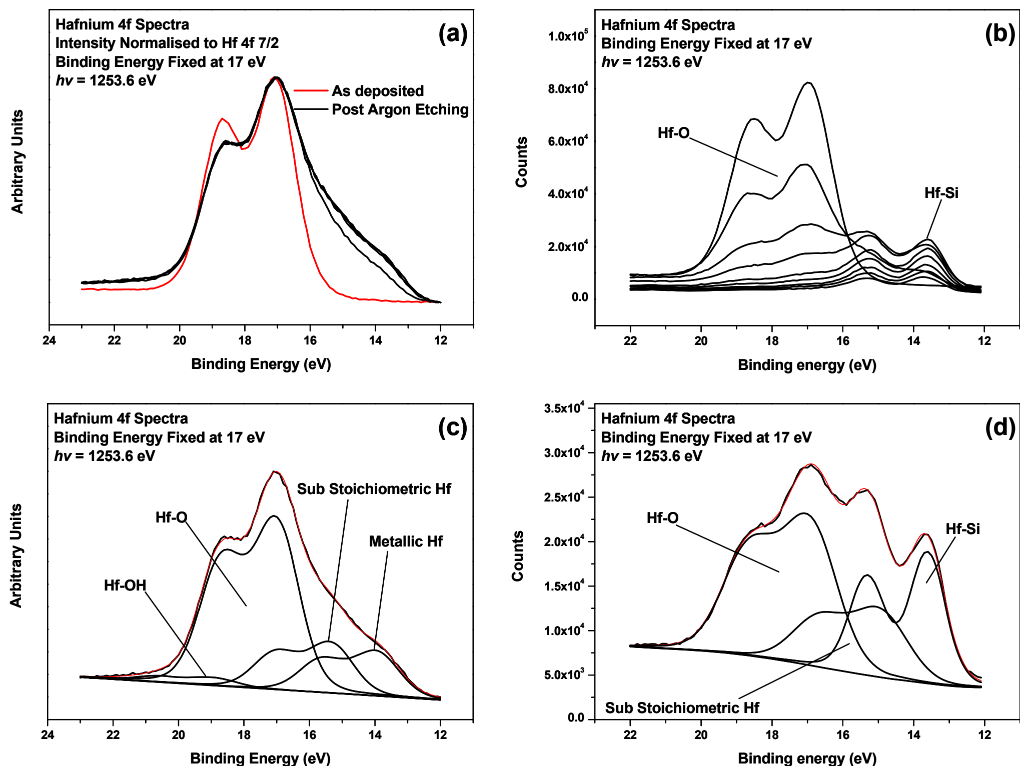

Figure 5.2 Photoemission spectra of the Hf 4f core-level, a) depth profile of 70 nm HfO_2 scanned after sequential argon bombardments, b) depth profile of 6-7 nm HfO_2 scanned after sequential argon bombardments, c) example of peak fitting for 'a', d) example of peak fitting for 'b'.

film by the argon bombardment leaving metallic hafnium in the sample. Figure 5.2b shows a similarly obtained depth profile from a thinner 6-7 nm HfO_2 film grown on silicon. The eventual removal of all oxygen from the film results in the formation of hafnium silicide. An example of the spectral analysis for this sample is shown in figure 5.2d.

Depth profiles similar to figure 5.2b have been reported in the past[10,11] and interpreted as evidence of silicide formation at the interface. Lebedinskii *et al*[12] showed that for thin films grown and analysed intermittently during sequential *in-situ* depositions, argon bombarding resulted in a depth profile identical to figure 5.2b even though no presence of silicide formation was detected during the deposition process. Argon bombardment depth profiles of hafnium oxide clearly result in artefacts that distort any analysis that could otherwise be conducted.

5.3.2 Oxygen Pressure during Deposition

The reduction of the interfacial oxide, grown during many high-κ deposition procedures on silicon, is vital for ensuring a sufficiently low EOT for device applications.[13,14] Varying the amount of oxygen that is supplied in order to ensure the growth of fully oxidised films has been suggested as a way to control this interfacial oxide[15]. The effect of four different oxygen flow rates on the growth of HfO_2 by PIAD on n and p type HF-last silicon substrates was investigated and presented here. The oxygen flow rates of 0, 2.5, 5 and 7 sccm were used.

Physical characterisation:

The oxygen flow rate can be seen, in figure 5.3a, to have a considerable impact on the amount of interfacial SiO_2. As the oxygen flow rate is reduced, the ratio of the integrated intensities from the interfacial silicon oxide signal to the signal from the silicon substrate is seen to decrease. This ratio can be used to determine the interfacial oxide thickness as described in section 2.2. The expression

$$d = l \cos\theta \ln[1 + \frac{R_{exp}}{R_0}] \quad (5.2)$$

required the use of constants l, R_0 and θ which were taken as 34.48 Å, 0.82 and 0° respectively. The thicknesses calculated by this method are shown in figure 5.3a. Figure 5.3b shows an example of the curve fitting used to determine the oxide-substrate ratio. The core-level chemical shift between the Si-O and Si bulk features for the thinnest interfacial oxide is notably less than expected for stiochiometric SiO_2 indicating that the interfacial oxide layer is SiO_x where $x < 2$

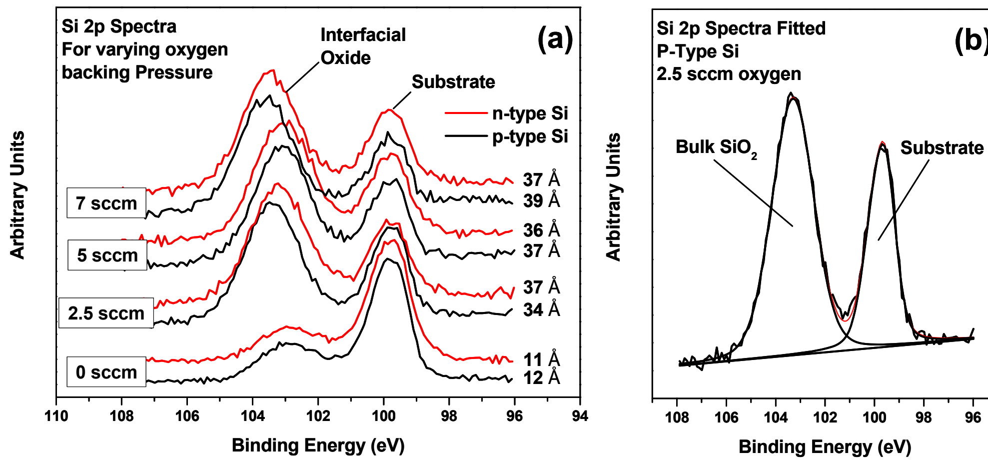

Figure 5.3 a) X-ray Photoemission Spectra of the silicon 2p core-level for PIAD HfO_2 on silicon grown under various oxygen flow rates. b) An example of the fitting for the Si 2p core-level.

Analysis of the binding energy separation between the O 1s and Hf 4f core-levels has been used to monitor the chemical state of the elements in the hafnium oxide films. It can be seen from figure 5.4 that reducing and even omitting the oxygen back pressure does not result in any detectable interfacial silicide formation which would be evidenced by an extra doublet feature shifted more than 3 eV to lower binding energy than the HfO_2 feature in the Hf 4f spectra. Neither is there any evidence of sub-stoichiometric hafnium oxide nor any noticeable change in the chemical state of the hafnium oxide film. As a reference, the Hf 4f and O 1s core-levels obtained from a 70nm thick HfO_2 film in included to show that the chemical state of the thin films match that of bulk HfO_2 films.

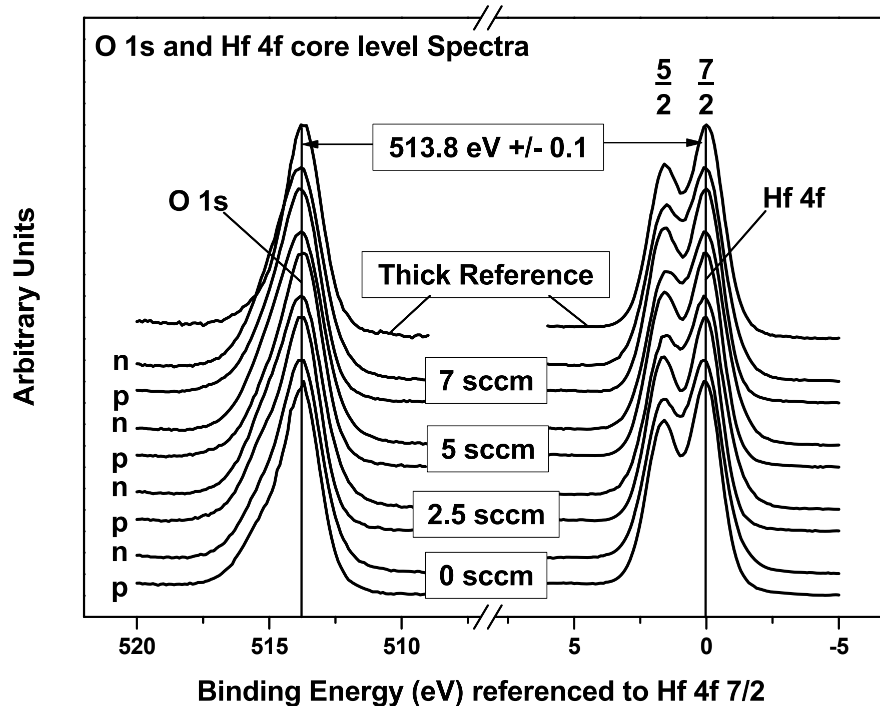

Figure 5.4 X-ray Photoemission Spectra of the oxygen 1s and the hafnium 4f core-level for PIAD HfO_2 on silicon grown under various oxygen flow rates

Electrical characterisation:

Figure 5.5 shows the current-voltage (I-V) characteristics of the ~ 4 nm HfO_2 films grown on p and n type silicon wafers, by PIAD, as a function of the oxygen flow rate during deposition. As the oxygen flow rate is decreased from 7 to 2.5 sccm, the increased leakage current corresponds to the reducing interfacial oxide thickness as determined by the XPS measurements. The thinner interfacial oxide would be expected to have reduced insulating properties as the thickness of the deposited HfO_2 is the same for all samples. The excessively high leakage-currents, even at low gate voltages, that can be seen from the I-V characteristic of the films grown with 0 sccm indicate that these films are not acting as effective insulating layers between the gate metal and the substrate. This is despite the fact that the XPS measurements showed no evidence of metallic hafnium.

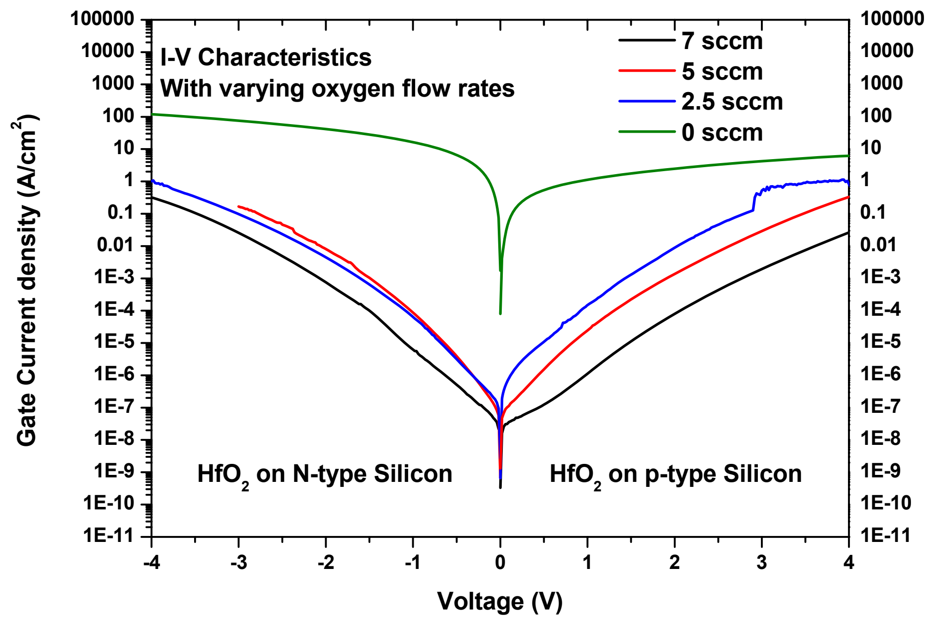

Figure 5.5 I-V characteristics for PIAD HfO_2 on both P and N-type silicon, grown under various oxygen flow rates

Figure 5.6 shows the raw C-V characteristics for the ~ 4 nm HfO_2 films grown on p-type silicon substrates under oxygen flow rates of 7 to 2.5 sccm. Since the films grown under 0 sccm oxygen flow rates did not display insulating properties, obtaining C-V characteristics from these samples was not possible. The increased capacitance with decreasing oxygen flow rates directly correlates with the decreased physical thickness of the insulating layers which agrees with both the increased gate leakage currents, seen in figure 5.5 and decreased interfacial oxide layer thickness as seen with XPS in figure 5.3.

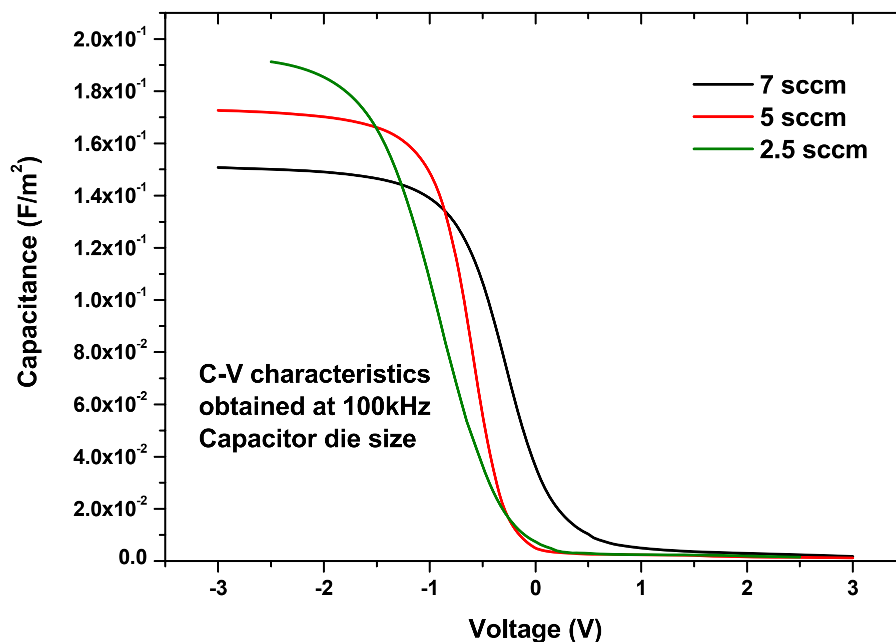

Figure 5.6 C-V characteristics for PIAD HfO_2, grown under various oxygen flow rates, on p-type silicon.

Since the changes in the electrical characteristics of the films grown with oxygen flow rates ranging from 7 to 2.5 sccm can be explained entirely by the changes in the interfacial oxide layers thickness, very little information about the HfO_2 can be obtained. The poor electrical characteristics of the films grown with 0 sccm oxygen flow rate, however, raises serious questions about the insulating quality of the hafnium oxide films grown by this technique. Further experiments have been undertaken with a view to acquiring a better understanding of the poor insulating properties seen for samples grown with 0 sccm flow rate.

5.3.3 Argon Ion Assist

The formation of significant interfacial oxide layers and the resultant high EOTs, seen in the previous section for all samples except those grown with 0 sccm oxygen flow rate, clearly show that the PIAD deposition process is unsuitable for future transistor fabrication. Since the omission of oxygen flowing during the deposition process resulted in non-insulating films, another method of controlling the

interfacial oxide thickness is required. This next section discusses the investigation into the cause of the interfacial oxide growth.

Origins of interfacial oxide growth:

The interfacial growth of SiO_2 during the deposition of hafnium oxide on silicon has been reported by many groups[11,16,17] as well as being discussed in the previous chapter. However, the growth of interfacial oxide in excess of 30 Å of SiO_2 in the above studies is larger than the values reported elsewhere. Experiments were carried out in order to determine when this interfacial oxide formed during the PIAD deposition process. As a preliminary check, a clean HF treated silicon wafer was exposed to the argon and oxygen plasma with an oxygen flow rate of 7 sccm, for a time comparable to the pre-deposition 'stabilisation period'. Figure 5.7 shows an XPS comparison of a silicon wafer exposed to the plasma as described above (but removed from the chamber without depositing HfO_2) with a non-exposed sample. Both wafers experienced equal exposure to air before XPS analysis. This result

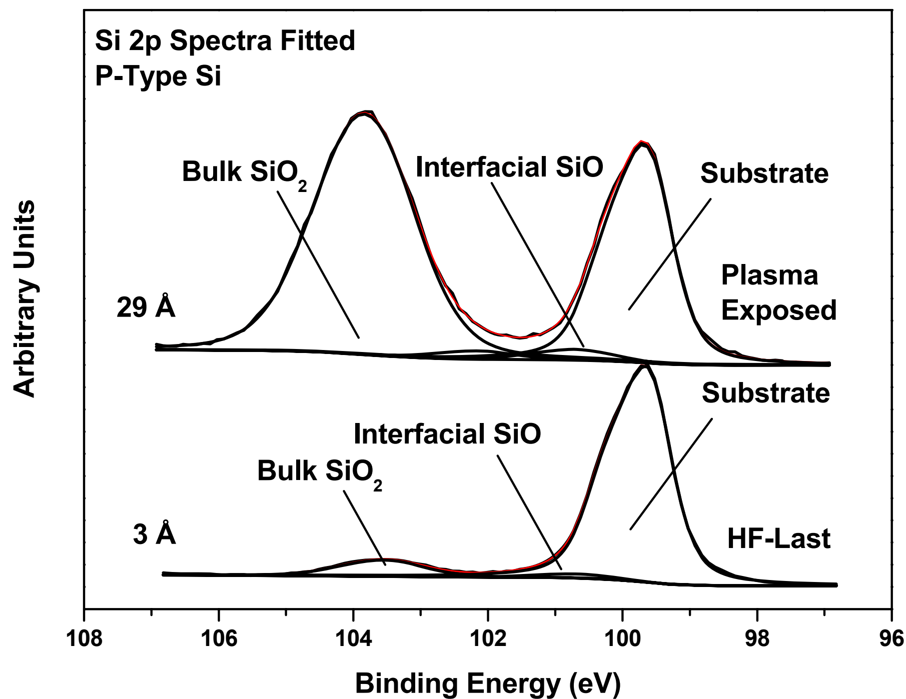

Figure 5.7 The Si 2p XPS of a HF silicon sample exposed to the predeposition PIAD stabalisation conditions and a HF silicon control sample.

suggests that almost all of the interfacial oxide growth occurs before any hafnium oxide is deposited.

In order to explore these findings, 30-40 Å hafnium oxide layers were grown on HF last silicon wafers under three different growth conditions. In all cases the substrate temperature was 150 °C and the oxygen flow rate was 7 sccm. For growth conditions A the film was grown without the aid of the plasma ion assist (i.e. conventional e-beam). For growth conditions B the film was grown in a two stage process involving the deposition of a 1 nm layer of hafnium oxide by conventional e-beam, as a buffer layer, followed by the PIAD of the remaining 1.5 nm film. For growth condition C the film was grown by PIAD in an identical fashion to the samples discussed section 5.3.2. It was hoped, for growth condition B, that the initial 1 nm HfO_2 film deposited without ion assist would suppress the plasma assisted oxidation of the underlying silicon. The sample labels have been tabulated in table 5.1. Growth conditions D which consisted of conventional e-beam deposition with no additional oxygen will be discussed later in this chapter but has been included here for completeness.

	Deposition Conditions	
Sample Label	**Oxygen Flow Rate**	**Plasma Ion Assist**
1	**5 sccm**	**Yes**
2	**2.5 sccm**	**Yes**
3	**0 sccm**	**Yes**
A	**7 sccm**	**No**
B	**7 sccm**	**2 Stage**
C	**7 sccm**	**Yes**
D	**0 sccm**	**No**

Table 5.1 Sample labels for *ex-situ* HfO_2 on silicon samples.

Figure 5.8 compares growth conditions A, B and C. The thickness of the interfacial oxide region for each sample has been calculated from these Si 2p core-level spectra using Equation 5.2 and has been included in the figure. It is clear that

conventional e-beam deposition without ion assist results in the thinnest interfacial oxide. Growth condition B which attempted to utilise the densification of the PIAD process while preventing the plasma enhanced interfacial oxide growth by first growing a 1nm HfO_2 film by conventional e-beam was found to be unsuccessful at completely preventing the interfacial oxide growth. This result implies that 1 nm of hafnium oxide is not a sufficient diffusion barrier for oxygen when in the presence of an oxygen plasma at 150 °C. Sample C was discussed previously as part of the oxygen flow rate variation study and is seen to have an interfacial oxide thickness of 36 Å.

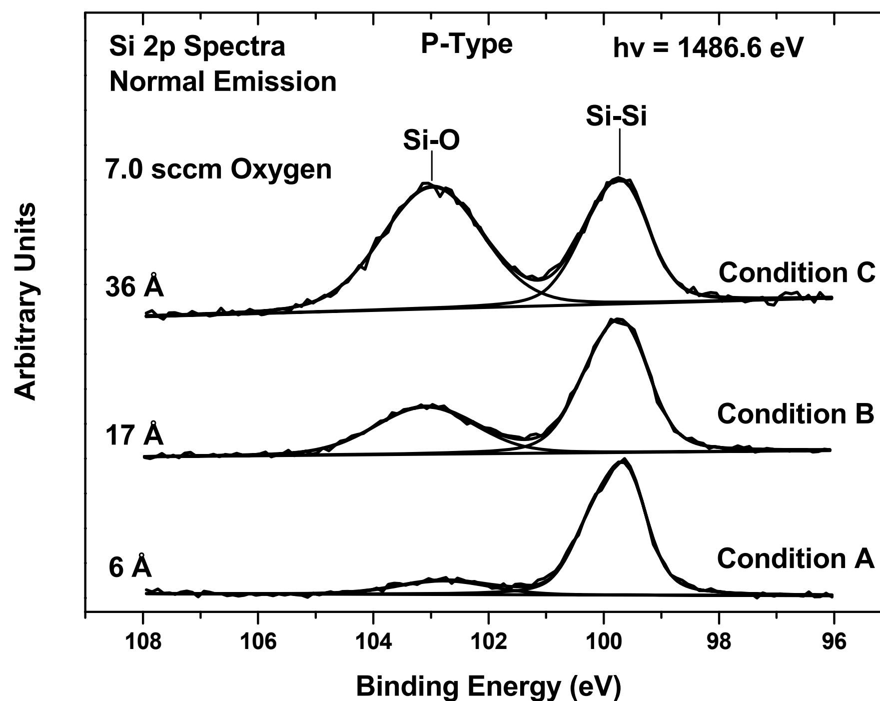

Figure 5.8 The Si 2p XPS spectra for HfO_2 grown on silicon with varying Plasma Ion assistance.

These thickness calculations have been shown to be quite reasonable when compared to High Resolution Transmission Electron Microscopy (HRTEM) supplied by Intel on these samples. These scans are shown in figure 5.9 and the silicon crystal lattice was used to obtain an accurate scale. The samples were labelled to correspond

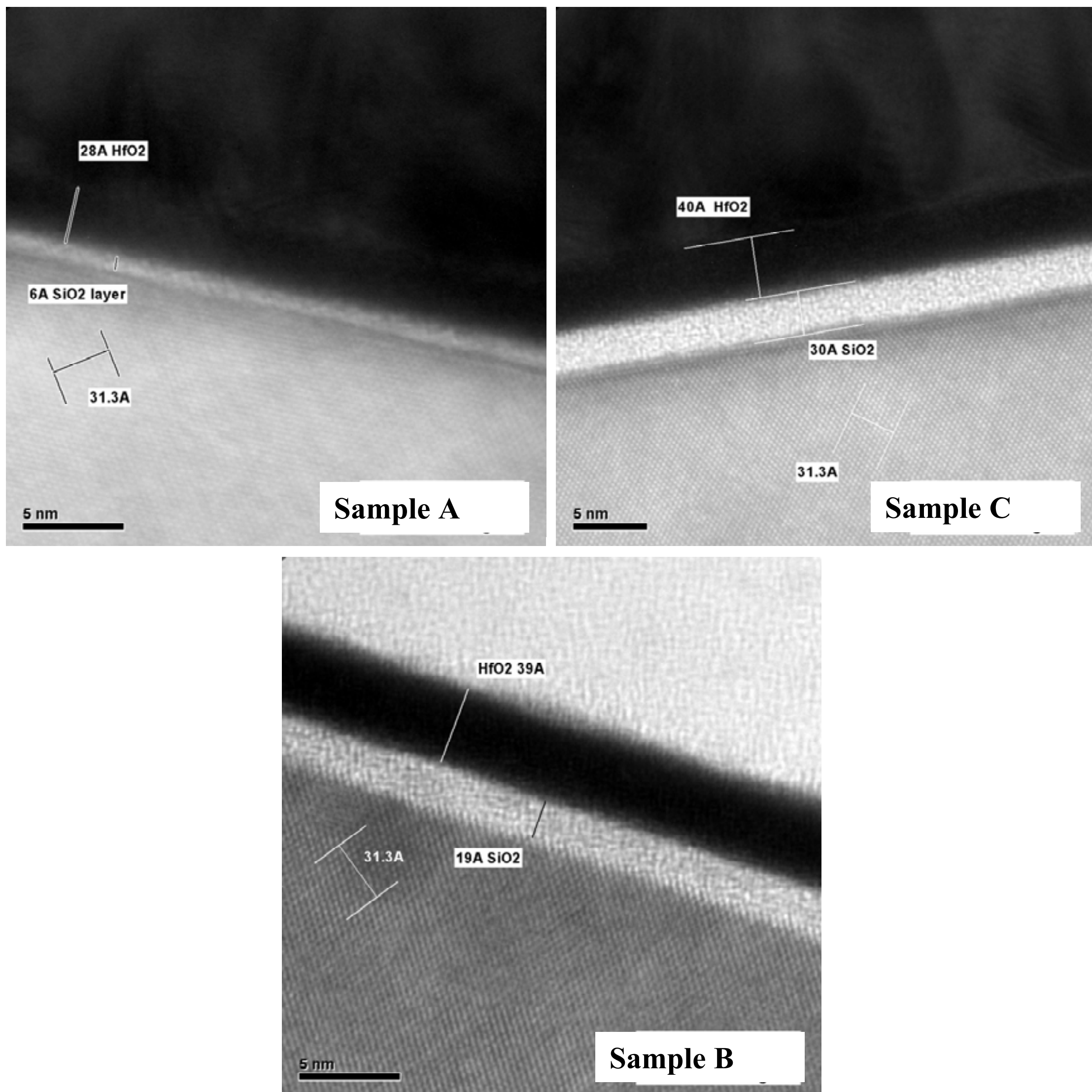

Figure 5.9 HRTEM of sample A-C. The thickness of the interfacial oxide is obtained using the silicon crystal lattice as a reference for scale. These images were supplied by R. Dunne and S. Cosgrove at Intel Ireland.

to the growth condition. The main uncertainties in the values for interfacial oxide thickness obtained from these HRTEM images are in defining the exact position of each interface. This is particularly noticeable for Sample A where the interface between SiO_x and the substrate as well as the interface between SiO_x and HfO_2 are not very clearly defined. One could easily make the case for the interfacial oxide being thicker by up to 50%.

Electrical characterisation:

The I-V and C-V characteristics of samples grown under condition A, B, and C on p and n type silicon wafers were analysed. The films with thicker interfacial oxides were seen to have lower leakage currents due to the increased thickness of the stacked dielectric layer. Figure 5.10 shows these characteristics for a sample grown under condition A and it is clear that, despite the very thin interfacial oxide layer, the hafnium oxide film, grown with 7 sccm oxygen flow rate and no plasma ion assist, has sufficient insulating quality to serve as a gate oxide.

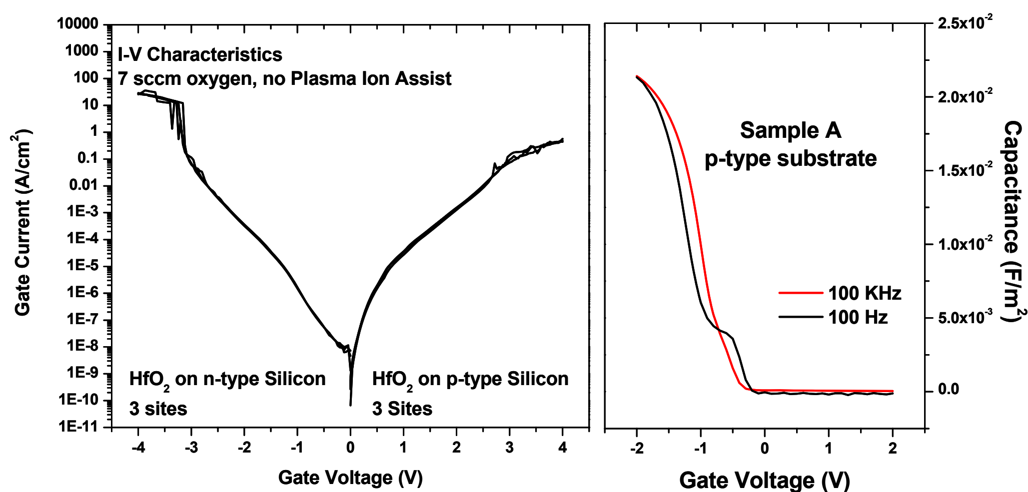

Figure 5.10 a) I-V characteristics for e-beam deposited HfO_2 on both p and n-type silicon, with no Plasma Ion assistance as well as b) C-V characteristics for a p-type sample at 100 Hz and 100 KHz.

5.3.4 Comparisons

A comparison of a sample grown under condition 3 (PIAD HfO_2 grown with no back pressure of oxygen) and a sample grown under condition A (e-beam deposited HfO_2 with 7 sccm oxygen flow rate) will now be made. Condition A results in a thinner interfacial oxide layer, as seen in figure 5.11a, but still has better insulating properties, shown by the I-V and C-V characteristics presented in 5.10, than film grown under condition 3 which displayed non-insulating behaviour. Here two possible explanations are considered. It would be easy to assume that the lack of oxygen gas during the growth of samples using condition 3 could have resulted in a

sub-stoichiometric hafnium oxide, or even partially metallic film. However, as mentioned previously, there is no evidence in the XPS spectra of the formation of anything other than fully oxidised stoichiometric HfO_2. Figure 5.11b shows that the high-κ films grown with excess oxygen flowing during deposition are chemically identical to those grown without oxygen flowing.

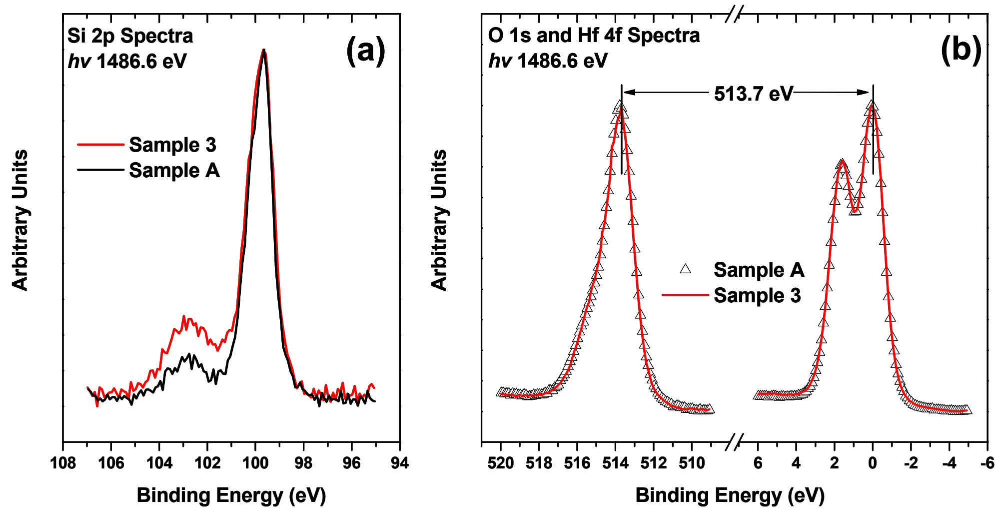

Figure 5.11 a) The Si 2p XPS spectra for samples 3 and A normalised to maximum signal and the silicon substrate at 99.6 eV binding Energy b) the O 1s and Hf 4f XPS spectra for samples 3 and A normalised to their maximum signal and the Binding Energy was referenced to 0 eV so that the O 1s and Hf 4f separation could be easily viewed.

Alternatively, the use of the argon plasma during the growth condition 3 could have resulted in a roughening of the sample surface. If this roughening was severe enough then, since e-beam deposition is a non-conformal deposition technique, the deposited hafnium oxide layer thickness could vary substantially from the predicted thickness. This could result in the formation of localised high conductivity channels between the gate metal and silicon substrates. Plasma roughening should not cause as much of a problem when oxygen is present in the growth chamber since a substantial oxide layer is grown before the deposition of hafnium oxide as previously discussed and shown in Figure 5.3.

In order to determine the cause of the poor electrical qualities displayed by samples grown under condition 3, a thin film hafnium oxide layer was grown on silicon with no ion assist and no oxygen flowing during deposition (condition D). This

film should have the same chemistry and electrical quality as samples grown under condition A (PIAD no O_2) but have the smoother interface of provided by interface 3 (e-beam 7 sccm O_2). Figure 5.12a shows the Si 2p XPS spectrum obtained from a sample grown under condition D. It displays a very thin interfacial oxide while the binding energy separation of the hafnium 4f and oxygen 1s core-levels, shown in figure 5.12b is consistent with stoichiometric HfO_2, which would indicate that the chemical state of the hafnium is unchanged by the lack of an oxygen backing pressure during the deposition process.

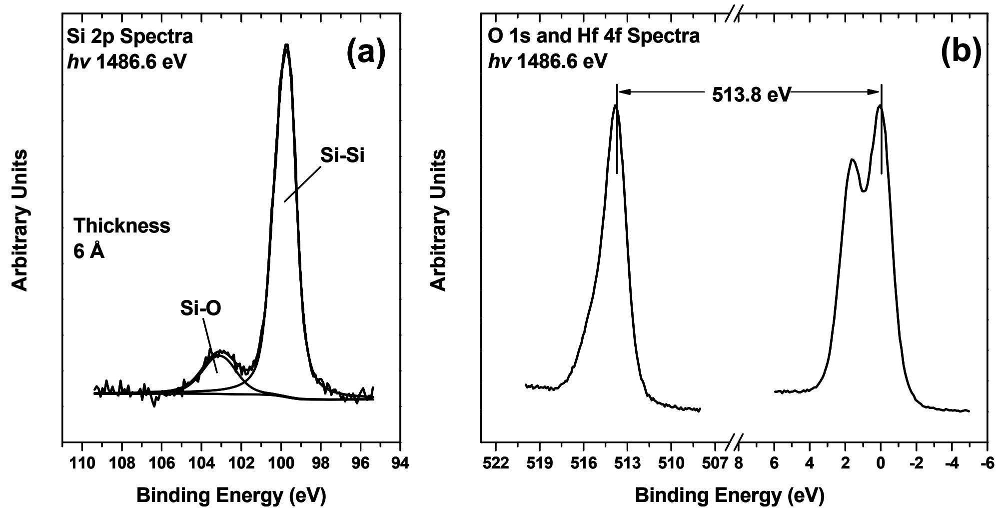

Figure 5.12 a) The Si 2p XPS spectra for samples grown under condition D normalised to maximum signal and the silicon substrate at 99.6 eV binding Energy b) the O 1s and Hf 4f XPS spectra for the same sample normalised to their maximum signal and the binding energy was referenced to 0 eV for the Hf 4f so that the O 1s and Hf 4f binding energy separation could be easily viewed.

Electrical

The I-V and C-V characteristics of 40 Å HfO_2, grown by e-beam deposition with no oxygen back pressure (condition D), are shown in figure 5.13 and confirm that an oxygen back pressure is not required in order to grow an insulating hafnium oxide film. It can be concluded from these studies that it is the argon ion assist process which causes sufficient surface damage prior to HfO_2 deposition that results in poor electrical characteristics.

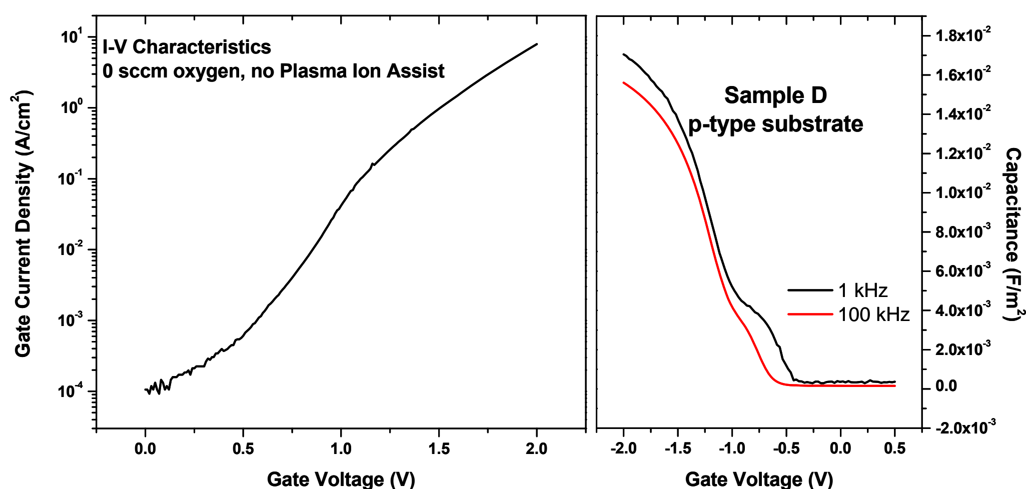

Figure 5.13 I-V and C-V characteristics for e-beam deposited HfO_2 on both p-type silicon, with no Plasma Ion assistance and no oxygen.

Collaborators working at the Tyndall National Institute in Cork Ireland performed a more in depth analysis of the electrical characteristics displayed by the samples discussed in this chapter.[18] The modelling of the C-V curves implied a dielectric constant of ~21 for all HfO_2 films regardless of the precise deposition procedure. This would suggest that the proposed densification of the films by PIAD does not yield a noticeable advantage in terms of the dielectric constant. Also, the dielectric constant of the interfacial oxide layer is seen to increase to ~ 6 for samples grown under condition A. This is consistent with the suggestion that sub-stoichiometric silicon oxide has a higher dielectric constant than SiO_2 and with the XPS results which indicate that the silicon oxide interfacial layer is SiO_X (where $X < 2$).[19]

5.4 Conclusion

In this chapter, the $HfO_2/SiO_x/Si$ interface formation during e-beam deposition was studied by *ex-situ* XPS. It was found that the combination of a plasma ion assist and an oxygen backing pressure results in a ~ 30 Å thick interfacial SiO_2 layer which is intolerably large for application in future MOS devices. Also the use of PIAD without an oxygen back pressure result in non-insulating layer, most likely due to

substantial roughening of the underlying silicon causing shorts through the HfO_2 film. The use of an oxygen backing pressure was found to not be a requirement for growing insulating films by e-beam deposition from HfO_2 pellets.

A 1 nm buffer layer grown by e-beam deposition was not sufficient to prevent the oxidation of the underlying silicon in the presence of an oxygen plasma with a wafer temperature of 150 °C. The electrical analysis carried out by others suggested that no increase in the dielectric constant of HfO_2 was achieved by the PIAD method and so no benefits from the use of this method were found in this study.

XPS results have been successfully correlated to the electrical characteristic of identical films. XPS has been used as a tool for monitoring interfacial oxide thickness in a quick and cost effective manner and was shown to be quite accurate in its quantitative estimations of the thickness when compared to HRTEM.

5.5 References

[1] M. -H. Cho, Y. S. Roh, C. N. Whang, K. Jeong, S. W. Nahm, D. –H. Ko, J. H. Lee, N. I. Lee, K. Fujihara, Appl. Phys. Lett. **81** (2002) 472

[2] H. Harris, K. Choi, N. Mehta, A. Chandolou, N. Biswas, G. Kipshidze, S. Nikishin, S. Gangopadhyay, H. Temkin, Appl. Phys. Lett. **81** (2002) 1065

[3] S. Pongratz, A. Zöller, J. Vac. Sci. Technol. A **10(4)** (1992) 1897

[4] M. F. Al-Kuaili, S. M. Durrani, E. E. Khawaja, J. Phys. D: Appl. Phys. **37** (2004) 1254-1261

[5] C. Driemeier, R M. Wallace, I. J. R. Baumvol ECS Transactions **11(4)** (2007) 91-102

[6] P. Liu, T. Kendelewicz, G. E. Brown, Jr, G. A. Parks, Surface Science **412/413** (1998) 287-314

[7] J. F. Moulder, W. F. Stickle, P. E. Sobol, K. D. Bomben, *Handbook of X-ray Photoelectron Spectroscopy* Perkin-Elmer Corporation, Physical Electronics Division (1992)

[8] M. Chen, X. Wang, Y.H. Yu, Z. L. Pei, X. D. Bai, C. Sun, R. F. Huang, L. S. Wen, Applied Surface Science **158** (2000) 134-140

[9] M. N. Islam, T. B. Ghosh, K. L. Chopra, H. N. Acharya, Thin Solid Films **280** (1996) 20-25

[10] S. J. Wang, P. C. Lim, A. C. H. Huan, C. L. Liu, J. W. Chai, S. Y. Chow, J. S Pan, Q. Li, C. K. Ong Appl. Phys. Lett. **82(13)** (2003) 2047-2049

[11] O. Renault, D. Samour, D. Rouchon, P. Holliger, A. -M. Papon, D. Blin, S. Marthon, Thin Solid Films **428** (2003) 190-194

[12] Y. Lebedinskii, A. Zenkevich, J. Vac. Sci. Technol. A **22(6)** (2004) 2261

[13] J. Robertson, Rep. Prog. Phys. **69** (2006) 327-396

[14] G. D. Wilk, R. M. Wallace, J. M. Anthony, J. Appl. Phys. **89(10)** (2001) 5243-5275

[15] D. –Y. Cho, S. –J. Oh, Y. J. Chang, T. W. Noh, R. Jung, J. –C. Lee, Appl. Phys. Lett. **88** (2006) 193502

[16] L. Xie, Y. Zhao, M. H. White, Solid State Electronics, **48** (2004) 2071-2077

[17] H. Y. Yu, M. F. Li, D. L. Kwong, Thin Solid Films **462-463** (2004) 110-113

[18] K. Cherkaoui, S. Monaghan, M. A. Negara, M. Modreanu, P. K. Hurley, D. O'Connell, S. McDonnell, G. Hughes, S. Wright, R. C. Barklie, P. Bailey, T. C. Q. Noakes, J. Appl. Phys. **104** (2008) 064113

[19] F. Giustino, A. Pasquarello, Microelectron. Eng. **80** (2005) 420

6 *In-situ* Atomic Layer Depositions of high-κ dielectric layers on GaAs(100) surfaces

6.1 Introduction

Historically, the need for higher speed operating systems in radar, communications and sensors drove the research on GaAs. This research opened up new markets such as global position systems (GPS's), wireless local area networking (WLAN) and global cellular communications to name a few. Kayali *et al*[1] describe GaAs as an 'enabler' for many of these technologies. The higher electron mobility of GaAs makes it an obvious candidate for replacing silicon as a substrate in high speed devices.

For n-type GaAs there exists an anomalous large frequency-dependant dispersion of accumulation capacitance[2] shown in figure 6.1. The work of Hasagawa and Sawada[2] discussed in detail the uncertainties of attributing this effect solely to high interface state density induced Fermi-level pinning. In that work, a model was proposed relying on the presence of a 'disordered non-stoichiometric semiconductor region' at the oxide substrate interface. In this model it is assumed that there is an 'exponentially decaying spatial distribution of interfacial traps into the insulator'. It was suggested in that study that this region could be due to an arsenic-deficient surface while it is also known that oxygen exposure of clean GaAs(110) causes Fermi level pinning[3].

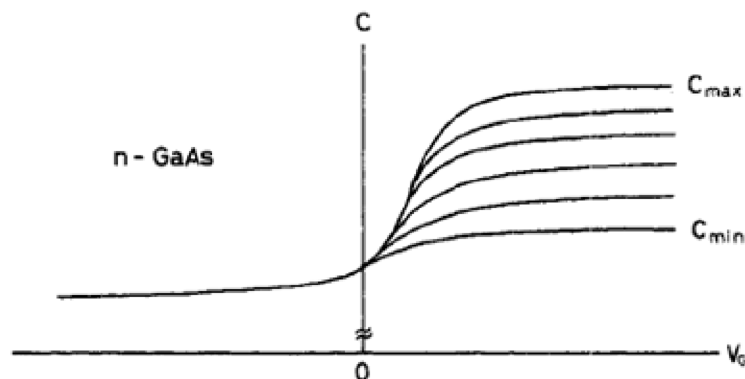

Figure 6.1 As frequency is increased, the capacitance on the accumulation side decreases from C_{max} to C_{min}. Figure taken from Hasegawa and Sawada.[2]

The work of Hale *et al*[4] concludes that donor and acceptor states in the bandgap at 0.5 eV and 0.75 eV above the valence band maximum caused by the bonding of a single Ga atom to two oxygen atoms causes a pinning of the Fermi level. Much has

been done to reduce this frequency dependant dispersion of accumulation capacitance. The insertion of silicon[5-8] or germanium[9] interlayers between the GaAs and insulator has been shown to be effective. Hale *et al*[4] have also postulated the use of Ga_2O as a passivation layer. While solutions such as the use of a silicon interlayer show promise, the origin of the 'low bandgap disordered region' is still poorly understood.

In this chapter, an investigation of the anomalous frequency dispersion of accumulation capacitance (C_{acc}) has been undertaken and an attempt has been made to correlate this electrical effect with a chemical analysis of the insulator/semiconductor interface. It was hoped that through a detailed *in-situ* analysis of each process step using XPS, a better understanding of how a silicon interlayer[5-8] between the GaAs and insulating layer reduces this frequency dependant dispersion of $C_{acc.}$ An investigation of different surface cleaning procedures for GaAs(100) single crystal surfaces as preparation for subsequent high-κ dielectric deposition will be presented. The aim was to develop procedures which resulted in an unpinned Fermi level at the GaAs/high-κ dielectric interface in order to allow inversion of the semiconductor for transistor operation.

The experiments that will be present in this chapter have been divided into 3 sections. Firstly the preliminary work on native oxide reduction by various methods along with the effects of depositing silicon onto GaAs surfaces will be presented and discussed here so as to better understand the effects of the early processing steps. Secondly the deposition of 1 nm thick Al_2O_3 and HfO_2 films directly onto both native oxide and chemically treated GaAs surfaces by ALD has been analysed *in-situ* with XPS and the effect of such depositions on the interfacial oxide will be presented. Thirdly, two different surface preparation techniques will be described and a full analysis of the effect of each surface treatment on electrical capacitance measurements, with and without a silicon interlayer, will be given.

The results that will be present are compared to important findings by other research groups. A selection of these important studies warrant discussion before the presentation of the results arising from this work. The chemical composition of the native oxide of GaAs has been studied extensively in the literature.[10-14] In particular Hollinger has provided a base-line for the deconvolution of the XPS spectra by

analysing the individual oxidation states from appropriate reference materials.[10] That work discusses the difficulties in assigning the observed chemical states in the native oxide to specific oxidation states. It suggests that assigning the As^{3+}, As^{5+} and Ga^{3+} signals to separate phases As_2O_3, As_2O_5 and Ga_2O_3 should not be done without further evidence. In that work, it is suggested that the oxide can be explained as an amorphous mix of AsO_3, AsO_4, AsO_6, GaO_4 and GaO_6 bonding environments. XPS analysis identifies core-level chemical shifts that could be due to separate phases or a 'single phase metastable non-stoichiometric oxide', the latter of which is supported by valence band analysis.[10] When referring to the native oxide of GaAs in this chapter it will occasionally be referred to as $GaAsO_x$.

Studies performed by Lebedev *et al*[11] in a controlled nitrogen/UHV environment have shown that NH_4OH reduces the native oxides on the GaAs surface, leaving a small amount of Ga-O bonds as well as elemental arsenic and arsenic hydroxide. Subsequent annealing at 450 °C removes all elemental arsenic, As-O(H) bonds and increases the Ga-O bond concentration. Chemical cleaning in a controlled inert gas environment, followed by chemical analysis in UHV without any intermediate exposure to air, allows for a detailed study of the changes induced in the chemical composition of the surface by a particular chemical. However, such cleaning procedures would be unrealistic for practical device fabrication. Standard cleaning procedures used in device processing are generally followed by short exposures to air prior to film depositions. In this chapter, *ex-situ* chemical cleans, carried out in a standard chemical fume-hood on both p-type and n-type GaAs, have been analysed with XPS. The effects of *in-situ* anneals to 300 °C and 450 °C have studied and these results will be compared to the study of Lebedev *et al*[11] and presented in section 6.3.2.

Previous *ex situ* studies of Al_2O_3 and HfO_2 ALD deposited directly on GaAs have reported an interfacial "self-cleaning" reaction process that effectively reduces the native As and Ga oxides. Ye *et al*[15] reports that the ALD process removes the native oxides and excess arsenic leaving a thin Ga-O interfacial layer. Later Frank *et al*[16] reported interfacial thinning of the native GaAs oxides by ALD Al_2O_3 using $Al(CH_3)_3$ (TMA) and H_2O as aluminium and oxygen precursors, respectively. This same study showed no native oxide thinning by ALD HfO_2 using $HfCl_4$ and H_2O as hafnium and oxygen precursors. Dalapati *et al*[17] used the same precursors as Frank *et*

al[16] on sulphur passivated GaAs substrates and specifically reported thin interfacial arsenic oxide after Al_2O_3 deposition seen with XPS. Huang *et al*[18] and Chang *et al*[19] report interfacial oxide removal of arsenic oxides on InGaAs using TMA and $Hf(NCH_3C_2H_5)_4$ (TEMA-Hf) as precursors for Al and Hf respectively. These authors also reported the presence of As_2O_5[18] or As_2O_x[19] ($5 \geq x > 3$) on the surface of the Al_2O_3 and HfO_2 layer respectively after deposition. This interfacial oxide self cleaning mechanism has been studied by *in-situ* monochromated XPS and the results will be compared to these previous works and presented in this chapter in section 6.3.3.

Studies such as these provided useful comparisons for the experiments that will be presented in this chapter. The early work on the native oxides of GaAs facilitated the peak identification process of the XPS core-level features, and the knowledge of the effects of NH_4OH on the native oxides as well as effects of direct high-k depositions onto GaAs substrates made the process of designing sensible and unique experiments easier.

6.2 Experimental

The surface preparations for the high-κ/Si/GaAs gate stacks, which are utilised for the reduction of the frequency dependant dispersion of accumulation capacitance, vary widely for the studies reported in literature. Many of the reported chemical cleans/passivations are sulphur based[20-23], while *in-situ* GaAs MBE growth followed by silicon interlayer depositions[5,24] have also been reported. In this work, which was carried out at the university of Texas at Dallas (UTD), sulphur based cleans were avoided to ensure that there was no contamination of the multi-technique deposition/characterisation UHV system (described in section 3.1 as system C). Reasonable electrical results have been reported using ammonium hydroxide based cleans prior to dielectric deposition[25] and these procedures have been taken as a starting point for this study.

6.2.1 Surface preparations

The samples characterised electrically in this work were n-type Si-doped GaAs(100) wafers with doping concentration of 5×10^{17} cm^{-3}. Doping concentrations varied for some samples used in the surface preparation studies. All chemically treated samples were first subjected to a 'degreasing' step which consisted of sequential 60 second immersions in acetone, methanol and isopropanol. This step was followed by a 3-minute etch in 29% ammonium hydroxide (NH_4OH) after which they were blown dry with N_2 and immediately placed into the UHV system load lock. Exposure to air was kept to a minimum between the different wet chemical steps and after the NH_4OH etching to facilitate repeatable results and minimise ambient contamination. Samples prepared in this manner are referred to as having the 'standard NH_4OH etch' in the following text. Many samples experienced a high-temperature anneal in UHV at a temperature of 300-350 °C for 30 minutes.

In an alternative pre-deposition treatment, GaAs samples were loaded into UHV as-received, with no chemical treatments. These samples were heated to a temperature of 430 °C for 15 minutes (to allow for the outgasing of moisture and removal of surface carbon). While this temperature was maintained, the wafer was exposed for 30 minutes to a flux of atomic hydrogen, generated using a hydrogen cracker source (cell temperature of 1400°C, $P_{H2}= 1\times10^{-6}$ mbar). After 30 minutes, the hydrogen flux was turned off and the sample was allowed to cool. Total cleaning time including ramping up and down in temperature was 75-90 minutes. This treatment is referred to as 'atomic hydrogen treatment (AHT)' in the text.

6.2.2 Depositions

Silicon depositions were conducted at a deposition rate of approximately 20 Å/min by e-beam deposition from a silicon source in a silicon crucible with the GaAs sample wafer kept at room temperature. This MBE deposition chamber is used solely for depositing group IV materials and non-group-IV substrates were kept at temperatures below 100 °C so as to ensure a reasonably contamination-free deposition environment. An alternative Si deposition method was the use of a silicon effusion

cell, in an adjacent UHV chamber, operated at 1400 °C which deposited Si at a rate of 2 Å/min. These techniques were used interchangeably as the deposition rate was found to have no noticeable effect on the electrical characteristics.

Both Al_2O_3 and HfO_2 dielectric layers were deposited on various starting surfaces by atomic layer deposition (ALD). Al_2O_3 was grown using a trimethyl-aluminum (TMA) precursor with H_2O oxidation pulses at a wafer temperature of 300 °C while the HfO_2 was grown using a tetrakis(ethylmethylamino)-hafnium (TEMA-Hf) precursor with H_2O oxidation pulses at a wafer temperature of 300 °C. 10 nm thick Al_2O_3 films were required for electrical analysis, however, since a 10 nm film would have been too thick for XPS analysis to yield any interfacial information, the depositions were performed in two stages. A 1 nm Al_2O_3 layer was grown followed by *in-situ* XPS analysis in an adjacent chamber before the deposition of an additional 9 nm. To form MOS capacitors, tantalum nitride (TaN) was RF sputtered, *ex-situ*, as the gate metal using shadow masks resulting in 150 nm-thick circular capacitors with an area of 3.14 x 10^{-4} cm^2. An *ex-situ* electron-beam-evaporated Ni/Au/Ge alloy annealed at 425 °C was used as the Ohmic back contact.[26]

6.2.3 Characterisation

After each *in-situ* processing step, up to and including the final deposition of the 10 nm Al_2O_3 layer, the surface was analysed *in-situ* with XPS to extract details of the evolution of the interface chemistry after each processing step. Electrical characterisation was carried out using a Cascade probe station with a Keithley 4200 for current voltage (I-V) characteristics and a HP 4284 LCR for capacitance voltage (C-V) measurements. The electrical data presented in this chapter was collected and analysed by colleagues in the Electrical Engineering Department of the National Science and Engineering Research Laboratory (NSERL) at the University of Texas at Dallas (UTD). As such a more detailed discussion of the modelling used to extract information about the electrical characteristics of these films from the C-V curves may be found in the future thesis of Arif Sonnet supervised by Prof. Eric Vogel at UTD. The conclusions drawn independently from chemical and electrical analysis

were then compared in a group environment so that the correlations between the two that are presented at the end of this chapter could be made.

6.3 Results

6.3.1 Native oxide, chemical composition and curve fitting

The native oxides present on as-received n-GaAs and p-GaAs were analysed by monochromated XPS and are present here in figure 6.2. The presence of As^{3+} and As^{5+} species can be clearly identified in the As 3d and As 2p 3/2 regions, due to their large core-level chemical shifts with respect to the As-Ga features. There is also a component identified here as As^{0} which is attributed to As-As bonds. In the case of the Ga oxides, the chemical shifts with respect to the Ga-As features are much smaller than those for arsenic and as such many groups have chosen to fit them with one Gaussian feature[11,12,22] rather than subdividing the oxide component into individual oxidation states.[13,14] The 2p 3/2 and 3d core-levels provide information from two very different sampling depths because of the large difference in kinetic energy of electrons emitted from these core-levels. Electrons excited from the 2p 3/2 core-levels have a low kinetic energy which makes them very surface sensitive.

Fitting the GaAs substrate signals has been aided by access to an oxide free surface as a reference spectrum. This reference spectrum was obtained by exposing the native oxide to atomic hydrogen with a substrate temperature of 430 °C, this process is explained in detail in section 3.4. The Lorentzian and Gaussian components of the Ga and As substrate features were determined from these oxide free samples for the 2p 3/2 and 3d spectra by fixing the spin orbit splitting and intensity ratios to accepted values[27] while allowing the Lorentzian and Gaussian widths to vary until the best fit was achieved. The Lorentzian and Gaussian components were then fixed for all substrate peaks throughout all future fitting procedures. This allowed any subsequent potential peak broadening to instead be attributed to the presence of chemically shifted components. Core-level binding energy separations were

calculated so that all substrate peaks could be referenced with respect to the As 3d binding energy when fitting more complex systems.

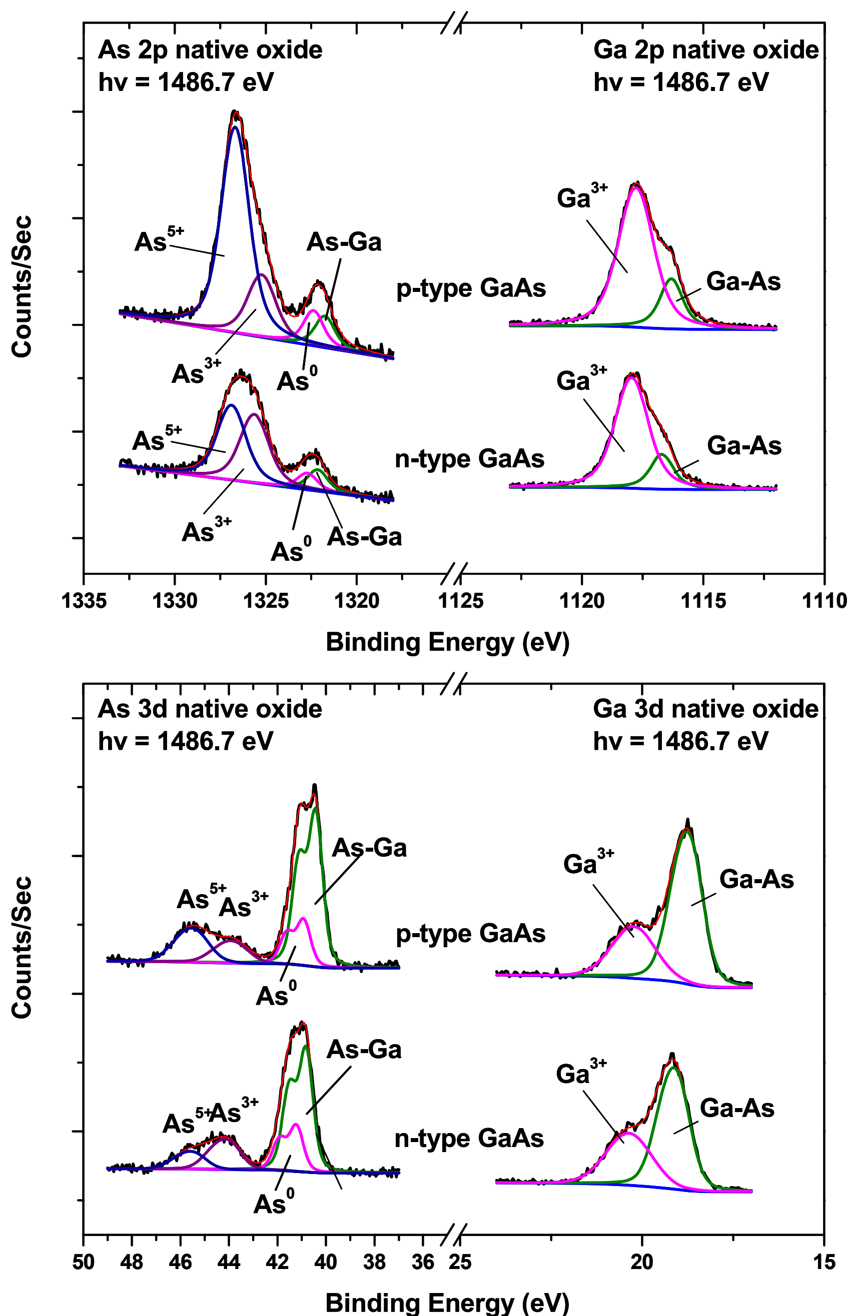

Figure 6.2 Arsenic and gallium 2p (Top) and 3d (Bottom) spectra for the native oxide on p and n type GaAs.

For each core-level, As 2p 3/2, As 3d, Ga 2p 3/2, Ga 3d, the Lorentzian peak widths remained fixed, since this component of the peak width is intrinsic to the core-

level and should not be affected by the bonding environment atom. Table 6.1 shows the fixed parameters used when fitting. To allow for the deconvolution of spectra containing more than one oxidation state, the Gaussian peak widths were left free but approximately equal to each other. It is well known that the peak widths of different oxidation states can vary from one another as in the case of SiO_2/Si.[28] In this system some oxidation states are primarily from the bulk oxide which would be highly disordered and with a high variation in bond angles that would result in a large Gaussian component, while others would be interfacial oxides that may still have retained substantial order from the underlying substrate and would therefore have much smaller Gaussian components.

	As 3d	As 2p 3/2	Ga 3d	Ga 2p 3/2
Lorentzian (eV)	0.24	0.84	0.22	0.61
Spin Orbit Splitting (eV)	-0.7	N/A	-0.45	N/A
Branching Ratio	0.667	N/A	0.667	N/A

Table 6.1 Fixed fitting parameters for Lorentzian peak width, Spin Orbit Splitting and Intensity Branching ratio determined by experiment, literature and theory respectively

In the case of this study the As^{3+}, As^{5+} and Ga^{3+} signals are all assumed to be from the bulk oxide; hence similar Gaussian widths are used across all samples to realistically analyse the oxides. This approach is considered reasonable since sub-oxides are rarely shown as detectable by XPS for the native-oxide/GaAs system in the literature. The Gaussian peak width for the As-As feature, that has been reported in most works on GaAs[10,11,14,20] has been fixed to be the same as that of the substrate. Table 6.2 gives a short list of the core-level chemical shifts for each core-level feature, as measured with respect to the relative substrate Ga-As feature, seen in the literature. These values were used as a starting point for peak fitting in this study. In the study by hollinger[10] the values are obtained from a range of 6 differently prepared samples. Three were grown by ultra-violet (UV) oxidation and three were grown by thermal oxidation.

Chemical State	Arsenic			Gallium
Reference:	As^0 (eV)	As^{3+} (eV)	As^{5+} (eV)	Ga^{3+} (eV)
20 (Arabasz)	-0.6	-3.2	-4.5	-1.4
22 (Ghudaoui)		-3.1	-4.5	-1.2
23 (Massies)		-3.1 (-3)		-0.9 (-1.1)
10 (Hollinger)	-0.5/-0.6	-2.93/-3.12	-4.13/-4.48	-1.2
11 (Lebedev)	-0.7	-3.2	-4.5	-1.2
14 (Schröder)	-0.6	-3	-3.8	-1.1

Table 6.2 Core-level chemical shifts (CLCS) of the oxidation states with respect to the bulk as found in literature for the As and Ga 3d (2p) spectra are shown.

Figure 6.2 shows that similar oxidation states are present in the native oxide for both n-GaAs and p-GaAs. The differences in the oxide intensity can easily be attributed to differences in the native oxide thickness. Since the pre-treatment histories of these samples are unknown and they are supplied by different manufacturers, no attempt has been made to attribute the differences in oxide thickness to the intrinsic properties of the n-GaAs or p-GaAs. Table 6.3 shows a breakdown of the fitting parameters extracted from the analysis shown in figure 6.2. For the 3d core-levels it can be seen that the core-level chemical shifts with respect to the substrate features extracted from the curve fitting procedure agree well with the range of value published in the literature. The areas for the individual features allow of the calculation of atomic percentages within the native oxide and also for the calculation of the native oxide thickness.

	N-type				P-Type			
	3d							
	As-Ga	As^0	As^{3+}	As^{5+}	As-Ga	As^0	As^{3+}	As^{5+}
BE (eV)	40.81	+0.4	+3.13	+4.57	40.41	+0.5	+3.27	+4.89
Gaussian (eV)	0.53	0.53	1.01	1.01	0.53	0.53	1.22	1.22
Area (a.u.)	235	88	75	43	295	88	60	91
	Ga-As	Ga^{3+}			Ga-As	Ga^{3+}		
BE (eV)	18.98	+1.21			18.62	+1.44		
Gaussian (eV)	0.68	1.22			0.68	1.16		
Area (a.u.)	205	124			256	118		
	2p							
	As-Ga	As^0	As^{3+}	As^{5+}	As-Ga	As^0	As^{3+}	As^{5+}
BE (eV)	1322.13	+ 0.57	+3.49	+4.74	1321.74	+0.62	+3.47	+4.93
Gaussian (eV)	0.77	0.77	1.37	1.37	0.77	0.77	1.32	1.32
Area (a.u.)	213	165	903	986	314	354	808	2661
	Ga-As	Ga^{3+}			Ga-As	Ga^{3+}		
BE (eV)	1116.7	+1.24			1116.34	+1.43		
Gaussian (eV)	0.63	1.16			0.63	1.24		
Area (a.u.)	604	2538			896	3314		

Table 6.3 The fitting parameters for the native oxide on n-type and p-type GaAs.

6.3.2 Surface Preparation

NH_4OH and UHV Anneals:

In this study, *ex-situ* chemical cleans of the native oxide using ammonium hydroxide (NH_4OH), carried out in a standard chemical fume-hood on both p-type and n-type GaAs, have been analysed with monochromated XPS. The effects of a subsequent *in-situ* anneal at 300 °C for 5 minutes has been studied in order to understand the effects on the chemical composition of the substrate surface when heating to this temperature, which occurs in the ALD reactor prior to dielectric deposition.[25] The effect of an *in-situ* anneal to 450 °C for 5 minutes was also analysed for comparison to synchrotron studies[11] where GaAs substrates were annealed at 450 °C in UHV after an NH_4OH etch. The n-type and p-type samples were supplied by different companies and were taken from 4 inch and 2 inch wafers respectively. The differently doped samples were mounted side by side on the same holder to ensure equivalent processing.

Following the standard NH_4OH etch, the surface chemical composition of the GaAs samples was analysed by XPS. The As 3d spectra, presented in figure 6.3, shows that NH_4OH removes the higher oxidation state (As^{5+}) for both n-GaAs and p-GaAs. For n-type and p-type GaAs, both of the high temperature anneals result in a reduction of the As-O related features. The ratio of As^{3+} + As^{5+} to the substrate signal is proportional to the thickness of the oxide layer. For As 3d region on n-type this ratio drops to 51% of the native oxide value after the standard NH_4OH etch, 24% after the 300 °C anneal and 7% after the 450 °C anneal. For the p-type samples the corresponding values are 51%, 30% and 15%.

The Ga 3d spectra, also displayed in figure 6.3, show a reduced oxide feature following the NH_4OH treatment and the core-level chemical shift between the oxide and substrate feature is seen to be reduced which indicates the removal of a higher binding energy component that was not previously resolved in the fitting of the native oxide but could have been attributed to $Ga(OH)_3$.[14] For both p and n type GaAs there is a clear increase in the Ga-O concentration after both the 300 °C and 450 °C UHV

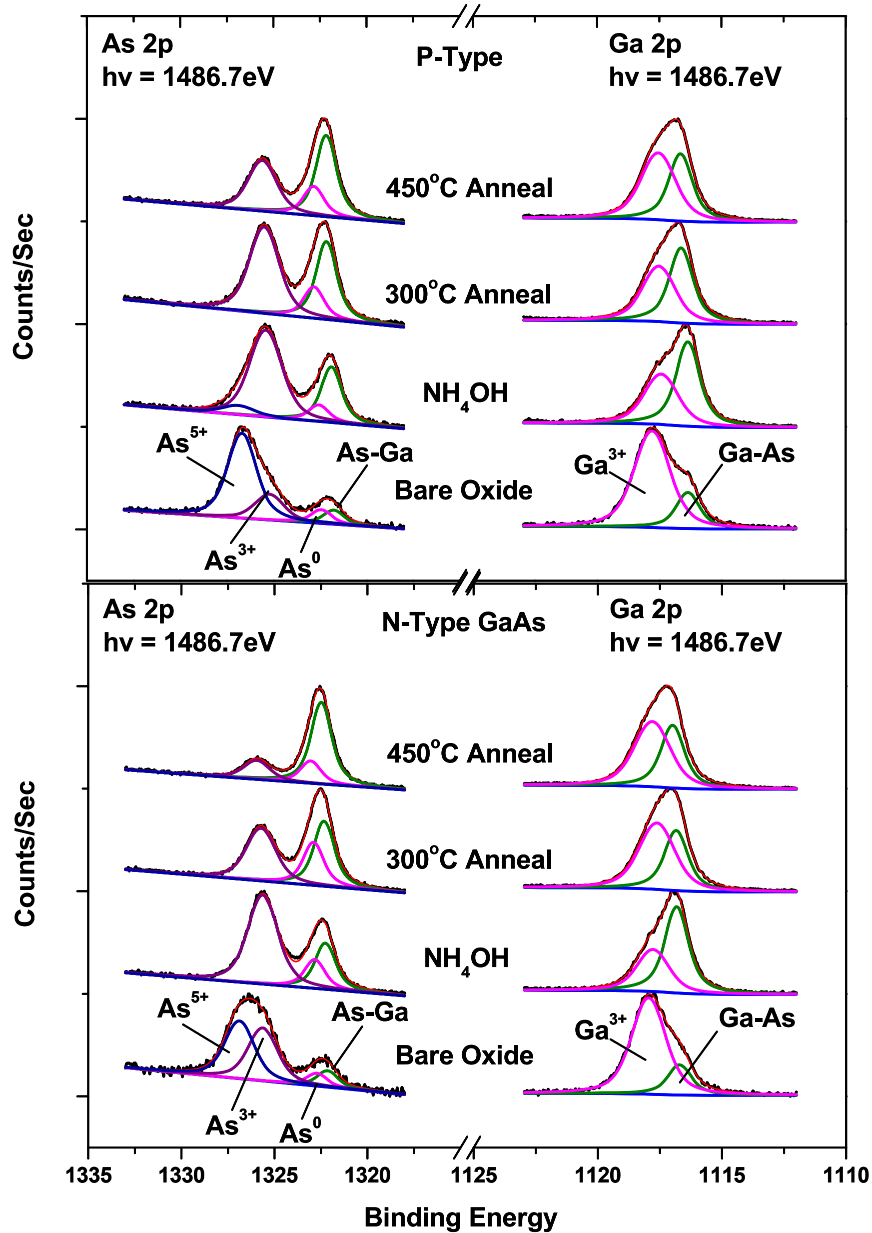

Figure 6.3 The As 3d and Ga 3d spectra for p-type (Top) and n-type (bottom) GaAs as the samples were processed from native oxide through to the final 450 °C UHV anneal.

anneals. Using the same approach as for the As 3d region the trend in the oxide-to-substrate ratio for the Ga 3d region as a percentage of the same ratio for the native oxide is 21%, 31% and 34% for n-type and 21%, 23% and 32% for p-type for the standard NH_4OH etch, 300 °C and 450 °C anneal respectively.

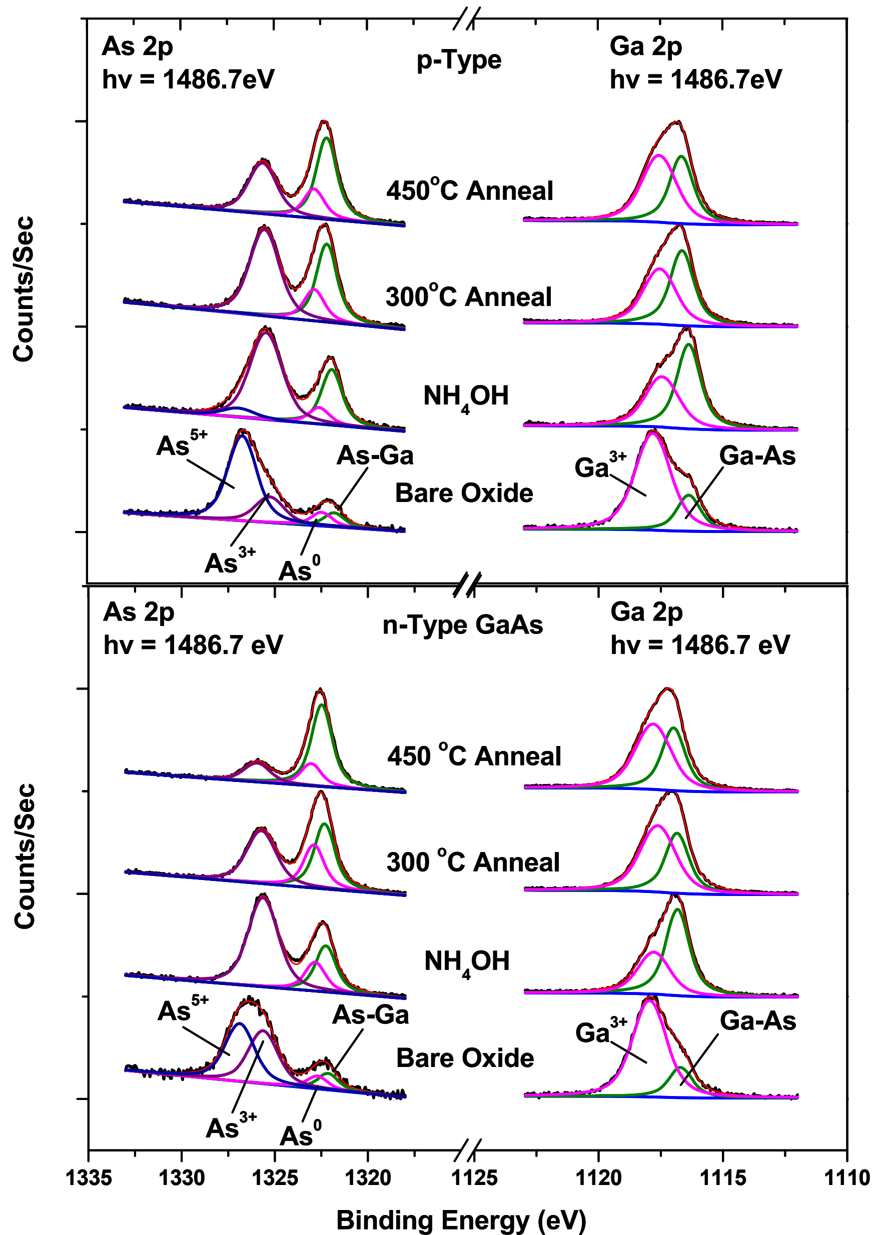

Figure 6.4 The As 2p and Ga 2p spectra for p-type (Top) and n-type (Bottom) GaAs as the samples were processed from Native oxide through to the final 450 °C UHV anneal.

Figure 6.4 shows the As 2p 3/2 and Ga 2p 3/2 core-level spectra for the same sample. The observed trends are exactly the same but exaggerated due to the decreased sampling depth in that low kinetic energy region. Again there is an intitial reduction in the total As-O and Ga-O bonds after the NH_4OH treatment. The following high-temperature anneals stimulate a transfer of oxygen from As-O environments to Ga-O environments. These studies show that the reduction in native

oxide by the standard NH_4OH etch occurs regardless of doping type for both gallium and arsenic oxides. However the high temperature anneals appear to reduce the As-O concentration on n-type GaAs to a greater degree than p-type.

Table 6.4 shows a breakdown of the atomic percentages for the various chemical components in the overlayer which effectively tabulates the trends discussed based on the observations from figure 6.3. These percentages are calculated using the integrated peak areas from in the individual features identified in figure 6.3 modified by the relative sensitivity factors[26x] (RSF's) for each element, 0.57 and 0.31 for the As 3d and Ga 3d respectively. Corrections for RSF use on ultra-thin films have not been made due to the negligible (20 eV) difference in the core-level kinetic energies.[27x] Similar calculations were not made for the As 2p and Ga 2p core-level spectra shown in figure 6.4 because the difference in kinetic energy between the As 2p and Ga 2p is ~ 200 eV which results in a change in sampling depth of over 20% which would invalidate the use of conventional RSF's on these ultra-thin films. A gallium-rich native oxide has been previously reported by Ghidaoui *et al.*[22] The As-As bonds are seen to make up a higher percentage of the overlayer after the NH_4OH treatment as has previously been reported by Lu *et al*[31] for a HCl based etch. NH_4OH has been shown by Lebedev *et al*[11] to completely remove As^{3+}, As^{5+} and Ga^{3+} signals but leave a strong As-As bond signal. The oxide related arsenic and gallium features shown after NH_4OH etching in this study are therefore most likely formed by the re-oxidation of the GaAs between sample etching and placement in UHV due to the lack of any chemical passivation of the surface.

Type	n-Type			p-type		
Process	%As-O	%As-As	%Ga-O	%As-O	%As-As	%Ga-O
Native	27	20	53	33	19	48
NH_4OH	30	44	26	33	36	31
300 °C	11	51	38	21	40	39
450 °C	5	36	59	10	39	51

Table 6.4 Atomic percentages of the native oxides constituent bonding environments as calculated from the integrated areas of the As 3d and Ga 3d features identified in figure 6.3 modified by their RSF's.

The oxygen 1s core-level spectra obtained from the same samples as the As and Ga 3d and 2p features shown in figure 6.3 and figure 6.4 are shown here in figure 6.5. These features are difficult to deconvolve due to the large number of oxygen related bonding environments and, in the case of the native oxide, a reasonable fit can even be obtained using only one wide Gaussian component. Therefore it is difficult to obtain any extra quantitative information from these spectra although trends extracted from the peak shape should still correlate with and confirm any trends seen in the arsenic and gallium oxide features. Since the arsenic and gallium core-level scans showed clear oxide related features with very different core-level chemical shifts with respect to their substrate features, it stands to reason that the native oxide should be fitted with at least two Gaussian components of different binding energies which can be assigned to O-As and O-Ga bonds as has been reported in literature.[11,31,32] In figure 6.5 the ratio of the integrated intensity of these two features was fixed to match the expected ratio ofAs-O to Ga-O bonds obtained from the As 3d and Ga 3d features and shown as percentages in table 6.4. In figure 6.5 it can be seen that this still results in a fit that matches well with the raw date and allows the O 1s core-level feature to serve as a check for the conclusions drawn from the fitting of the As 3d and Ga 3d features.

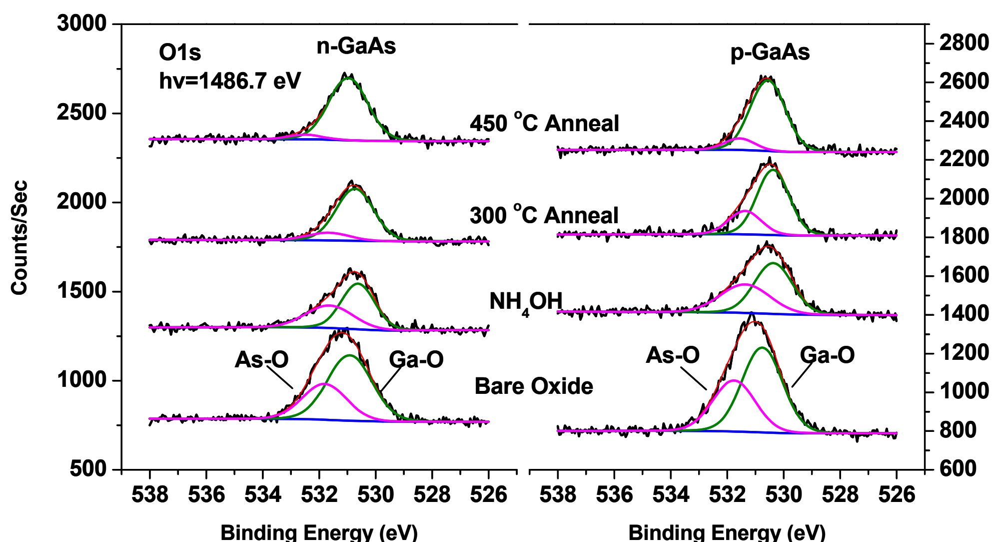

Figure 6.5 Oxygen 1s spectra for n and p type GaAs from native oxide through to 450 °C annealed sample. Peak widths were allowed to vary to accommodate a fixed ratio for the As to Ga related oxygen components.

Analysis of the carbon 1s feature showed the trace amounts of carbon, left after the NH_4OH treatment, are removed by the UHV anneal.

Following the NH_4OH treatment the oxygen 1s spectra shows a decrease in its total area which agrees with the reduction in the As^{5+} and Ga-O related features. Calculating the total area of the oxygen 1s spectra shows that the high temperature anneals do not have a significant impact on total oxygen concentration indicating that the majority of the oxygen simply transfers from As to more energetically favourable Ga-O bonding environments rather than desorbing in agreement with K. Tone *et al.*[33] This is in agreement with XPS and TPD results reported by other groups[12,14] which state that temperatures of >580 °C are required for complete desorption of oxidised Ga, as well as TPD studies which show the removal of As from GaAsOx at temperature < 400 °C in the form of As and As_2 without the removal of O.[33] Those authors concede that the 'parent' desorbing molecule could be As_4 rather than As_2 since the mass of As_4 could not be measured by their equipment but this does not change the conclusion that oxygen is not seen to be removed. In that study a temperature of 475 °C was shown to be required to begin the desorption of Ga and Ga_2O species.

Thickness Calculations:

As previously explained in section 2.2, the ratio of the overlayer to substrate signals is proportional to the thickness of the film. The 'effective' thickness of arsenic oxide (As^{3+}+As^{5+}), elemental arsenic (As^0) and gallium oxide (Ga^{3+}) can be determined from the following expression:

$$\frac{I_x}{I_S} = \frac{I_A^\infty}{I_S^\infty}\left[\frac{\{1-\exp[\frac{-d_x}{l_{x,x}(\cos\theta)}]\}}{\exp[\frac{-d_{AsOx}}{l_{S,AsOx}(\cos\theta)}+\frac{-d_{As}}{l_{S,As}(\cos\theta)}+\frac{-d_{GaOx}}{l_{S,GaOx}(\cos\theta)}]}\right] \quad (6.1)$$

Where I_x and d_x are the integrated intensity and film thickness respectively for the overlayer component (arsenic oxide AsOx, elemental arsenic As or gallium oxide GaOx) being measure and I_S is the integrated intensity for the relevant As or Ga substrate signal.

The values for the electron attenuation length (EAL) were determined using software supplied by National Institute for Standards and Technology (NIST).[34] Values of 26.42 Å and 26.78 Å were determined for electron with 1443 eV (As 3d) and 1466 eV (Ga 3d) kinetic energy respectively in a $GaAsO_4$ layer ~20 Å thick with a density of 3.72 gcm^{-3}. The density was assumed to be ~70 % of the accepted values for bulk GaAs[35,36] as shown by Tanner *et al.*[37] The value of R_0 was determined as suggested by Seah and Spencer[38] from the relationship

$$\frac{I_A^\infty}{I_S^\infty} = \frac{\rho_A l_A M_S}{\rho_S l_S M_A} \tag{6.2}$$

resulting in values of 0.54, 1.49 and 0.53 for As-O, As and Ga-O respectively. Constants ρ_x and M_x defined in section 2.2 as the atomic density and molecular mass can be found in the literature.[35,36] Compound A is assumed to be stoichiometric $GaAsO_4$ while S is the GaAs substrate. The value of θ, the photoelectron take-off angle with respect to the surface, was 45° for all measurements.

Since the $GaAsO_4$ is treated as having a single density, the attenuating properties and therefore the value of l_x is the same for x = AsOx, As or GaOx. Although reliable data exists on the values of ρ and M for As, As_2O_3, As_2O_5 and Ga_2O_3, the treatment of the $GaAsO_4$ as having a single density is due to the suggestion by Hollinger *et al*[10] that the oxide is a 'single phase metastable non-stoichiometric oxide' and can not be assumed to have the same physical properties as pure As_2O_3, As_2O_5 or Ga_2O_3.

Table 6.5 shows the calculated 'effective' thickness of the individual components of the overlayer and the total thickness (d), for n and p type GaAs, for each step of the experiment. The observed trends show a good correlation with those seen using the integrated areas and relevant RSF's in table 6.4.

Type	n-Type (Å)				p-type (Å)			
Process	d_{AsOx}	d_{As}	d_{GaOx}	d	d_{AsOx}	d_{As}	d_{GaOx}	D
Native	7.6	1.7	10	19.3	9.1	1.4	7.7	25.3
NH_4OH	6.5	2.6	2.7	11.8	6.4	2	3.1	17.4
300 °C	3	4.3	4.7	12	3.9	2.2	4	15.2
450 °C	0.9	2.1	6.8	9.8	1.9	2.3	6	15.5

Table 6.5 Effective thicknesses in angstrom for arsenic and gallium related oxides and elemental arsenic.

<u>H Cracker:</u>

GaAs *in-situ* cleaning with atomic hydrogen[39-42] allows for the study of films deposited on an oxide free surface without growing the samples by *in-situ* MBE.[5,24] Figure 6.6 shows a comparison of hydrogen cleaned samples with ammonium hydroxide cleaned samples. Both As and Ga oxide components are removed to below the detection limits of XPS as illustrated in figure 6.6a and figure 6.6b, and there was no evidence of residual carbon contamination. There is still a detectable presence of a small oxygen 1s signal in figure 6.6c. The ratio of O 1s to As 3d signal is less than 10% of the same ratio for NH_4OH treated samples.

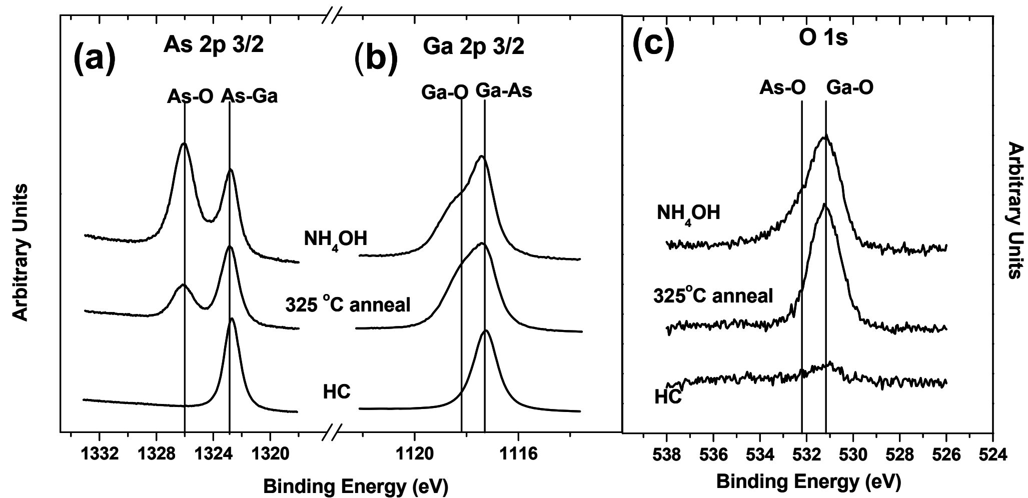

Figure 6.6 Comparison of the oxide removal capabilities of the standard NH_4OH etch, the subsequent UHV anneal and the AHT on n-GaAs using a) As 2p b) Ga 2p and c) O 1s spectra.

Using empirically derived relative sensitivity factors[26x] for the As and Ga 2p and 3d core-levels, the atomic percentages of arsenic and gallium can be determined from the AHT GaAs with two different sampling depths which can be described by

$$3\lambda \cos\theta \tag{6.3}$$

where λ is the inelastic mean free path which is approximately 25 Å for the 3d core-levels and 7.9 Å and 12.5 Å for the As and Ga 2p core-level respectively[33] and θ is the take-off angle of the photoelectrons which for this system was 45°.

	3d (~53 Å sampling depth)	2p (~15-25 Å sampling depth)
Arsenic	46%	57%
Gallium	54%	43%

Table 6.6 Stiochiometry of the GaAs surface at two different sampling depths

The stiochiometry calculations for the AHT cleaned surface using the 3d core-levels show the Ga:As to be approximately 1:1 although the slight As deficiency in the substrate would not be unexpected after a 430 °C anneal. The 11% increase in the As concentration for the more surface sensitive 2p core-levels could be attributed to an arsenic terminated surface since, with a sampling depth of 15 Å for the As 2p spectra, 63% of the signal comes from the top 5 Å or 1-2 monolayers.

Silicon Deposition:

In order to better understand the bonding structure at the Si/GaAs interface, sequential depositions of Si on NH_4OH treated GaAs samples were performed in a UHV MBE chamber at target deposition rates of approximately ~ 20 Å/min with a substrate temperature of 70 °C and the XPS spectra of the interfacial chemical reactions were acquired. The samples in this study were not annealed in UHV after the standard NH_4OH etch.

Figure 6.7a shows that the initial silicon depositions result in the reduction of the As-O bond concentration to below detectable limits, as seen by other groups.[43-45] Curve fitting suggests that there is a concurrent increase in the surface concentration

of elemental arsenic designated as As^0 indicating that the arsenic remains after the As-O bond is broken. This is to be expected since not enough thermal energy is supplied in this experiment to facilitate the desorption of As_2 or As_4 species. The ratio of Ga-O/GaAs is seen to vary only slightly throughout the silicon deposition. This is reported, although not shown by Ivanco *et al*[43] who goes on to show that Si depositions at higher temperatures result in the reduction of Ga-O in agreement with Jiménez *et al*.[44,45]

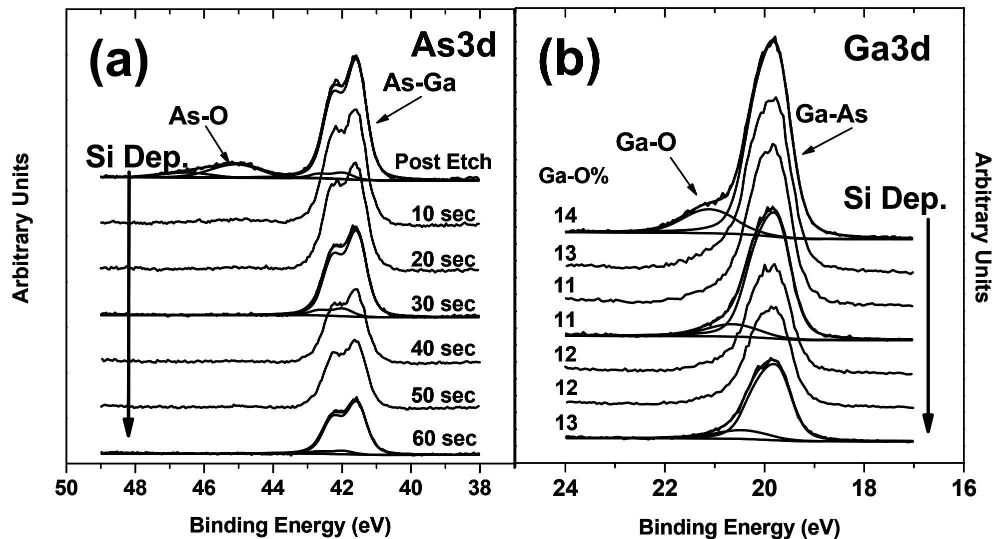

Figure 6.7 As 3d and Ga 3d spectra for sequential depositions of Si on NH_4OH treated n-type GaAs.

It is also apparent in figure 6.7b that there is a substantial shift in the Ga-O related feature to a lower binding energy as the silicon deposition progresses. The lack of change in the GaO/GaAs ratio makes it difficult to attribute this shift solely to the removal of a higher binding energy $Ga(OH)_3$[14] component as in the case of NH_4OH treated samples. Instead a possible explanation considering the involvement of the deposited silicon will be discussed later.

Figure 6.8 shows the growth of the silicon 2p signal and the attenuation of the gallium 3p signal which are separated by only 7 eV. The position of the silicon peak at 102 eV binding energy, after the first deposition, is consistent with silicon existing in an oxidised state. As mentioned by Ivanco *et al*[44] the growth of the Si signal in an oxidised state along with a concurrent decrease in oxidised arsenic signal suggests

that the silicon atoms replace arsenic in the $GaAsO_x$ layer because Si-O bonds are more thermodynamically stable.[36] When all of the As-O bonds have been replaced by Si-O bonds there is a significant increase in the intensity of the Si-Si related feature indicating the rest of the deposited silicon layer is unoxidised.

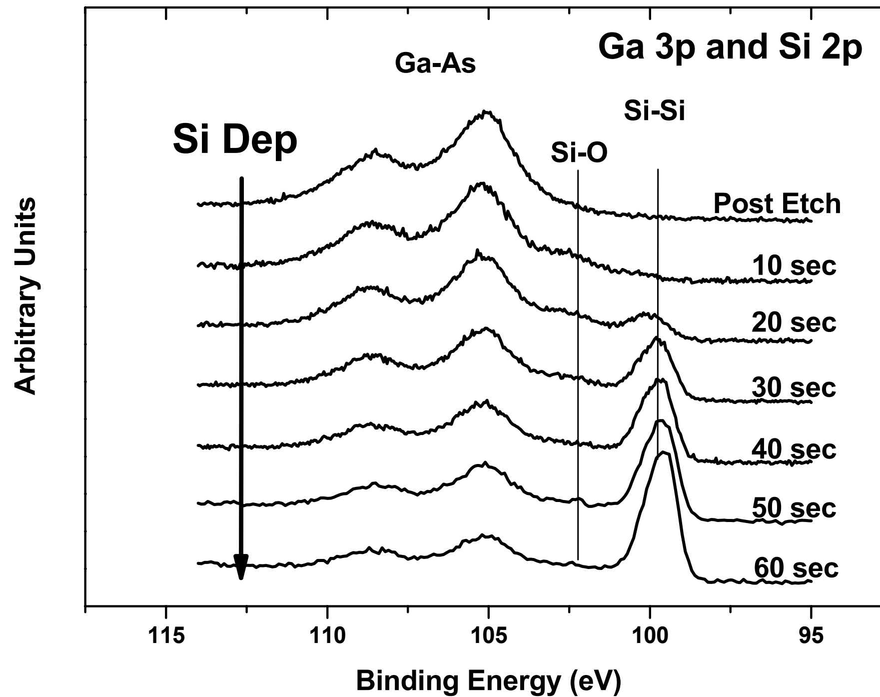

Figure 6.8 Ga 3p and Si 2p spectra for sequential depositions of Si on NH_4OH treated N-type GaAs.

An example of the curve fitting for the Ga 3p/Si 2p spectra is shown in figure 6.9. Fitting was performed by fixing all variables excluding the peak area for the Ga 3p core-level substrate component to match that for a clean reference sample. The ratio of gallium oxide to substrate signal as well as the core-level shift was fixed to reflect the results of fits for the Ga 3d spectra. The 80 eV difference in the kinetic energy of electrons emitted from the 3d and 3p core-levels was considered and so the oxide to substrate ratio (R_{exp}') of the 3p peak was set 7% higher than the same ratio (R_{exp}) for the 3d core-level to account for the difference in the EAL from the expression:

$$R_{exp}' = R_{exp} \frac{\exp\left(\frac{d}{l'}\right) - 1}{\exp\left(\frac{d}{l}\right) - 1} \tag{6.4}$$

This expression is obtained by rearranging the standard thickness expression, Equation 2.12, in terms of R_0. This constant is the same for all core-levels of a given element and so the equations for the Ga 3d and Ga 3p in terms of R_0 can be set as equal. An estimate for the expected value of R_{exp}' from the Ga 3p feature can be extracted from equation 6.4. The two Si-O components were required for consistently good fits for each deposition but are not assigned to specific oxide states since the precise bonding structure is unknown. The values for *l* and *l*' were calculated using software provided by NIST[34] as 26.81 Å and 25.32 Å.

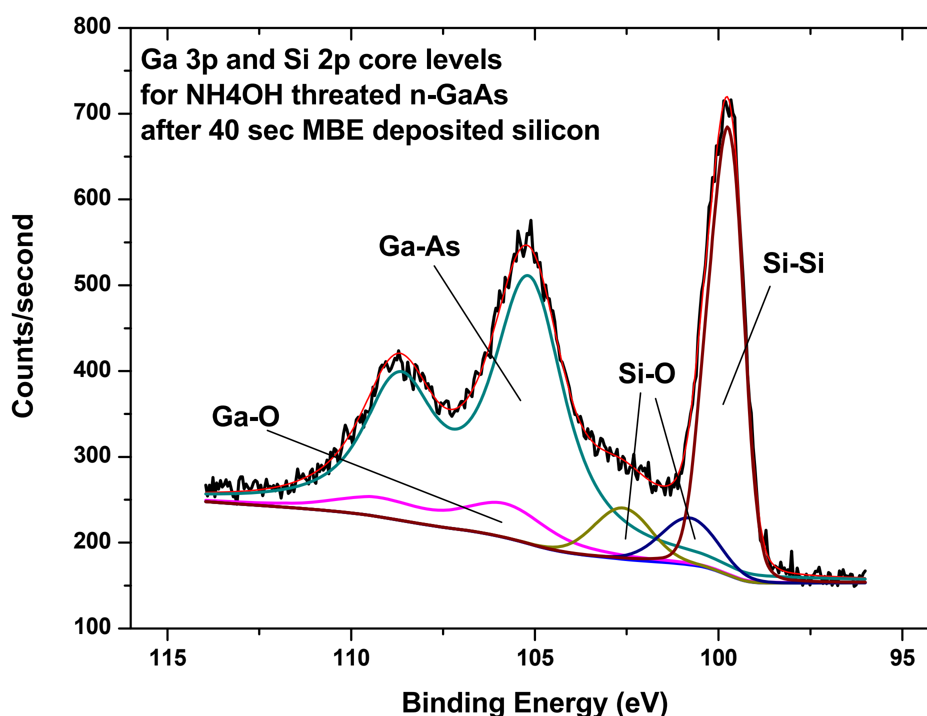

Figure 6.9 Example of the fitting for the Ga 3p and Si 2p core-levels.

A decrease in the integrated intensity of the Si-O features with continued silicon depositions suggests the silicon oxide remains at the interface rather than being transported to the surface. The shift to lower binding energy of the Ga 3d oxide feature after the first silicon deposition seen in figure 6.7b can now be explained by

the presence of Si-O bonds. There is a change from a Ga-O-As like environment to a Ga-O-Si like environment. The difference in the electronegatives of silicon and arsenic, which are 1.9 and 2.2 respectively, results in a different charge distribution for the Ga-O-As and Ga-O-Si systems. Silicon-oxygen bonds will be more ionic and result in a greater charge transfer than arsenic-oxygen bond which lowers total charge transfer between that oxygen atom and the gallium in the Ga-O-Si system. Since the magnitude of core-level chemical shifts is related to the charge transfer between atoms as described in section 2.2, this would be expected to decrease the detected binding energy of electrons excited from those Ga atoms.

Thickness calculations, tabulated in table 6.7, were carried out in a manner similar to measurements made for the native oxide using equation 6.1. Throughout the depositions, the layers were assumed to be stacked as schematically shown in figure 6.10 which allowed for thickness to be calculated layer by layer as described by Equations 2.19 and 2.20 where the first layer is a compound Ga-O and As-O layer covered by Si-O and finally Si.

Deposition Time	Thickness of individual layers					
	d_{GaOx}	d_{AsOx}	d_{As}	d_{SiOx}	d_{Si}	d_{Total}
NH_4OH	3.8	5.3	0.4			9.5
10	4.3	1.2	1	2.7		9.2
20	3.8	0.3	1	4.2	1.3	10.6
30	3.9		1	4.3	4.5	13.7
40	4.1		0.8	4.5	7.1	16.5
50	4.1		1	4.9	8.8	18.8
60	4.5		0.7	4.8	13.1	23.1

Table 6.7 Tabulated data for the calculated thicknesses of each layer as silicon is deposited onto GaAs.

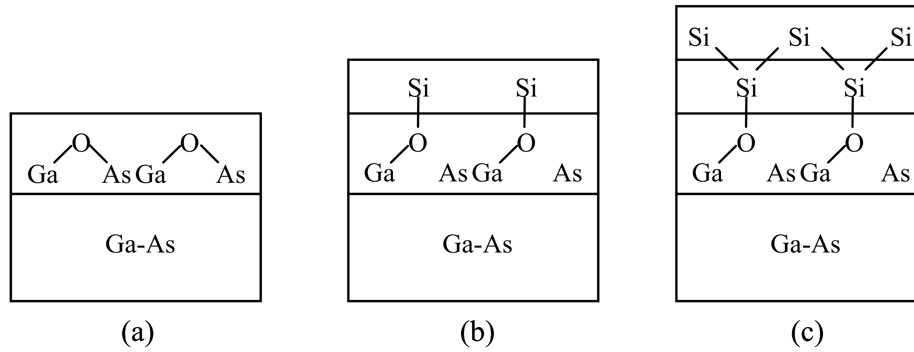

Figure 6.10 Bonding environments on GaAs after (a) NH_4OH treatment (b) initial Si depositions (c) continued Si depositions.

The value of R_0 for Si/GaAs was calculated as 0.55 from the values for atomic density ρ and molecular mass M of 2.33 g cm^{-3} and 28.09 respectively[35,36] as well as l of 28.23 Å, for silicon, taken from Seah and Spencer.[38] Since the signals for silicon and gallium came from different core-levels, the photoionisation cross-section for the Si 2p and Ga 3p peaks need to be considered and so equation 1.2 becomes:

$$\frac{I_A^\infty}{I_S^\infty} = \frac{\rho_A l_A \sigma_A M_S}{\rho_S l_S \sigma_S M_A} \qquad (6.5)$$

These values for the photoionisation cross-section σ are taken from Yeh and Lindau[46] for Al Kα photons. The calculated thicknesses for each of the depositions support the conclusion that silicon breaks the arsenic oxygen bond forming a layer of silicon oxide. The liberated arsenic remains as elemental arsenic as seen by the increase in the effective thickness of As^0. The Si-O layer seems to self limit at approximately 4.5-5 Å while variations in the Ga-O layer thickness are less than 1 Å.

6.3.3 XPS of high-κ layers on GaAs

Thin, 1 nm layers of Al_2O_3 and HfO_2 were deposited on GaAs by atomic layer deposition (ALD). In this section, the 'self-cleaning' of the As and Ga oxides by Al_2O_3 (TMA precursor) and HfO_2 (TEMA-Hf) films deposited on both the native oxides and NH_4OH treated GaAs(100) surfaces has been studied by *in-situ* chemical

analysis. The samples used were n-type silicon doped GaAs(100) with a doping concentration of 5 x 10^{17} cm^{-3}.

Figure 6.11 shows the As 2p and Ga 2p features for the untreated native Ga and As oxides. Also shown are the As 2p and Ga 2p regions after the deposition of 1 nm Al_2O_3 and HfO_2 films on similar starting surfaces. The native oxide is seen to contain the usual As^{3+} As^{5+} and Ga^{3+} signals. After the 1 nm deposition of Al_2O_3, the arsenic oxide feature is greatly reduced and can be fitted with only the presence of a reduced but not removed As^{5+} feature indicating the removal of the lower As^{3+} oxidation state. In contrast, the deposition of 1 nm HfO_2 is seen to remove the As^{5+} feature while leaving a reduced but still observable As^{3+} feature. The Ga 2p oxide feature is also seen to be reduced in both cases. As before, the native gallium oxidation states are not well resolved and have been fitted here with a single peak. Both ALD precursors are seen to reduce the total concentrate of Ga-O bonds. After the deposition of HfO_2, the peak is seen to shift to a lower binding energy when compared to the deposition of the Al_2O_3 film indicating that TEMA-Hf preferentially reduces the higher oxidation states of both gallium and arsenic.

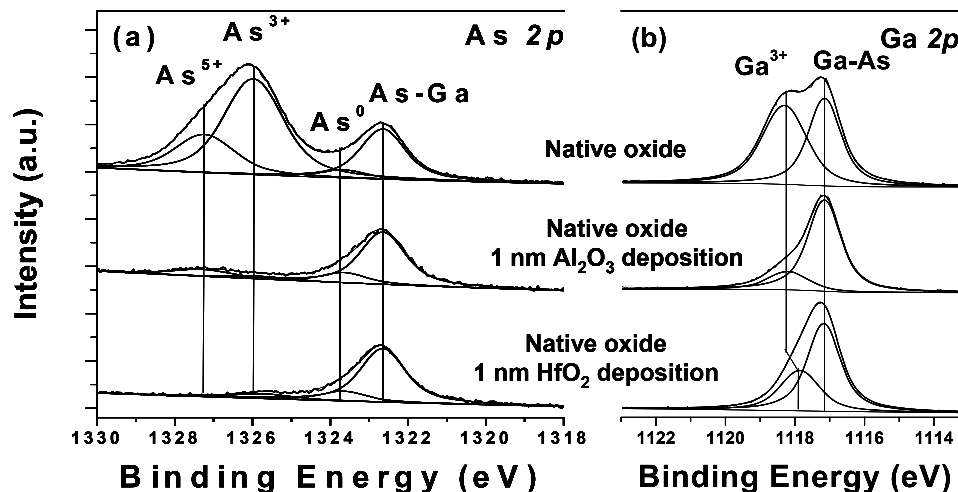

Figure 6.11 As and Ga 2p features for *in-situ* ALD deposition of Al_2O_3 and HfO_2 onto untreated GaAs with a native oxide layer.

The treatment of GaAs with NH_4OH can be seen in figure 6.12 to remove the As^{5+} component from the As 2p spectra as well as reducing the gallium oxide concentration in comparison to the native oxide. This was discussed in detail earlier in

this chapter (page 125-130). Subsequent deposition of 1 nm of a TMA Al_2O_3 by ALD is seen to again reduce the gallium oxide concentration and remove the As^{3+} component, leaving the interface arsenic oxide free. The deposition of a 1 nm TEMA-Hf HfO_2 film by ALD is seen to reduce the gallium oxide concentration along with a concurrent reduction in the binding energy of this component as well as reducing, but not removing, the As^{3+} component.

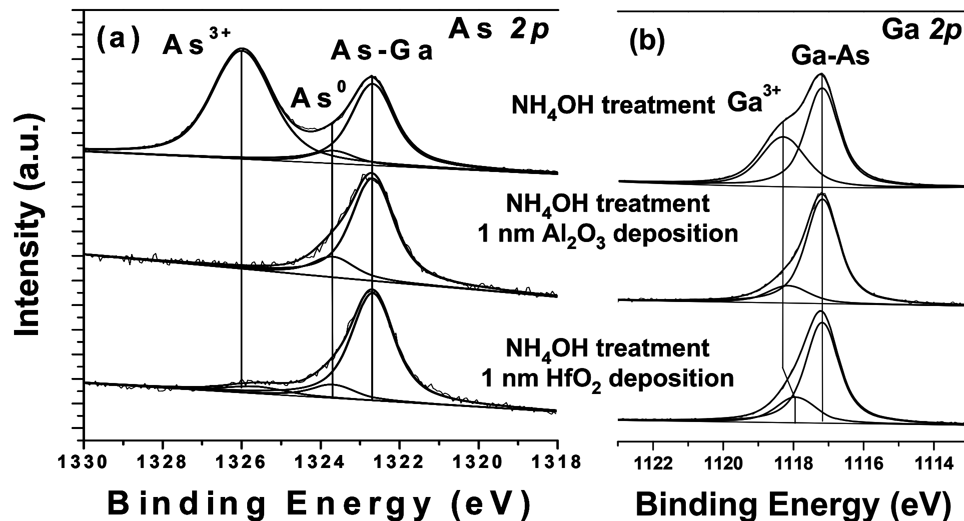

Figure 6.12 **As 2p and Ga 2p features for *in-situ* ALD deposition of Al_2O_3 and HfO_2 onto NH_4OH GaAs.**

For both the NH_4OH treated and untreated GaAs, the deposition of high-κ Al_2O_3 or HfO_2 causes a reduction in the gallium oxide concentration. The As 2p feature is similar for both surfaces after the deposition of HfO_2. This is most likely due to the similar concentrations of the As^{3+} feature for both surfaces prior to deposition. While the deposition of Al_2O_3 is also seen to reduce both arsenic oxide components, the selective removal of the As^{5+} by other means, such as NH_4OH treatment, allows for an arsenic oxide free interface after ALD. This appears to contradict the work of Dalapati *et al*[17] whose study clearly showed evidence of arsenic oxide after ALD of Al_2O_3 onto a presumably oxide free surface. However, that work utilised *ex-situ* XPS and so a possible reason for the difference in results could be the diffusion of oxygen through the thin 1-2 nm Al_2O_3 film to the interface, post ALD and prior to XPS analysis. The reduction in the total amount of GaAs oxides by ALD of

Al_2O_3 agrees with the work of Frank *et al.*[16] The reduction of the same oxide by ALD of HfO_2 does not agree with that study. This is most likely due to the use of different precursors for hafnium. We note that there is no evidence of As_2O_5 on the surface of the Al_2O_3 film as has been previously reported[18,19] for films grown on InGaAs, which indicates that this transport of As_2O_5 to the surface may be intrinsic to InGaAs substrates.

6.3.4 XPS of high-κ layers on GaAs: Effect of silicon interlayer

To examine how the interfacial chemistry correlates with the anomalous frequency dispersion of the maximum capacitance in accumulation, four samples with clearly different interfaces were prepared. Table 6.8 shows the processing conditions for each of the four samples that will be discussed throughout the remainder of this chapter. This sample set allowed Al_2O_3 layers grown on both ammonium hydroxide treated (NH_4OH + *in-situ* anneal) and atomic hydrogen treated (AHT) GaAs surfaces, to be studied with and without the use of a silicon interlayer. Following the surface preparation procedures, the Al_2O_3 films were deposited in two stages. First a 1 nm layer was grown and the interface was analysed *in-situ* with XPS. The samples were then transferred *in-situ* back to the ALD reactor and the remaining 9 nm were grown. The time period between the growth of the 1 nm and 9 nm layers while the sample was being transferred and analysed was approximately 3-3.5 hours. During that time the sample was in UHV (better than 1 x 10^{-9} mbar).

Sample	A	B	C	D
Degrease	✓		✓	
NH_4OH	✓		✓	
In-situ Anneal 325 °C	✓		✓	
AHT		✓		✓
Si interlayer deposition			✓	✓
ALD of 1 nm Al_2O_3	✓	✓	✓	✓
ALD of 9 nm Al_2O_3	✓	✓	✓	✓

Table 6.8 Sample labels for *In-situ* Al_2O_3 on GaAs.

The interfaces, as analysed by XPS, after each process will be discussed in detail before the electrical characteristics are discussed and a correlation between the two are made. The two starting surfaces shown in figure 6.13, NH_4OH + *in-situ*

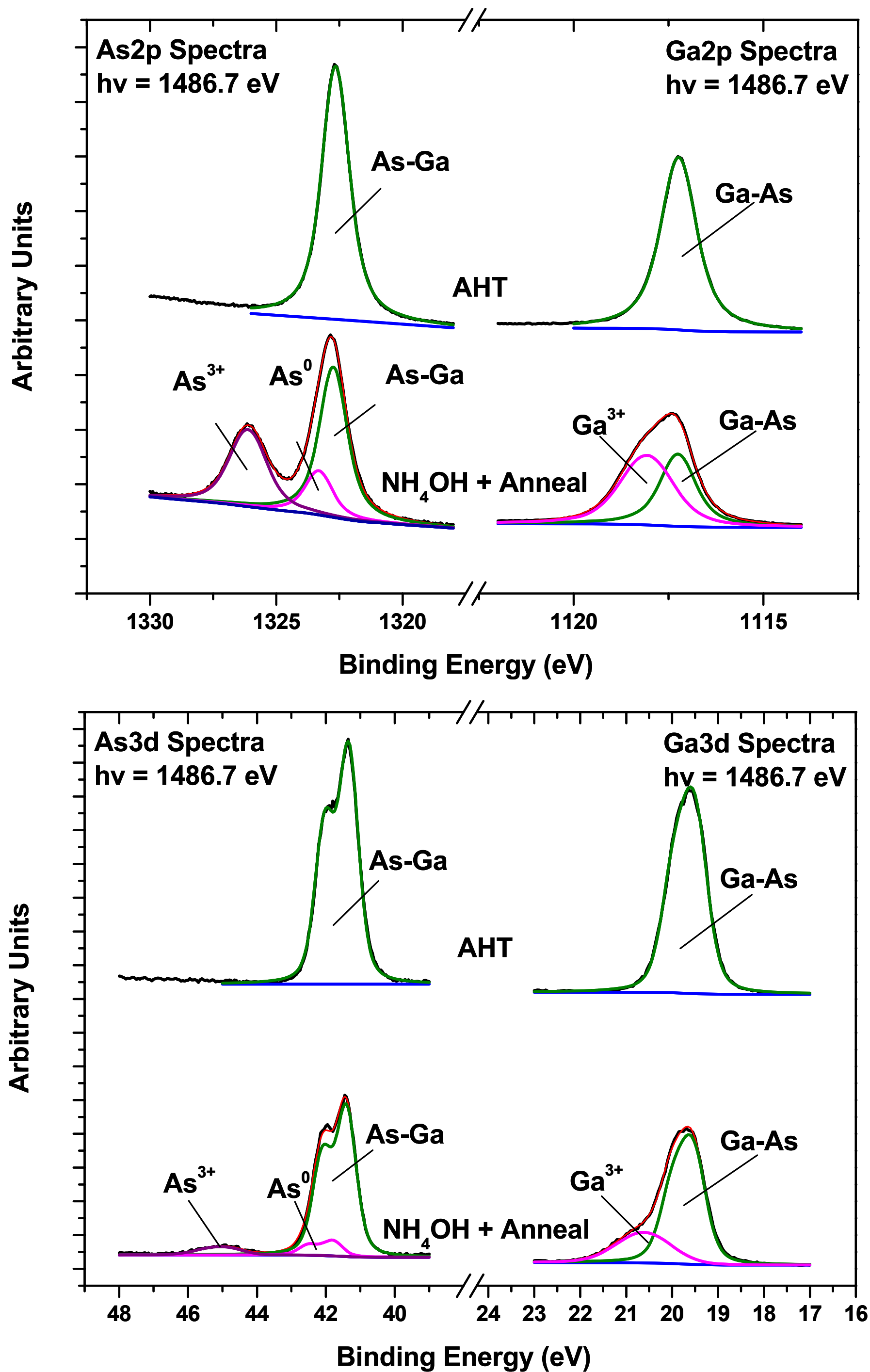

Figure 6.13 As 2p and Ga 2p regions (Top) and As 3d and Ga 3d regions (Bottom) for both NH_4OH + Anneal and AHT starting surfaces.

anneal and AHT, have been discussed earlier but they shall be compared here and the important differences will be highlighted for the sake of completeness. Figure 6.13 shows that the AHT samples which are the starting surface for samples B and D are free of arsenic and gallium oxides as well as elemental arsenic. The NH_4OH + anneal treated samples which are the starting surface for samples A and C show evidence of thin As^{3+} and Ga^{3+} oxides seen by XPS as well as some elemental arsenic.

The second processing step was the deposition of a silicon interlayer which has been shown to electrically passivate the high-κ/GaAs interface and result in a reduction in the anomalous frequency dependant dispersion of accumulation capacitance.[5-8] This processing step was only performed on samples C (NH_4OH treated) and D (AHT) and the silicon was deposited with the substrate temperature less than 20 °C. The gallium 3d spectra deconvolved in figure 6.14 show that for the AHT sample there is still no evidence of gallium oxides after silicon deposition which

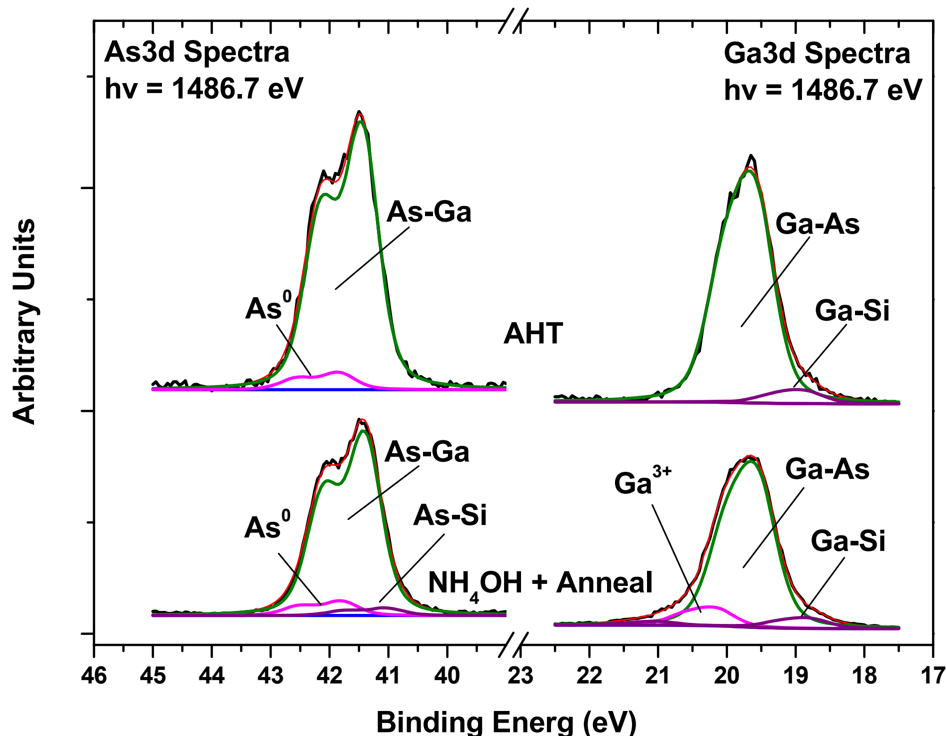

Figure 6.14 As and Ga 3d spectra for AHT and NH4OH+Anneal treated samples after the deposition of silicon.

indicates that there was no additional oxygen contamination during the deposition process. There is however an additional lower binding energy component separated from the gallium substrate peak by ~ 0.75 eV. This has been tentatively assigned to Ga-Si bonds in the figures but it could also be due to Ga-Ga bonds. Ivanco *et al*[39a] deconvoles Ga-Si and Ga-Ga bonds after the high temperature deposition of silicon. In that study, they assign a feature with a CLCS of -0.45 eV to Ga-Si while assigning a feature with a CLCS of -0.82 eV to Ga-Ga bonds. Chambers *et al*[47] however, assigned features having CLCS's with respect to the substrate ranging from 0.35-0.75 eV all to Ga-Si. The spectra for the NH_4OH + anneal treated sample can be fitted in a similar fashion but requires the addition of a gallium oxide component. The As 3d spectra for the AHT sample in the same figure clearly shows the presence of element arsenic however, there is no lower binding energy shoulder that could be attributed As-Si as seen by Ivanco *et al*.[44] The NH_4OH + anneal sample shows evidence of elemental arsenic as well as a possible As-Si feature. The increased attenuation of the low kinetic 2p core-level energy electrons by the silicon overlayer made accurate curve fitting harder and so these spectra were not used for the remainder of the interface analysis.

The emergence of an elemental arsenic feature on the AHT sample can be attributed to silicon disrupting the Ga-As bonds at the interface and releasing arsenic as it bonds to gallium. For the thickness calculations, the fortuitous close proximity of the Ga 3p and Si 2p was exploited. Figure 6.15a and figure 6.15b shows these spectra for the NH_4OH + anneal treated and AHT samples. To aid in curve fitting, the core-level chemical shifts and the R_{exp} values for GaOx/GaAs and GaSi/GaAs were taken from the curve fitting of the less convoluted Ga 3d feature and modified as mentioned early (page 135-136). As might be expected, the concentration of Si-O bonds is much lower when silicon is deposited onto the AHT surface.

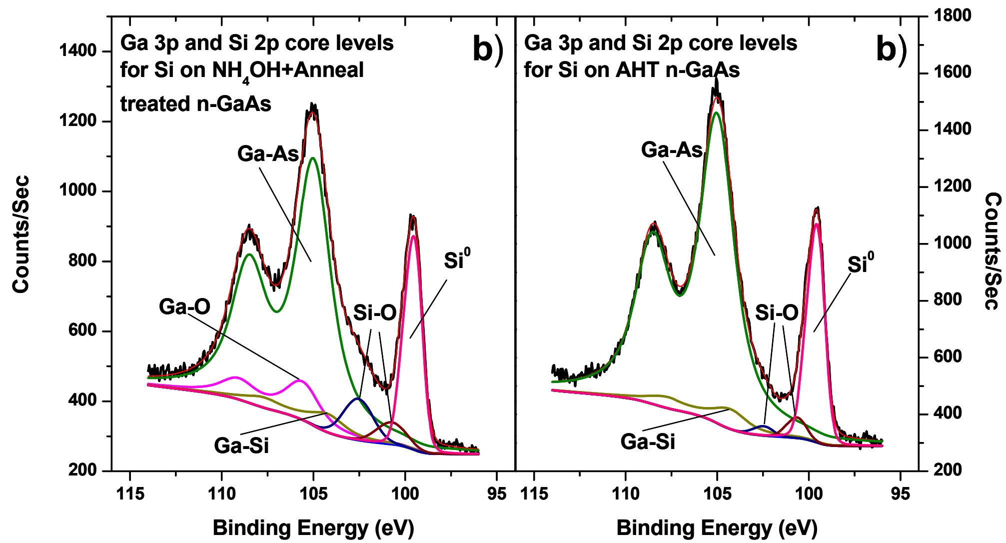

Figure 6.15 Ga 3p and Si 2p for silicon deposited on a) NH_4OH+Anneal treated and b) AHT surfaces.

The presence of a small Si-O feature reflects the small concentration of oxygen remaining on the surface after AHT cleaning (page 132). While calculating the thickness of the various layers, shown in table 6.9, the Ga-Si component is assumed to be due to silicon atoms that have broken Ga-As bonds, so this layer is assumed to be mixed with the remaining oxide layer. Unfortunately the Si^0 feature should be made up of silicon from the overlayer and silicon in the silicide bonds since only very small chemical shifts are generally detected for silicides with respect to a bulk silicon signal. This means that there will be a slight over estimation of the silicon overlayer thickness. If the Ga-Si feature is actually due to Ga-Ga bonds then no such overestimation would be expected.

Sample	Thickness of individual layers					
	d_{GaOx}	D_{GaSi}	d_{As}	d_{SiOx}	d_{Si}	d_{Total}
C	3.9	0.7	0.8	3.1	4.1	12.6
D	0	0.8	0.8	1.1	4.7	7.4

Table 6.9 Thickness calculations for samples C and D after the deposition of silicon.

Comparing samples C (NH_4OH treated starting surface) and D (AHT starting surface) after the silicon deposition, it can be seen that, despite the very different

arsenic bonding environments prior to silicon deposition, both samples are left arsenic oxide free and with the clear presence of element arsenic after the deposition of silicon. Both samples also contain Ga-Si bonds. The main differences between the two samples are the slight presence of an As-Si feature for the AHT sample, the greater concentration of Si-O bonds for the NH_4OH + anneal sample and most importantly the clear presence of Ga-O bonds for the NH_4OH + anneal treated sample.

The deposition of Al_2O_3 on samples A-D was done in two steps of 1 nm and 9 nm to allow for the chemical analysis of the high-κ/substrate interface after the 1 nm deposition. The Al_2O_3 deposition conditions where the same for samples A though D and the interfaces shall be discussed in turn. Figure 6.16 shows the Al 2p features after the 1 nm deposition. The most notable difference between the samples is that the integrated intensity for samples C and D (Al_2O_3 grown on silicon interlayers) is only 70% of the intensity for samples A and B (Al_2O_3 grown directly onto GaAs) . This implies that the thickness of the Al_2O_3 layer is slightly thinner when deposited onto a

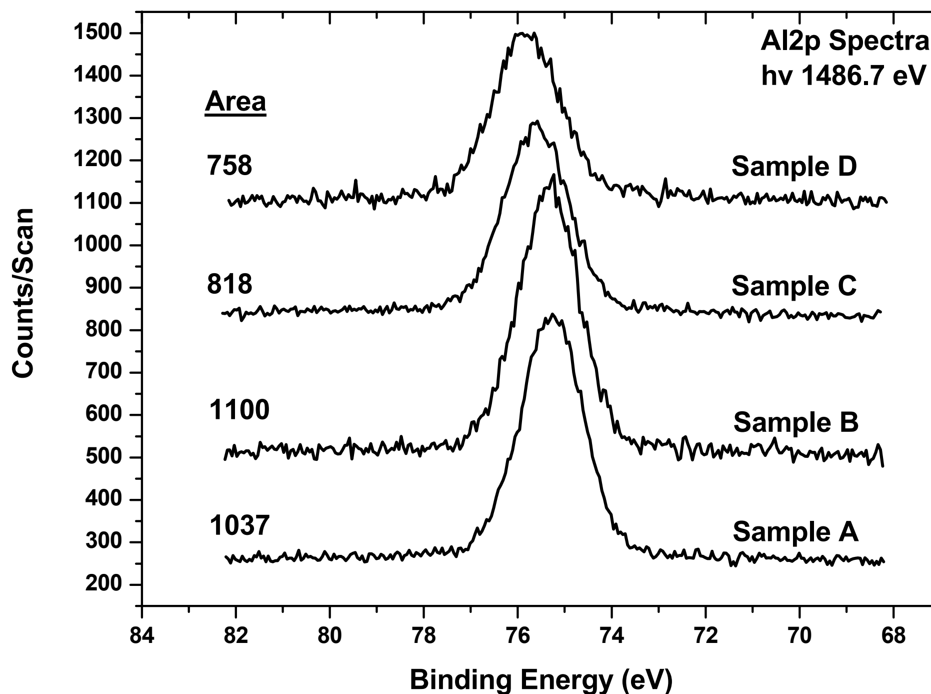

Figure 6.16 Al 2p spectra for samples A through D. Peak positions are normalised to As 3d at 41.56 eV. Features for sample B-D have been offset on the Y-Axis. Integrated peak areas are included.

silicon substrate, suggesting that the growth of the first monolayer is slower on silicon than on GaAs since subsequent layers should grow at a rate independent of the original substrate. The peak positions have been referenced to the As 3d substrate peak at 41.56 eV, as the charging effects will be different for each sample. A slight 0.3 and 0.5 eV shift to higher binding energies is detected for samples C and D, respectively. XPS spectra show no sign of carbon features above the background noise which indicates that all of the CH_3 is successfully desorbed and no detectable carbon contamination is added by the ALD process.

Figure 6.17 shows the curve fitting analysis for the arsenic 3d and gallium 3d. Note that all samples are arsenic oxide free, but show a detectable presence of elemental arsenic. From the As 3d and Ga 3d spectra, the following general observations can be made. For sample A (Al_2O_3 on NH_4OH GaAs), there is a clear presence of element arsenic and Ga-O bonds. Sample B (Al_2O_3 on AHT GaAs) looks similar although the concentration of Ga-O is much lower. Sample C (Al_2O_3 on Si on

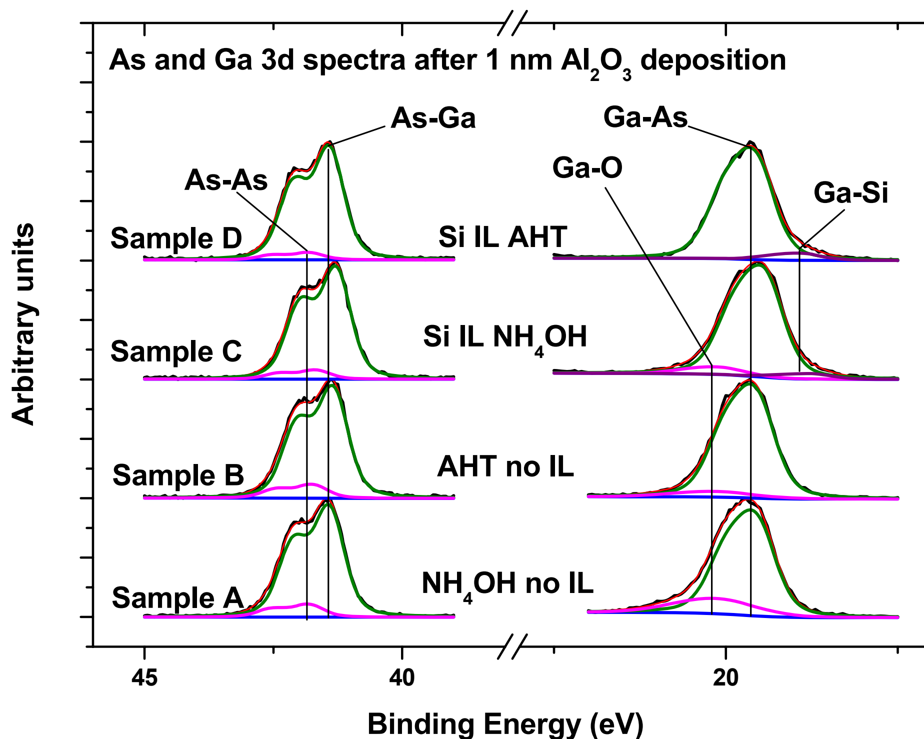

Figure 6.17 As and Ga 3d features for sample A-D following ALD of Al_2O_3. All curves have been normalised to maximum intensities allowing strongly attenuated signals to be seen as easily as others.

NH_4OH GaAs) still shows signs of both Ga-O and Ga-Si (or possibly Ga-Ga) bonds while the As-Si bonds are presumably desorbed during the ALD process. Sample D Al_2O_3 on Si on AHT GaAs) shows signs of Ga-Si (or possibly Ga-Ga) bonds but is the only sample to show no evidence of Ga-O bonds.

The ratio of the oxide to substrate signals for samples A and C (NH_4OH + anneal treated samples without and with a silicon interlayer respectively) is reduced to approximately 60% of its value from before the deposition of Al_2O_3. Reduction of gallium oxide for sample A is expected as this effect has already been discussed when using TMA as the ALD precursor for aluminium. However, the same explanation for sample C would require the self-cleaning reactions to take place through a buffer layer approximately 7 Å of Si and Si-O. Since there is no change in the GaAs/Si interface for sample D (Al_2O_3 on Si on AHT GaAs) following the deposition of Al_2O_3 it seems unreasonable to assume that TMA interacts with the Ga-O under the Si layer in the case of sample C. Yamada *et al*[40] reports the desorption of Ga_2O species at temperatures as low as 350 °C. The ALD requires a substrate temperature of 300 °C. The interaction of silicon with the Ga-O bonds may facilitate a lower desorption temperature and could be a possible explanation for the reduction in Ga-O bonding for sample C after the deposition of Al_2O_3.

The Ga 3p and Si 2p spectra for samples C and D (samples with a silicon interlayer prepared by NH_4OH and AHT respectively) are shown in figure 6.18. An increase in the concentration on Si-O bonds after the deposition of Al_2O_3 is noted for both samples and is assumed to be at the Si/Al_2O_3 interface. For the purpose of calculating the thicknesses of the individual layer, the thickness of the Si-O layer at the Si/GaAs interface was assumed to have remained unchanged. This allowed for the remainder of the Si-O signal to be attributed to silicon oxide at the Si/Al_2O_3 interface.

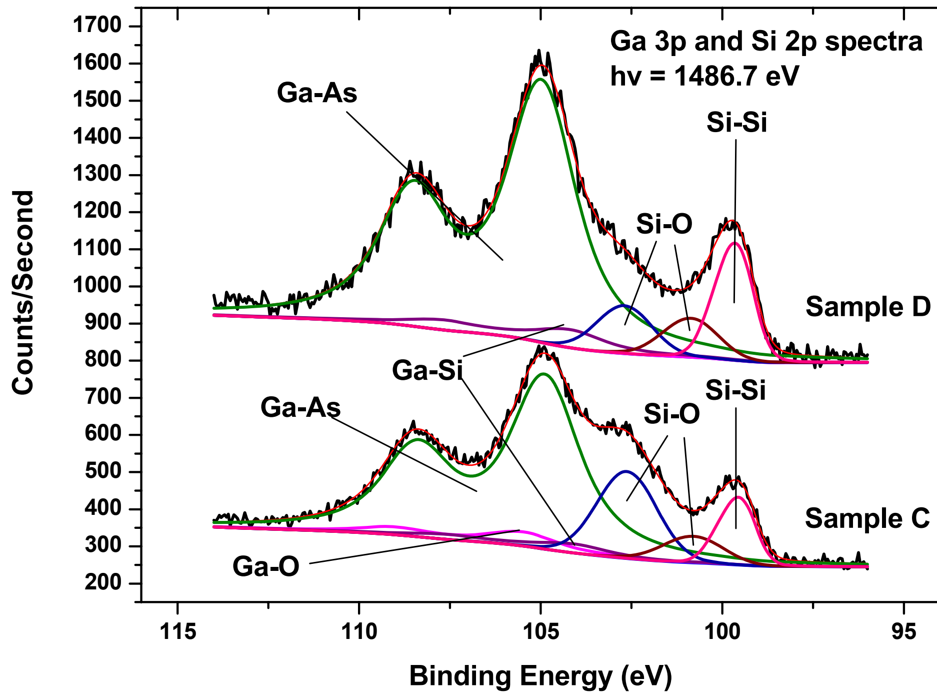

Figure 6.18 Ga 3p and Si 2p spectra for samples C and D after the ALD of 1 nm Al_2O_3.

The main focus of this study was to examine the effects of a silicon interlayer on the anomalous frequency dependant dispersion of accumulation capacitance that is seen on n-type GaAs.[2] C-V characteristics were studied at room temperature for a range of frequencies on each of the above samples. Figure 6.19 shows plots of this data and it can be seen clearly that sample D (Al_2O_3 on Si on AHT GaAs) is the only sample to display a reduced dispersion of accumulation capacitance even though there is still a clear shift in the flat band voltage for which will be discussed later. Firstly an attempt will be made to correlate the electrical results with the photoemission data discussed earlier.

The striking difference between C-V characteristics C and D despite both utilising a silicon interlayer is attributed to presence (C) and absence (D) of surface oxides before silicon deposition. Such differences however are seen to have little effect on the electrical characteristic when the silicon interlayer is not used as in samples A (surface oxides present) and B (no surface oxides) and this is due to the presence of interfacial oxides after high-κ deposition regardless of the starting surface as seen in figure 6.17. Comparing the electrical data seen in figure 6.19 to the

chemical analysis conducted earlier in this section and shown in figure 6.17, the only feature that is unique to sample D is its complete lack of a gallium oxide signal. All samples have displayed a lack of arsenic oxide and a detectable presence of elemental arsenic. Sample B does show a slight reduction in the dispersion of accumulation capacitance which is consistent with the argument that gallium oxide species are primarily responsible for the anomalous frequency dispersion effect since the only chemically observed difference between samples A and B was the reduced intensity of the gallium oxide feature for sample B.

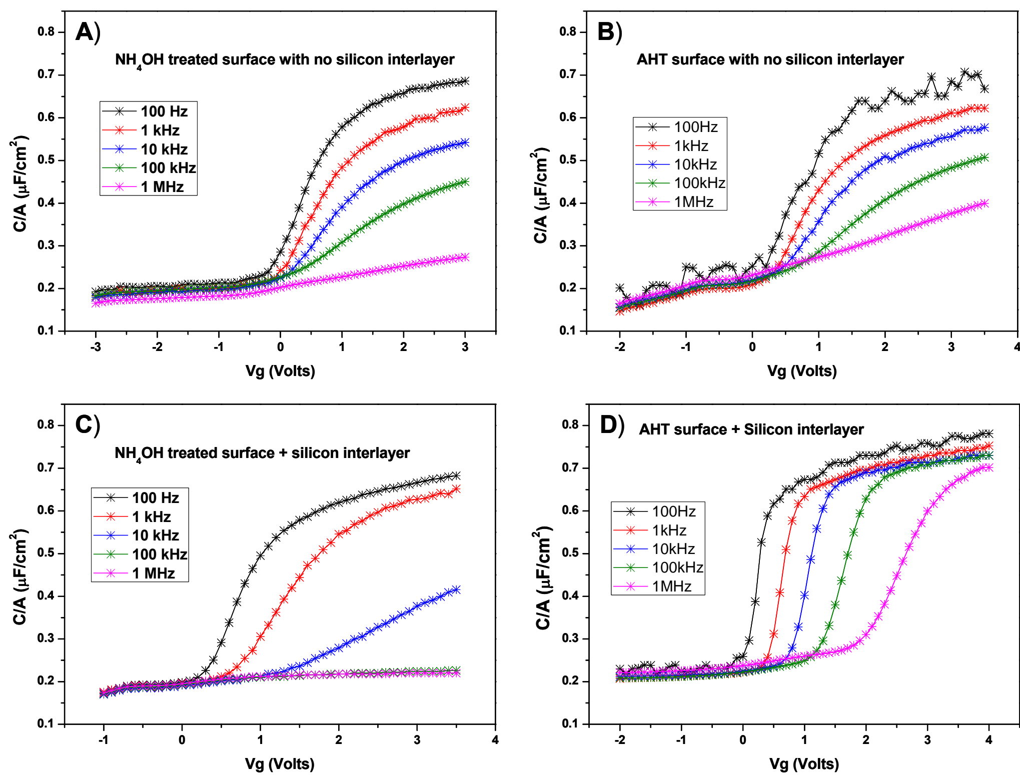

Figure 6.19 C-V characteristics for samples A-D with capacitance given per unit area.

In comparison to other studies, it should be noted that the Si interlayer thickness for sample D of approximately 7 Å is substantially lower than the optimal thickness suggested by Oktyabrsky *et al*[7] of 15 Å. In that study, silicon interlayers of 5, 7 and 10 Å showed little to no improvement in the maximum capacitance for a 1 MHz sweep. It is possible that the *ex-situ* deposition of the high-κ material in that study required the silicon to be of a sufficient thickness to act as an oxygen diffusion barrier for the duration of time the sample was exposed to atmosphere prior to the gate

dielectric deposition. In this present study, the *in-situ* deposition of the high-κ material allowed for a thinner interlayer to achieve similarly high maximum capacitance for the 1 MHz sweep.

Hasegawa and Sawada[2] (HS) discussed how it should not be assumed that high interface state densities alone are responsible for pinning the Fermi level and causing the anomalous frequency dependant dispersion of accumulation capacitance on n-type GaAs. They stated that modelling the C-V characteristics of high-κ/nGaAs using standard Nicollian and Brews (NB) interfaces states[48] requires not only extremely high interface state densities but also unrealistic capture cross sections of physical dimensions greater than the device size. They have shown that the anomalous frequency dispersion of accumulation capacitance can be modelled by assuming that interface traps are not limited to the surface but instead have an exponentially decaying spatial distribution into the dielectric. A valid reason for the use of a different model in the case of a high-κ/GaAs interface is the possible presence of a 'disorder low band-gap region' at the interface. If we assume that the reduced frequency dependant dispersion of accumulation capacitance seen when Al_2O_3 is deposition on an interfacial oxide free silicon/nGaAs surface (sample D) is due to the absence of the disordered low bandgap region then the standard NB theoretical model can be used to determine the interface state density. This has been modelled and shown in figure 6.20a and the extracted value for the interface state density (D_{it}) was 5 x 10^{-13} cm^{-2} eV^{-1}. Using an interface state density (D_{it}) of 5 x 10^{-13} cm^{-2} eV^{-1} in the HS model which assumes the presence of a disordered low bandgap region, results in the theoretical C-V characteristics shown in figure 6.20b. This shows that the presence or absence of the disorder low bandgap region rather than solely a high interface state density can explain the frequency dependant dispersion of accumulation capacitance.

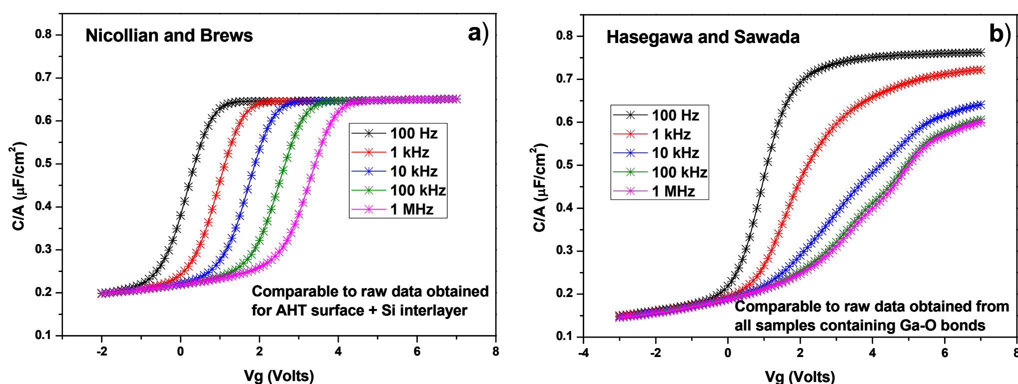

Figure 6.20 a) Nicollian and Brews[48] and b) Hasegawa and Sawada[2] models using 5 x 10^{13} cm^{-2} eV^{-1} as a parameter for interface state density.

The results from the chemical analysis here, when combine the C-V characteristics and interface state density modelling, implies that a Al_2O_3/nGaAs system could have equally high interface state densities to a Al_2O_3/Si/nGaAs system but the presence of Ga-O would cause it to display the frequency dependant dispersion of accumulation capacitance while the Al_2O_3/Si/nGaAs system would not.

6.4 Conclusion

The high-κ on GaAs system has been studied *in-situ* with monochromated XPS during various stages of the cleaning and deposition processes. A detailed analysis was made on NH_4OH treatment and *in-situ* high temperature anneals on GaAs native oxide. When compared to other studies it could be concluded that while the NH_4OH may remove most of the native oxide, it does not passivate the surface and so a thin oxide layer will always be present. The *in-situ* anneals showed that at temperatures greater than 300 °C a bond conversion process takes place were oxygen bonded to arsenic transfers to Ga-O bonds. Exposure of an untreated GaAs surface to atomic hydrogen at a substrate temperature of more than 400 °C was found to be an effective way of removing both arsenic and gallium oxides.

The deposition of Al_2O_3 and HfO_2 by ALD using TMA and TEMA-Hf as sources for Al and Hf respectively on NH_4OH treated and GaAs native oxide showed that both reduced the interfacial gallium and arsenic oxide to below there original

levels. It was found that TMA preferential removed the lower coordination number oxidation states while TEMA-Hf preferential removed the high coordination number oxidation states. Because aluminium oxidises in a Al^{3+} oxidation state the selective removal of As^{3+} is consistent. First principle calculations have shown that higher coordination of the Hf in HfO_2 is more stable than lower coordination[49] and so the selective removal of As^{5+} may be energetically favourable rather than forcing the Hf into lower coordination to remove As^{3+}.

The investigation of how the use of a silicon interlayer improves the C-V characteristics of the high-κ/nGaAs showed that Ga-O bonds are the most likely cause of the frequency dependant dispersion of accumulation capacitance. When this result was considered along with the work of Hasagawa and Sawada[2] it could be concluded that a gallium oxide interfacial region is the disordered low bandgap region which is assumed to be present for the application of their interface state density model.

6.5 References

[1] S. Kayali, G. Ponchak, R. Shaw, JPL 96-25 (1996)

[2] H. Hasegawa and T. Sawada, IEEE Trans. Electron Devices **27**, (1980) 1055

[3] W.E. Spicer, I. Lindau, P.E. Gregory. C.M. Garner, P. Pianetta and P.W. Chye, J. Vac. Sci. Technol. **13** (1976) 780

[4] M. J. Hale, S. I. Yi, J. Z. Sexton, A. C. Kummel and M. Passlack, J. Chem. Phys. **119**, (2003) 6719

[5] H. Hasegawa, M. Akazawa, H. Ishii and K. Matsuzaki, J. Vac. Sci. Technol. B **7**, (1989) 870

[6] J. L. Freeouf, D. A. Buchanan, S. L. Wright, T. N. Jackson and B. Robinson, Appl. Phys. Lett. **57**, (1990) 1919

[7] S. Oktyabrsky, V. Tokranov, M. Yakimov, R. Moore, S. Koveshnikov, W. Tsai, F. Zhu and J. C. Lee, Mater. Sci. Eng., B **135**, (2006) 272

[8] S. J. Koester, E. W. Kiewra, Y. Sun, D. A. Neumayer, J. A. Ott, M. Copel, D. K. Sadana, D. J. Webb, J. Fompeyrine, J. P. Locquet, C. Marchiori, M. Sousa and R. Germann, Appl. Phys. Lett. **89**, (2006) 042104

[9] H.-S. Kim, I. Ok, M. Zhang, C. Choi, T. Lee, F. Zhu, G. Thareja, L. Yu and J.C. Lee Appl. Phys. Lett. **88** (2006) 252906

[10] G. Hollinger, R. Skheyta-Kabbani and M. Gendry, Phys Rev B **49** (1994) 11159

[11] M. V. Lebedev, D. Ensling, R. Hunger, T. Mayer and W. Jaegermann, Applied Surface Science **229** (2004) 226

[12] T. Van Buuren, M. K. Weilmeier, I. Athwal, K. M. Colbow, J. A. Mackenzie, T. Tiedje, P. C. Wong and K. A. R. Mitchell, Appl. Phys. Lett **59(4)** (1991) 464

[13] J. Ivanco, T. Kubota and H. Kobayashi, J. of Appl. Phys. **97** (2005) 073712

[14] F. Schröder, W. Storm, M . Altebockwinkel, L. Wiedmann and A. Benninghoven, J. Vac. Sci. Technol. B **10(4)** (1992) 1291

[15] P. D. Ye, G. D. Wilk, B. Yang, J. Kwo, S. N. G. Chu, S. Nakahara, H. –J. L. Gossmann, J. P. Mannaerts, M. Hong, K.K. Ng and J. Bude. Appl. Phys. Lett **83** (2003) 180

[16] M. M. Frank, G. D. Wilk, D. Starodub, T. Gustafsson, E. Garfunkal, Y. J. Chabal, J. Grazul and D. A. Muller, Appl. Phys. Lett. **86** (2005) 152904

[17] G. K. Dalapati, Y. Tong, W. -Y. Loh, H. K. Mun and B. J. Cho IEEE Trans. Electron Devices **54(8)** (2007) 1831

[18] M. L. Huang, Y. C. Chang, C. H. Chang, Y. J. Lee, P. Chang, J. Kwo, T. B. Wu and M. Hong, Appl. Phys. Lett **87** (2005) 252104

[19] C. H. Chang. Y. K. Chiou, Y. C. Chang, K. Y Lee, T. D. Lin, T. B. Wu, M. Hong and J. Kwo, Appl. Phys. Lett. **89** (2006) 242911

[20] S. Arabasz, E. Bergignat, G. Hollinger, J. Szuber, Vaccum **80** (2006) 888

[21] I. Ok, H.-S. Kim, M. Zhang, C.-Y. Kang, S. J. Rhee, C. Choi, S. A. Krishnan, T. Lee, F. Zhu, G. Thareja, J. C. Lee, IEEE Electron Device Letters **27** (2006) 145

[22] D.Ghidaoui, S. B. Lyon, G.E. Thompson, J. Walton, Corrosion Science **44** (2002) 501

[23] J. Massies and J. P. Contour, J. Appl. Phys. **58** (1985) 806

[24] S. Oktyabrsky, V. Tokranov, M. Yakimov, R. Moore, S. Koveshnikov, W. Tsai, F. Zhu, J. C. Lee Materials Science and Engineering B **135** (2006) 272

[25] Y. Xuan, H.C. Lin and P. D. Ye, IEEE Trans. Electron Devices **54** (2007) 1811

[26] N. Braslau, J. Vac. Sci. Technol. **19** (1981) 803

[27] C. D. Wagner, A. V. Naumkin, A. Kraut-Vass, J. W. Allison, C. J. Powell and J. R. Rumble Jr. *NIST X-ray Photoelectron Spectroscopy Database* located @ http://srdata.nist.gov/xps/

[28] F. J. Himpsel, F.R. McFreely, A. Taleb-Ibrahimi, J.A. Yarmoff and G. Hollinger, Phys. Rev. B **38**, (1988) 6084

[29] C. D. Wagner, L. E. Davis, M. V. Zeller, J. A. Taylor, R. H. Raymond and L. H. Cole, Surface and Interface Analysis **3(5)** (1981) 211

[30] R. O'Connor, S. McDonnell, G. Hughes, K. E. Smith, Surface Science **600** (2006) 532

[31] Z. H. Lu, C. Lagarde, E. Sacher, J. F. Currie, and A. Yelon, J. Vac. Sci. Technol. A **7(3)** (1989) 647

[32] G. Hughes, R. Ludeke, J. F. Morar and J. L. Jordan, J. Vac. Sci. Technol. B **3(4)** (1985) 1079

[33] K. Tone, M. Yamada, Y. Ide and Y, Katayama, Jpn. J. Appl. Phys. **31** (1992) L721

[34] C. J Powell, A Jablonski, *NIST Electron Effective-Attenuation-Length Database* version 1.0 copyright 2001

[35] G.W.C. Kaye, T.H. Laby *Tables of Physical and Chemical Constants* (16th edition) Longman: Harlow (1995)

[36] D. R. Lide, *CRC Handbook of Chemistry and Physics* (88th edition) CRC Pres: Boca Raton, FL, (2000)

[37] B. K. Tanner, D. A. Allwood, N. J. Mason, Materials Science and Engineering B **80** (2001) 99

[38] M. P. Seah and S. J. Spencer, Surf. Interface Anal. **33** (2002) 640

[39] T. Akatsu, A. Plößl, H. Stenzel, U. Gösele, J. Appl. Phys. **86(12)** (1999) 7146

[40] Y. Ide, M. Yamada, JVST A (**12)4** (1994) 1858

[41] M. Yamada, Y. Ide, Jpn. J. Appl. Phys. **33** (1994) L671

[42] M. Yamada, Y. Ide, K. Tone, Jpn. J. Appl. Phys. **31** (1992) L1157

[43] I. Jiménez, F. J. Palomaresa and J. L. Sacedón, Phys Rev B **49(16)** (1994) 11117

[44] J. Ivanco, T. Kubota, H. Kobayahsi, J. Appl. Phys. **97** (2005) 073712

[45] I. Jiménez, J. L. Sacedón, JVST B **12(6)** (1994) 3095

[46] J. J. Yeh and I. Lindau, Atomic Data and Nuclear Data Tables **32** (1985) 1

[47] A. Chambers, V. A. Loebs, Phys Rev B **47(15)** (1993) 9513

[48] E. H. Nicollian and J. R. Brews, MOS Physics and Technology, Wiley, Hoboken, NJ, (1982)

[49] G. Jun and K. Cho, Mater. Res. Soc. Symp. Proc. **747** (2003) 5.1.1

7 Characterisation of hafnium germanate dielectric films on germanium(100) substrates

7.1 Introduction

As discussed in the introduction to this thesis, much of the early semiconductor research was conducted on germanium as well as silicon. The poor electrical quality of the GeO_x/Ge system compared to the SiO_2/Si system resulted in germanium failing to become the dominant substrate of choice by the semiconductor industry. Germanium's higher electron and hole mobilities when compared to silicon give it the potential to provide higher performance devices than even strained silicon layers[1], and the move away from the SiO_2/Si removes one of the main advantages that silicon has over germanium, namely the excellent quality of the native oxide. Germanium is far less abundant than silicon and is estimated as 1.3 parts per million (ppm) in the earth's crust[2] in comparison to silicon 2.7×10^5ppm which makes its use inherently more costly. However, germanium on insulator (GOI) technologies have been demonstrated[3,4] and provide the possibility of utilising the mobility and GaAs lattice matching advantages on germanium without incurring the cost of manufacturing germanium wafers.

The prevention of unfavourable GeO_x species at the germanium/insulator interface is one of the main goals in fabricating high quality MOSFETs devices using germanium. To this end, many interlayers have been suggested for use in high-κ/Ge systems.[5-9] In this chapter a fundamental study of the interfacial chemistry present for hafnium germanate (HGO) films on germanium is undertaken. In particular, the interfacial chemistry of films grown with germanium oxynitride, silicon and germanium nitride interlayers will be examined. Preliminary work of the surface preparation of germanium substrates will also be presented. The HGO films were studied as a preliminary trial before moving to nitrided hafnium germanate films. The electrical characteristics of GeON/Ge show promise,[10] however, the dielectric constant of GeON is not high enough to allow for long term scaling of device dimensions. It is hoped that the addition of hafnium into the GeON film will provide a high-κ dielectric option while preserving the good characteristics of the GeON/Ge interface. This chapter outlines the exploratory study of the HGO/interlayer/Ge systems monitored by *in-situ* monochromatic XPS.

7.2 Experimental

7.2.1 Samples

These experiments were carried out at the University of Texas at Dallas using the UHV system C described in section 3.1. For these studies 1 cm x 1cm pieces were cut from 3 inch germanium wafers of (100) orientation doped n-type with a concentration of 1.54×10^{18} -1.88×10^{17} dopants/cm^{-3} using Sb and resulting in a resistivity of 0.005 Ω cm - 0.02 Ω cm. Before the growth of GeN, GeON or Si interlayers on the germanium samples, the substrates were prepared by *in-situ* UV ozone treatment which was explained in section 3.4 and results in a carbon free GeO_x layer. GeON interfacial layers can then be prepared by nitriding the GeO_x in a nitrogen plasma as described in section 3.4. This was achieved by striking a plasma and low power (10W) over a HfO_2 sputter target. This power is low enough that no hafnium is detected by XPS even after 60 minutes of nitridation. Before Si or GeN interlayers were grown, the germanium substrate was cleaned of all oxygen by heating to 400 °C after UV ozone cleaning. This procedure is similar to the flash cleaning of silicon performed in section 4.2.1. Silicon depositions were conducted at a deposition rate of approximately 20 Å/min by e-beam deposition from a silicon source in a silicon crucible with the Ge sample wafer kept at room temperature in the MBE deposition chamber of the multi-technique deposition/characterisation UHV system. GeN was formed by the nitridation of the clean germanium substrate in the same way as GeON was formed.

The growth of HGO was achieved by co-sputtering from separate HfO_2 and Ge targets in a back pressure of 1×10^{-6} mbar of oxygen using an argon plasma with an argon flow rate of 80 sccm (providing a growth pressure of 10 mtorr). Due to the high sputtering coefficient of germanium, the powers on the HfO_2 and Ge targets were 150 W and 30 W respectively.

7.2.2 Characterisation:

The chemical characterisation was carried out using XPS and ultra-violet spectroscopy (UPS) in system 'C' described in chapter 3. The samples were transported under vacuum between the UV ozone treatment chamber, the interlayer/high-κ deposition chambers and the analysis chamber. Electrical characterisation was carried out after the *in-situ* deposition of aluminium as a back contact and the *ex-situ* deposition of platinum as a front contact through a shadow mask.

7.3 Results

7.3.1 Native oxide and fitting

Like silicon, germanium forms a thin native oxide layer in air. In the case of silicon, a chemically grown oxide layer is often used as a barrier to protect the surface of the silicon from carbon contamination. Unlike SiO_2 the native germanium oxide (GeO_2) is water soluble and is therefore unstable in air, making it unsuitable to be used as a barrier layer to protect the germanium substrate from carbon contamination. Due to this fact removing this oxide and passivating the germanium surface is not a trivial task.

Figure 7.1 shows the XPS spectra of Ge 3d and 2p regions for an untreated native oxide covered germanium wafer. Works by other authors show that the oxidation of germanium is similar to silicon in that it can be deconvolved into four oxidation states.[11,12] While similar spectra are often fitted with only a single interfacial and bulk oxide component,[13,14] the use of a monochromated x-ray source in this study allowed for all 4 oxidation states to be detected. Reports on the magnitude of the chemical shifts for each of these states indicate that the binding energy separation between the different oxidation states 0.85-0.91 eV per electron.[11,12] When fitting the spectra shown in figure 7.1, the binding energy of the Ge 2p substrate component was referenced to the substrate signal from the Ge 3d region in order to ensure that the

oxide features in the surface sensitive Ge 2p region did not distort the fitting process. The required separation between these components was found to be 1187.69 eV from an oxide free substrate and the binding energy of the Ge 2p substrate feature was allowed to vary only ± 0.05 eV from this value since no greater experimental accuracy can be claimed. Referencing the spectra to the Ge 3d core-level position for clean germanium negates both the positive shift in binding energy expected due to sample charging, seen on many oxides, as well as the negative shift in binding energy due to band bending which would be expected for oxidised n-type germanium. Measurement of the amount of band bending due to the over-layers is not possible since no trustworthy binding energy reference other than the substrate is available.

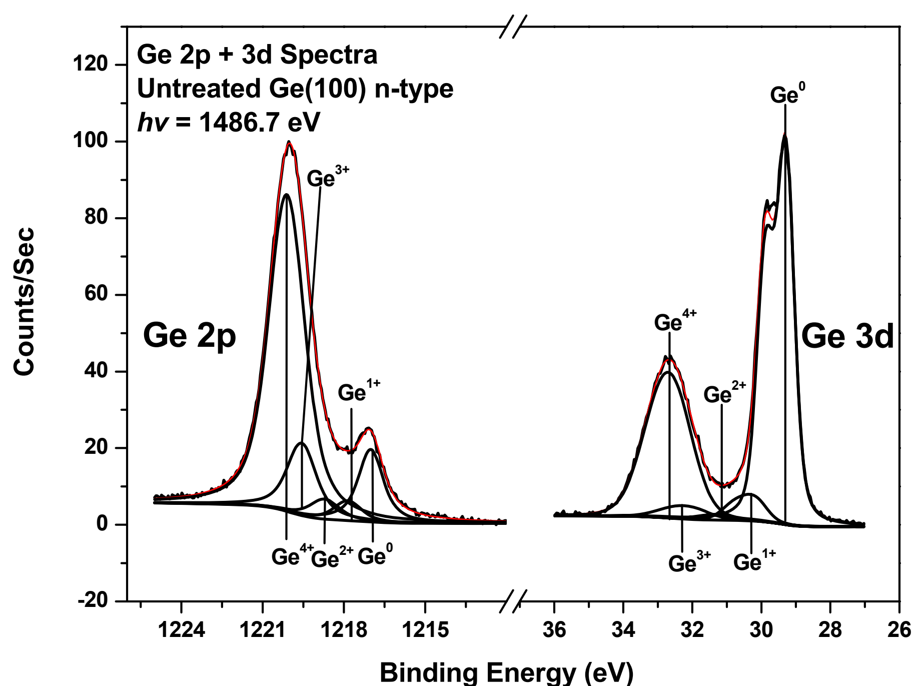

Figure 7.1 The Ge 2p and Ge 3d XPS spectra for the native oxide on germanium

In this work, the core-level chemical shift (CLCS) for the Ge^{4+} state was left as a free parameter in order to obtain the best fit which resulted in a value for the CLCS of 3.1 eV for the Ge 2p core-level and 3.19 eV for the Ge 3d. As a starting point for the sub-oxides they were spaced evenly between the substrate and bulk oxide peak. While this results in a reasonable fit for the native oxide, since the suboxide signals are relatively small in comparison to the bulk oxide and substrate features, fitting thinner oxides that will be shown throughout this chapter required that the sub-

oxides be spaced 0.85(0.91) eV from the Ge 2p(3d) substrate core-level. This results in the Ge^{3+} and Ge^{4+} features being separated by only 0.55(0.46) eV for the Ge 2p(3d) regions but good fits can be obtained with these CLCS fixed for a variety of different thermally and chemically treated samples that will be shown throughout this study.

As discussed in chapter 2, the availability of two strong core-level features with very different binding energies allows for an overlayer thickness to be accurately established if the electron attenuation lengths for each core-level are known,[15] without any knowledge of the expected ratio (R_0) between overlayer and substrate that is normally obtained theoretically or from a clean substrate and an infinitely thick overlayer. Equation 2.13, repeated here as 7.1, then gives an expression

$$\frac{I_{S,HKE}}{I_{A,HKE}}\left[\exp[\frac{+d}{l_{HKE}(\cos\theta)}]-1\right]=\frac{I_{S,LKE}}{I_{A,LKE}}\left[\exp[\frac{+d}{l_{LKE}(\cos\theta)}]-1\right] \quad (7.1)$$

from which the overlayer thickness can be deduced. The electron attenuation lengths for the high kinetic energy core-level (Ge 3d) and low kinetic energy core-level (Ge 2p) were found to be 28.4 Å and 7.3 Å respectively from the NIST EAL database.[16] These were calculated assuming a density for GeO_2 of 4.25 g/cm^3 taken from Kaye *et al*.[17] The calculated thickness for the native oxide of the untreated samples was 11.2 Å.

7.3.2 Native oxide removal

There have been many reports of sample preparation methods for germanium substrates. Okumura *et al*[18] preparing samples for MBE, reports a surface preparation technique involving sequential chemical oxide formation using H_2O_2 and removal with HCl/H_2O(1:4), followed by the growth of a sub-stoichiometric protective oxide using $NH_4OH/H_2O_2/H_2O$(0.5:1:10) with no subsequent deionised water rinse. This oxide can then be removed by UHV annealing to 400 °C with no detectable surface contamination seen on the final surface. Hovis *et al*[19] reported that for atomically clean, carbon free, samples for STM studies, the chemical preparation suggested by Okumura *et al*[18] must be followed by UV/ozone exposure. The samples would then be outgassed at 300 °C for 5 hours before flashing to 727 °C while maintaining a

pressure better than 5×10^{-10}Torr. Other reported surface preparations include successful sulphur passivation[20] and NH_3 treatments[5] while Choi *et al*[21] reported successful hydrogen passivation with hydrofluoric acid (HF) is possible. The germanium oxide can be 'flash cleaned' in vacuum in a manner similar to silicon oxide but at much lower temperatures as 390 °C is sufficient to desorb the oxygen from the germanium substrate.[22] Also, pre-treating the sample by UV/ozone oxidation can be helpful for removing carbon prior to oxide removal.[19,22] The use of deionised water is known to dissolve the bulk of the oxide leaving only sub-oxides that are not water soluble.[19]

Figure 7.2 shows raw XPS data obtained after each of the cleaning steps taken in this study and the results are similar to the work of Zhang *et al.*[22] Sample charging has been accounted for by referencing to the Ge 3d substrate peak at 29.28 eV. A typical spectrum obtained from an untreated sample is shown as (a) while the effects of four surface treatments on the Ge 2p, O 1s and C 1s signals are also summarised. These include a 20 second deionised water (DIW) rinse (b) and a 10 minute HF (10%) etch (c), both of which appear to have similar affects on the surfaces. They remove the bulk GeO_2 but leave noticeable sub-oxide and carbon signals. High temperature annealing to 400 °C (d) appears to remove all oxides but does not remove all carbon, while UV-ozone (e) followed annealing (f) removes both surface oxides and carbon

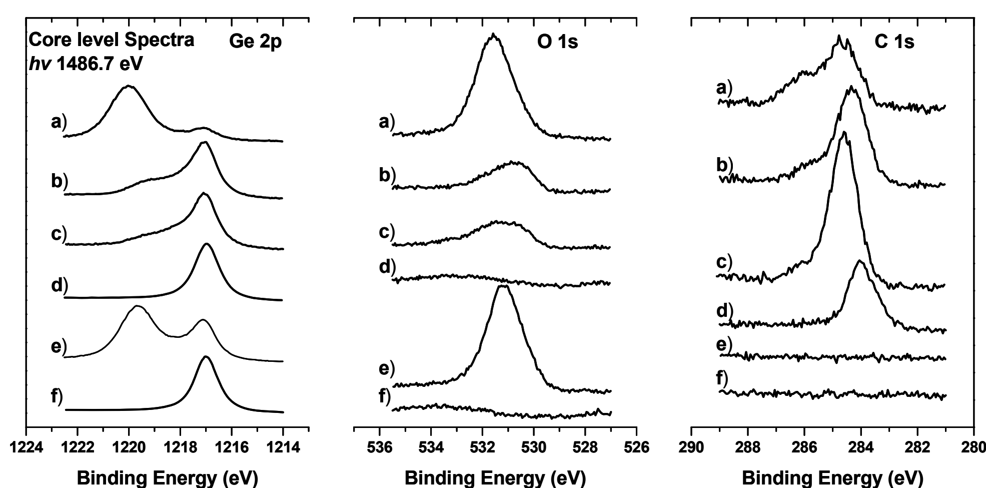

Figure 7.2 The Ge 2p, O 1s and C 1s XPS spectra for a range of surface treatments, a) untreated, b) 20secs DIW rinse, c) 10 min HF (10%) emersion, d) 400 °C flash clean, e) 20min UV/ozone exposure, f) sample e) after a 400 °C flash clean.

contamination resulting in the cleanest samples achieved during this work. Table 7.1outlines the treatment procedures for each sample.

Sample	DIW Rinse	HF Etch	UV Ozone	400 °C Anneal
A				
B	✓			
C		✓		
D				✓
E			✓	
F			✓	✓

Table 7.1 Clean procedures performed on samples a-f shown in figure 7.2.

Water, Hydrofluoric Acid and *in-situ* annealing

Figure 7.3 shows a peak fitted comparison of 400 °C annealed, DIW treated and HF treated germanium substrates. All treatments were performed on separate 'out of the box' samples with no additional pre-treatments and the spectra are referenced

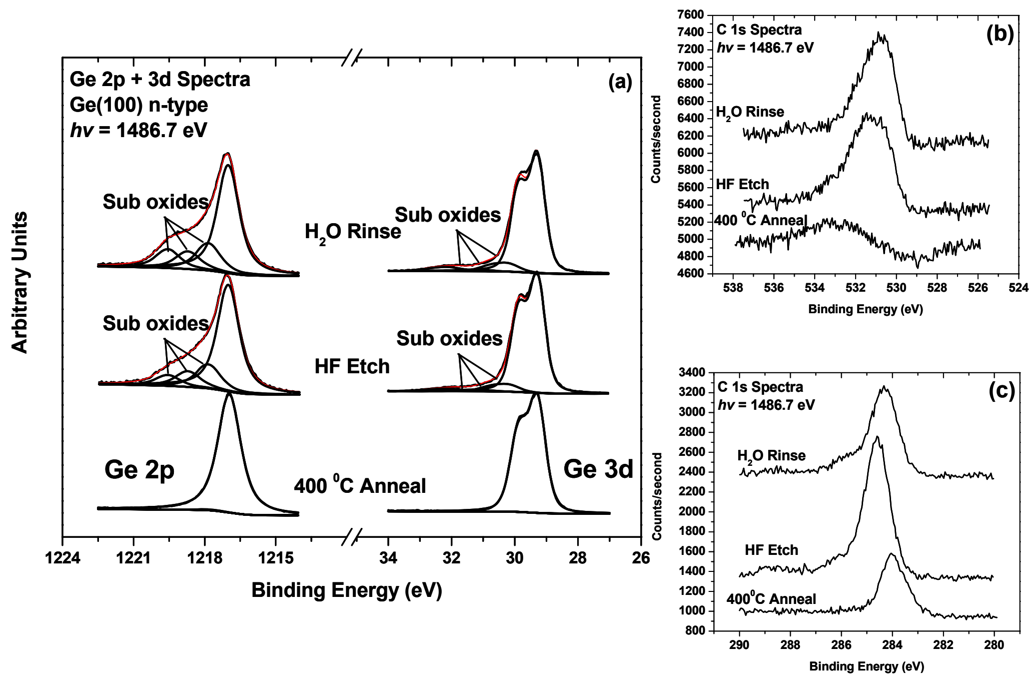

Figure 7.3 a) The deconvolved Ge 3d XPS core-level for sample b-d) along with the O 1s and C 1s core-levels.

to the known binding energy of the Ge 3d core-level from clean germanium (sample f). As in the case of the native oxide spectra, this referencing procedure compensates for surface charging affects.

The surface sensitive 2p region in figure 7.3a shows clearly the presence of all 3 sub-oxide features after H_2O and HF treatments and the calculated oxide thicknesses were found to be 2.8 Å and 1.7 Å respectively which are both effectively equal to or less than one monolayer. The native GeO_2 is known to be unstable in water and is easily removed. However the sub-oxides are not water soluble and their removal by H_2O would not have been expected. While the HF treatment may indeed have removed the sub-oxides, its failure to passivate the surface would have allowed for the rapid re-growth of sub-oxides between etching and the placement of the samples in vacuum.

As seen in figure 7.3a and figure 7.3b annealing to 400 °C completely removes the native oxide, however figure 7.3c shows that the surface is still contaminated by carbon. The C 1s core-level is found to be 0.5 eV lower in binding energy than the 284.5 eV expected for typical surface contamination. This normally indicates the formation of a carbide,[23] however, it has been noted by Zhang *et al*[22] that there is no known germanium carbide. Nevertheless, they still suggest that the shift in binding energy most likely indicates that the carbon is chemisorbed on the germanium substrate. The shift in the binding energy of the carbon 1s core-level also suggests that referencing to surface carbon, as has been done by other groups, in order to yield information about banding bending may be unreliable.[24] Also, when comparing the Ge 2p and 3d features after the 400 °C anneal to sample (f) from figure 7.2 the peak widths are found to be slightly larger for sample (d) which would indicate a greater variation in the number of bonding environments. This is typically seen, to a greater extent, after the argon bombardment of crystals and so could be interpreted as indicating a slightly damaged surface.[25] Since the HF treatment showed no significant improvement over a simple H_2O rinse, HF was not used in any pre-treatments on germanium for the rest of these studies.

UV-Ozone cleaning:

A more successful germanium cleaning procedure is *in-situ* UV ozone cleaning. After rinsing the germanium samples in DI water, to remove the bulk GeO_2, the samples were placed in the UHV system where they were exposed to UV ozone for 20 mins as described in the section 3.4. It can be seen in figure 7.4 that, along with increasing the amount of oxidised germanium to a thickness of 6.9 Å, this procedure completely removes all carbon.

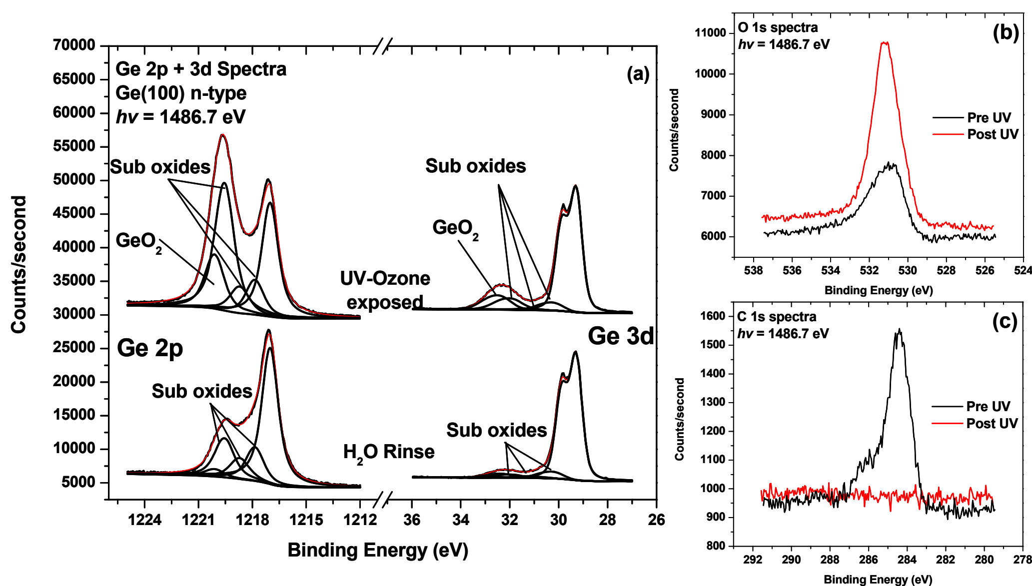

Figure 7.4 a) The deconvolved Ge 3d and 2p XPS core-level for sample b) and e) along with the O 1s and C 1s core-levels of the surface before and after UV-ozone cleaning.

Unlike the native oxides seen in Figure 7.1 the UV ozone exposed samples show a strong Ge^{3+} feature. This would indicate that the *in-situ*, ozone grown germanium oxide is chemically different to the native oxide which grows in air. This oxidised surface can be nitrided to form GeON or the oxide can be removed, if required, by flashing the sample to 430 °C which leaves the surface oxygen and carbon free. It is spectra from these samples, shown in figure 7.5 that have been used as a reference for the Ge 2p and 3d peak widths and binding energy separation.

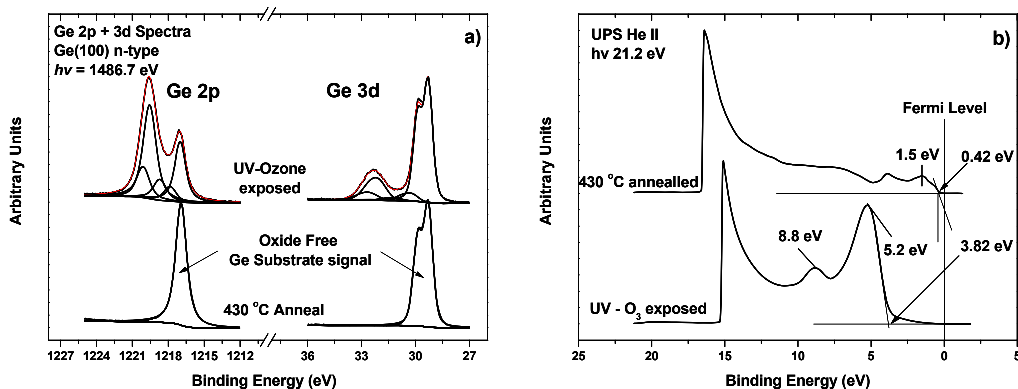

Figure 7.5 a) The deconvolved Ge 3d and 2p XPS core-level for sample e-f) as well as b) UPS spectra of the valence band structure of the same samples.

Included in figure 7.5b are the valence band spectra obtained by UPS at 21.2 eV which clearly shows the separation between the valence band states and the Fermi level for the UV ozone exposed samples along with the reduction in this offset for the oxide free surface. A separation between the valence band maximum (VBM) and the Fermi of 0.42 eV for the clean germanium indicates that the Fermi level is in the upper half of the gap which is to be expected for an n-type germanium sample. A VBM of 3.8 eV below the Fermi level for the UV ozone exposed sample is close to the value of 4 eV reported by Ohta *et al*.[26] Prabhakaran *et al*[27] describes a feature at 1.38 eV below the valence band maximum as indicating a clean surface while a feature at 5.2 eV is expected after oxidation. The features seen at binding energies of 1.5 eV and 5.2 eV for the clean and oxidised germanium in this study can be used to indicate a clean and oxidised surface in a similar manner.

7.3.3 Interlayers

The poor quality of GeO_2 as a dielectric material has resulted in studies where interlayers are grown to prevent the formation of GeO_x species at the high-κ germanium interface. Bai *et al*[6] utilised a crystalline silicon interlayer, while Sugawara *et al*[7] has compared GeO_x, GeON, and TaON interlayers. Kim *et al*[8] and Elshocht *et al*[9] used NH_3 anneals to form thin GeON interlayers. Maeda *et al*[9] suggested that Ge_3N_4 would make a suitable oxygen diffusion barrier enabling its use as an interlayer in germanium metal-insulator-semiconductor structures. Presented in

this section is a spectroscopic study of GeN, GeON and Si layers grown on germanium with the view to using these films as interlayers in high-κ/interlayer/Ge systems. These samples were prepared as described in chapter 3.4 and 7.2.1. Figure 7.6 illustrates the difference in the core-level spectra of the Ge 2p and 3d regions for GeO_2/Ge, GeON/Ge and GeN/Ge interfaces. The noticeable shift in the overlayer's binding energy with respect to the substrate as the nitrogen is introduced confirms that the germanium bonding environment has been changed.

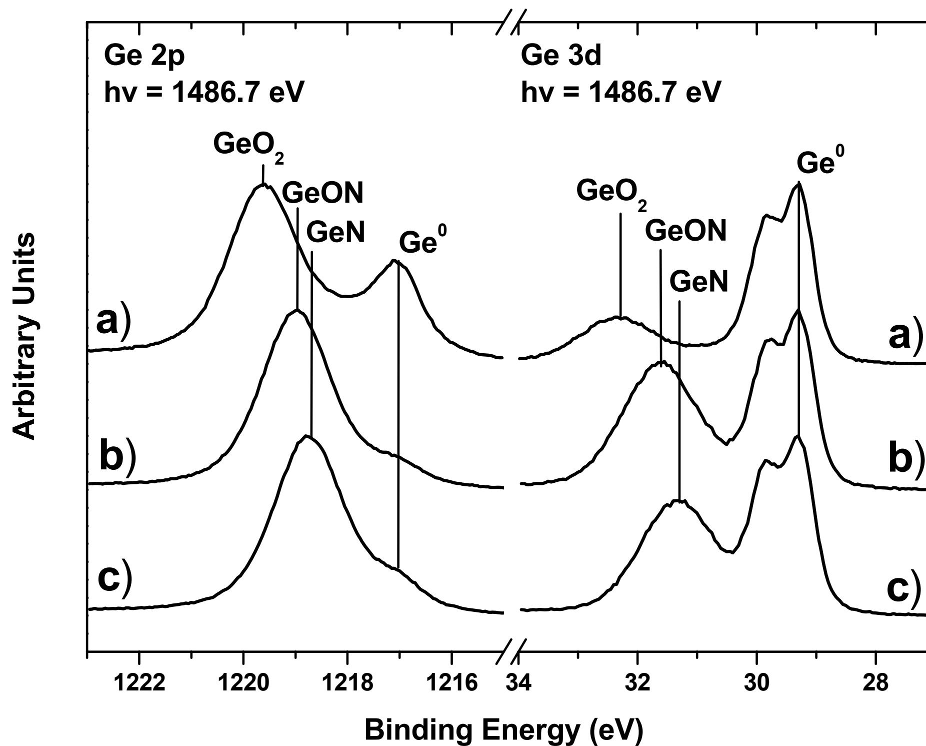

Figure 7.6 The Ge 2p and 3d XPS core-level spectra for a) UV/ozone treated Ge, b) UV/ozone treated germanium post nitridation and c) cleaned germanium post nitridation.

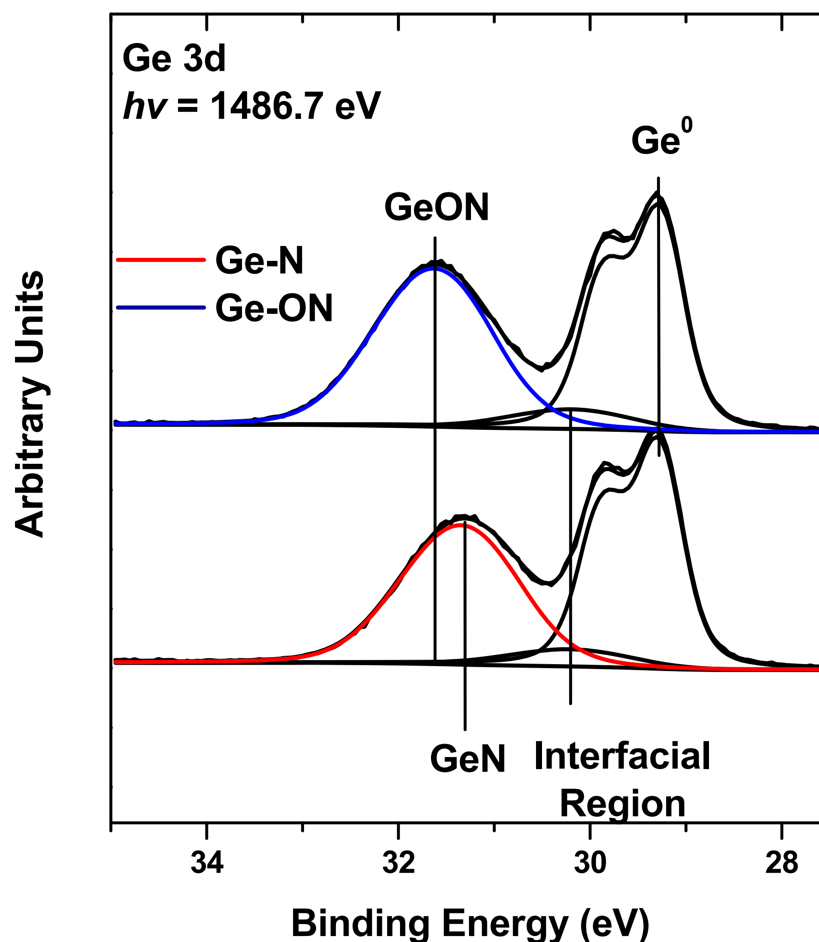

Figure 7.7 The cure fitted Ge 3d XPS core-level spectra of the GeON and GeN interlayers.

These core-level spectra have been deconvolved into three components (substrate, interface and overlayer) to allow for thickness approximations to be made and the fits are shown in figure 7.7. The thicknesses for the GeON and GeN have been calculated as 11.8 Å and 9.5 Å respectively using the assumption that the atomic densities are approximately the same for GeON and GeN as GeO_2. In reality their densities are most likely greater than GeO_2, however, reliable estimates for the densities of layers grown in this fashion could not be made. If the density of Si_3N_4 can be used as an analogue then the density for the GeN layer could be greater than GeO_2 by up to 50% [28] which results in lower values for the electron attenuation length and would mean that the films are actually thinner than what was calculated. The core-

level chemical shifts in the Ge 2p (3d) region between the overlayer and substrate features is 2.73 (2.55) eV for the GeO layer after UV-O_3 oxidation. This lowers to 2.14 (1.88) eV after nitridation, while the nitridation of a clean germanium substrate results in a CLCS of 1.85 (1.64) eV.

Figure 7.8 shows the oxygen 1s, nitrogen 1s and carbon 1s signals for a) UV ozone exposed germanium, b) nitrided germanium oxide and c) nitrided germanium. It is clear that both the GeON and GeN layers remain carbon free after the nitridation process, however there is a small but detectable O 1s signal after the nitridation of the clean germanium substrate. Since the nitridation is performed using a low powered nitrogen plasma struck over a hafnium oxide target, it is possible that some of that sputtered oxygen may become incorporated into the film. From the binding energy of the small oxygen 1s component on sample (c) it would appear that any oxygen is present in a GeON environment rather than GeO_x. There is a noticeable shift in binding energy in the O 1s feature from 531.1 eV for sample (a), as nitrogen is introduced into the overlayer, to 530.7 eV for sample (b). Also the N 1s feature shifts to lower binding energy as the oxygen content is reduced. The similar peak areas of the N 1s signal shows that the attempts to add approximately equal amounts of nitrogen to samples (b) and (c) were successful to a first approximation.

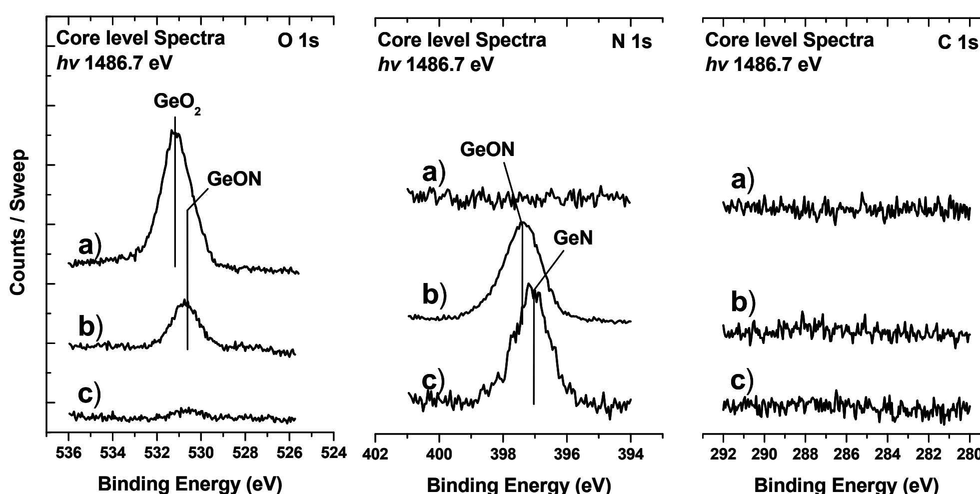

Figure 7.8 The O 1s, N 1s and C 1s XPS core-level spectra for a) UV/ozone treated Ge, b) UV/ozone treated germanium post nitridation and c) cleaned germanium post nitridation.

The differences in the core-level chemical shift seen between the substrate and overlayer features in figure 7.7 as well as the binding energy shifts seen in the O 1s and N 1s core-level spectra in figure 7.8 can be explained by a simple charge transfer model involving only the electronegatives of the three atoms. The higher the local negative charge density around a particular atom, the lower the force of attraction between an outer electrons and the positive nucleus which results in a lower effective binding energy being measured for the electrons in that atom. When an oxygen atom is replaced by a nitrogen atom, the nitrogen draws less charge from the germanium atom as it is a less electronegative element. This results in the remaining oxygen and germanium atoms having more charge than in the original system resulting in a shift of the Ge-O features in both the O 1s and Ge 2p (3d) core-level spectra to lower binding energy. A subsequent shift to lower binding energy for the Ge overlayer features as well as the N 1s feature can be expected when the remaining oxygen atom is replaced with a second nitrogen atom.

Silicon Interlayers:

To avoid the formation of GeO_2 at the high-κ germanium interface, some groups have grown a thin epitaxial layer of silicon on the germanium substrate.[6] In order to study the chemistry of interface formation, thin layers of amorphous silicon have been grown on germanium before the HGO is deposited and investigated by XPS. The surface before silicon deposition was oxygen and carbon free, clean germanium prepared by the standard UV ozone cleaning followed by a 430 °C anneal. The silicon was deposited in an MBE deposition chamber which at the time of deposition had only been used for silicon and germanium depositions to ensure no contamination from non-group IV materials. The depositions were conducted at room temperature and so the silicon layers would be expected to be amorphous. The deposition times and conditions were identical to the silicon interlayers grown on GaAs during the study of the electrical characteristics of silicon interlayers in the Al_2O_3/Si/GaAs, as such the thickness of the silicon layer is expected to be approximately 7 Å.

Figure 7.9 shows the XPS Ge 3d core-level spectra before and after silicon deposition. The peak heights have been normalised to their maximum intensities but

the binding energies have been unaltered. Since there is no oxygen present before or after the silicon deposition it is believed that surface charging effects would be minimal and approximately equal in both cases. The shift to a lower binding energy can be attributed to an increase in band bending at the silicon germanium interface resulting from the Fermi level moving down the germanium bandgap.

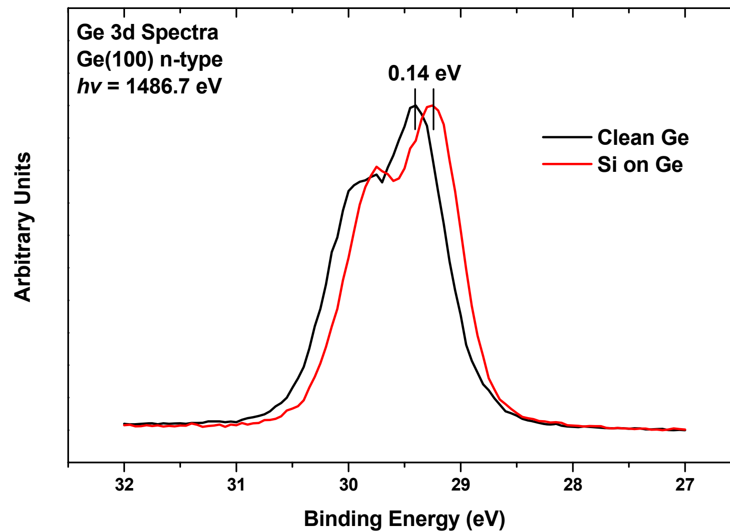

Figure 7.9 The Ge 3d XPS for clean germanium and silicon deposited on clean germanium. The binding energies have not been altered from the raw data.

In the work of Margaritondo *et al*[29] it is explained how the depth into the substrate over which this bending takes place is normally orders of magnitude greater than the sampling depth of XPS and because of this it is normal to see a shift in the peaks energy rather than an asymmetric broadening on one side of the peak. The shift seen in figure 7.9 of 0.14 eV is less than half the value of the band-gap for germanium which is 0.67 eV. Higher shifts have been noted by other groups[24] when analysing flash cleaned and oxidised n-type germanium samples. However in these works, the carbon 1s core-level position was fixed to account for surface charging effects. This can lead to large inaccuracies in measurements on germanium since the carbon on the germanium substrates, after flashing cleaning, could be chemisorbed to the underlying germanium and can not therefore be used as a reference for the core-levels since it could alter the result by as much as 0.5 eV. Here surface charging is not thought to be an issue and the banding bending seen in figure 7.9 is consistent with an overlayer deposited on n-type germanium.

7.3.4 Hafnium Germanate

The electrical qualities of the hafnium germanate (HGO) films deposited on silicon substrates has been previously studied by Sivasubramani.[30] In those experiments the films were grown using the same deposition and characterisation tool as the work described in this chapter. Here the interfacial chemistry of this dielectric layer in contact with GeN, GeON and Si interlayers was studied. Preliminary analysis of bulk, 7 nm, films allows for the reference core-level spectra to be identified without being complicated by the signals from interfacial regions or the underlying substrate. The Ge 2p, O 1s and Hf 4f XPS core-level spectra have been selected as the major core-levels for the hafnium germanate system and are shown in figure 7.10. The selection of the highly surface sensitive Ge 2p region over the Ge 3d, which is more commonly used for bulk analysis, is because of the overlap in the Hf 5p 3/2 and Ge 3d signals making any detailed analysis of a hafnium rich system very difficult.

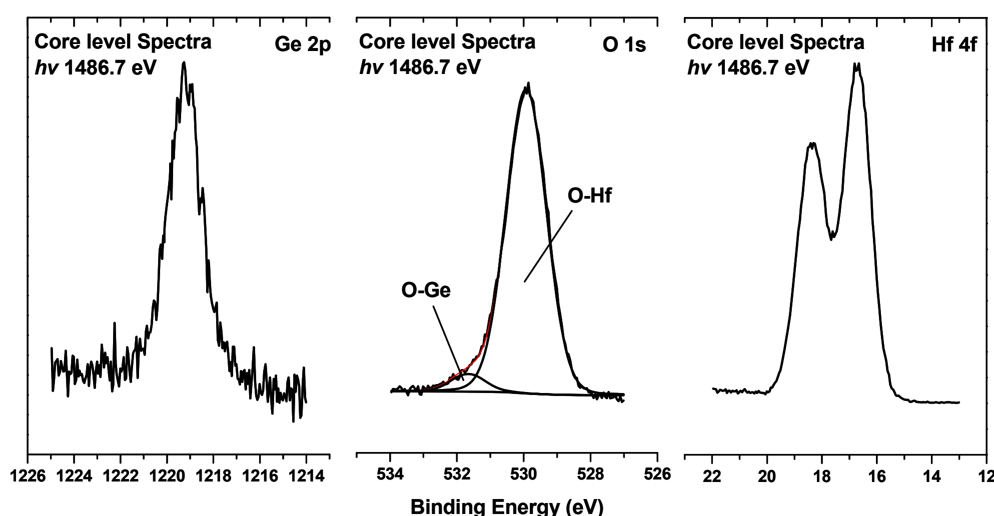

Figure 7.10 The Ge 2p, O 1s and Hf 4f XPS core-levels for 7 nm HfGeO films grown on a silicon substrate.

The intensity ratio of the Ge 2p to the Hf 4f core-level spectra allows for the stiochiometry of the HGO films to be measured. Achieving a low germanium content is thought to be desirable in order to achieve the highest possible dielectric constant. From these features we can see that a ratio of 1:6 Ge:Hf was achieved. The O 1s spectra show two clear components. These have been assigned to oxygen in GeO_x and HfO_x and have been used as a baseline in the later analysis of thin HGO films.

HGO on nitrided germanium

The deposition of thin layers (~10 Å) of hafnium germanate (HGO) on GeN and GeON interlayers were analysed with XPS. The lack of sufficient bulk sensitivity in the Ge 2p core-level to supply information about the interface, along with the overlap in the Hf 5p 3/2 and Ge 3d core-levels means that information about the various oxidation states present can only be found in the O 1s core-level features. Ordinarily oxygen species found in common surface contamination layers makes the O 1s core-level unreliable for detailed analysis using conventional XPS. However the combination of the improved resolution resulting from the use of monochromatic XPS along with the experiment being carried out entirely *in-situ* means that useful information can be extracted from this analysis.

Figure 7.11 shows the oxygen 1s core-levels for HGO grown on both GeN and GeON interlayers. The assignment of the features at 531.7 and 529.9 eV can be made with confidence by referencing to the bulk O 1s feature in figure 7.10. Figure 7.11a clearly shows that the addition of a third component is required in order to achieve a

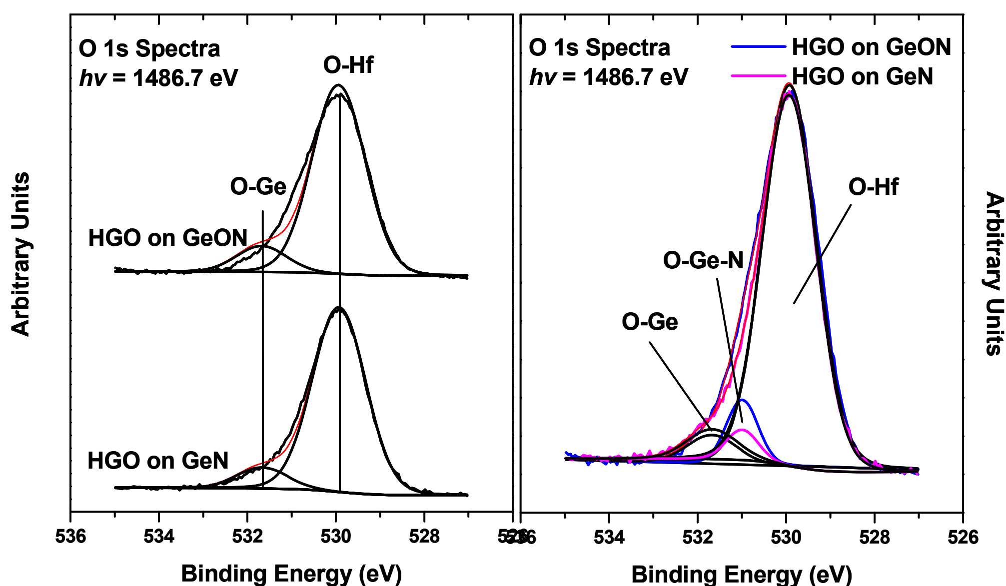

Figure 7.11 The O 1s XPS spectra for HGO on GeN and GeON interlayers. a) shows the attempt to fit the spectra with only 2 components. b) shows the better fits obtained with a 3rd GeON component.

good fit. The peak position of this component is fixed to be equivalent to that of oxygen in a GeON environment as seen in figure 7.7 and the resultant fits, shown in figure 7.11b, have been overlayed so that the difference in the component assigned to GeON can be more clearly seen. The HGO on a GeN interlayer system is found to have a lower GeON concentration than that of HGO grown directly on GeON, which can be expected since any GeON must be grown via the oxidation of GeN. Figure 7.11 does confirm that the HGO on GeON and GeN systems retain unique interfacial chemistries after the deposition of HGO.

HGO on Silicon interlayer

The main reason for inserting a silicon interlayer in this study is to prevent the formation of unfavourable GeO_2 at the high-κ germanium interface. The complete oxidation of the silicon interlayer during the deposition process could result in the formation of GeO_2 at the silicon germanium interface. Since GeOx species are present in the HGO film, detecting interfacial GeO_2, using the germanium core-levels, cannot be done with any great degree of certainty so instead, the Si 2p core-level is analysed. Figure 7.12 shows the Si 2p core-level XPS spectrum of the thin silicon interlayer

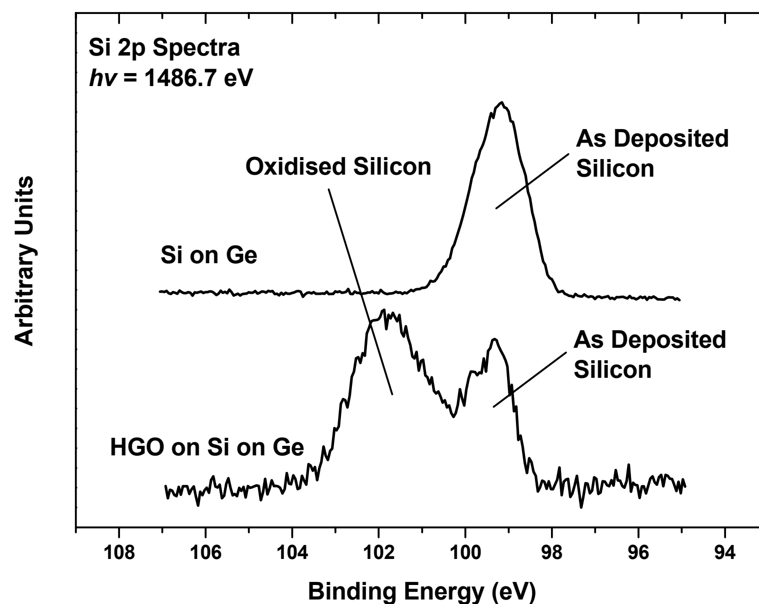

Figure 7.12 The Si 2p XPS core-level spectra before and after HGO depositions on the Si interlayer.

deposited on germanium prior to HGO deposition is silicon oxide free. Following HGO deposition, while there is an oxide component, there is a significant unoxidised silicon signal present. This unoxidised silicon is evidence that oxygen did not diffuse entirely through the film and as such the Si/Ge interface should be GeO_x free.

Continued work focused on the affect of a post deposition anneal in N_2 for 30 minutes on the chemical properties of the HGO films in the HGO/GeON/Ge system. Such anneals were found to be essential in order for MOS capacitor structures constructed using such HGO/GeON/Ge stacks to swept from accumulation to inversion. Figure 7.11a showed 2 distinct oxygen features assigned to both Ge-O and Hf-O bonding environments were present in the HGO film after deposition. The affect of a PDA anneal is shown in figure 7.13 and it is obvious that the distinction between the two oxygen environments is lost which would indicate that the use of a PDA is required in order to merge separate HfO_2 and GeO_2 regions into hafnium germanate.

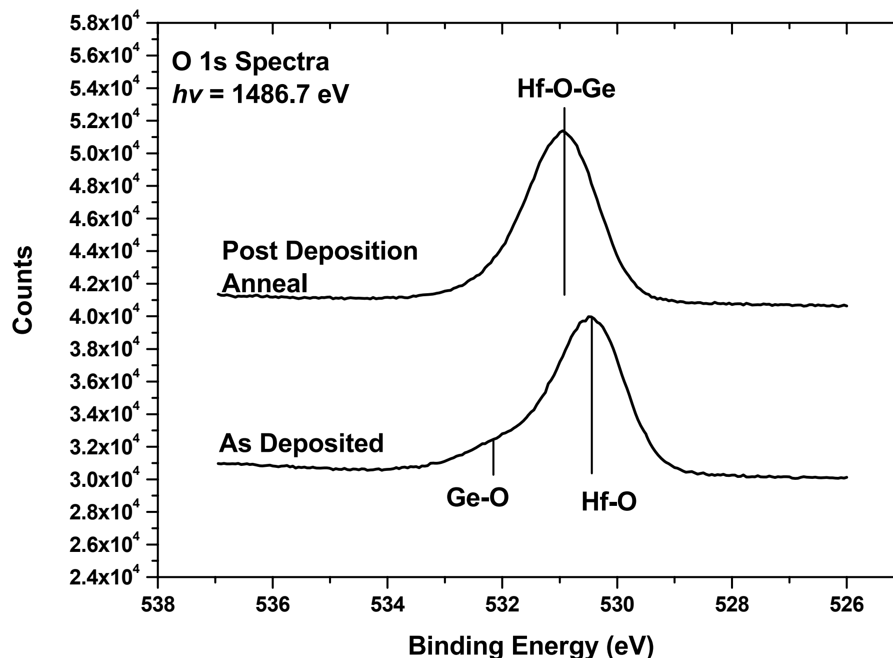

Figure 7.13 The O 1s core-level spectra of HGO/GeON/Ge before and after a Post deposition anneal.

7.4 Conclusion

The hafnium germanate on germanium system has been studied *in-situ* with XPS during various stages of the cleaning and deposition process. A preliminary study was conducted on various cleaning methods. It was found that while a 20 sec deionised water rinse removed the bulk of the native oxide leaving only a single monolayer of suboxides, *in-situ* exposure to UV-ozone was required to remove carbon contamination from the germanium surface. However subsequent anneals UHV to a temperature of 400 °C would complete remove the UV grown oxide and result in a clean, oxide and carbon free substrate.

Three interlayers were chosen for interface characterisation based on the electrical studies published by other groups.[6-9] The use of the multi-deposition and analytical tool (chamber C described in section 3.1) allowed for the chemical properties of these interlayers to be explored. Hafnium germanate was grown on each of the three interlayers and it was found that for both GeN and Si interlayers, there remained un-oxidised components which suggests that both layers act as sufficient oxygen diffusion barriers that should prevent the oxidation of the underlying germanium.

From the oxygen 1s core level spectra it was clear that the as deposited hafnium germanate films were segregated into HfO_2 and GeO_x phases. Post deposition anneals at 400 °C in N_2 for 30 minutes resulted in a single O 1s feature implying that a true hafnium germanate was formed. These PDA's were found to be essential in order to switch the channel region between accumulation and inversion

7.5 References

[1] H. R. Huff, D. C. Gilmer *High Dielectric Constant Material: VLSI MOSFET Applications* Springer series in Advanced Microelectronics **16** (2005)

[2] G.W.C. Kaye, T.H. Laby *Tables of Physical and Chemical Constants* (16th edition) Longman: Harlow (1995)

[3] S. Nakaharai, T. Tezuka, N. Sugiyama, Y. Moriyama, S. –I. Takagi, Appl Phys Lett **83** (2003) 3516

[4] Y. Liu, K. Gopalakrishnan, P. B.Griffen, K. Ma, M. D. Deal, J. D. Plummer IDEM Techn. Digest (2004) 1001

[5] S. Van Elshocht, B. Brijs, M. Caymax, T. Conard, T. Chiarella, S. De Gendt, B. De Jaeger, S. Kubicek, M. Meuris, B. Onsia, O. Richard, I. Teerlinck, J. Van Steenbergen, C. Zhao, M. Heyns, Appl. Phys. Lett. **85(17)** 2004 3824-3826

[6] W. P. Bai, N. Lu, D. –L. Kwong, IEEE Elec. Device Lett. **26(6)** (2005) 378-380

[7] T. Sugawara, Y. Oshima, R. Sreenivasan, P. McIntyre, Appl. Phys. Lett. **90** (2007)112912

[8] H. Kim, P. McIntyre, C. O. Chui, K. C. Saraswat, M. –H. Cho, Appl. Phys. Lett. **85(14)** (2004) 2902-2904

[9] T. Maeda, T. Yasuda, M. Nishizawa, N. Miyata, Y. Morita, S. Takagi, J.Appl. Phys. **100** (2006) 014101

[10] H. Kim, C. O. Chui, K. C. Saraswat, H. –H. Cho, P. C. McIntyre, Appl. Phys. Lett. **85** (2004) 2902

[11] N. A. Tabet, M. A. Salim, A. L. Al-Oteibi, Journal of Electron Spectroscopy and Related Phenomena **101-103** (1999) 233-238

[12] P. W. Wang, Y. Qi, D. O. Henderson, Journal of Non-Crystalline Solids **224** (1998) 31-35

[13] A. Cattoni, R. Bertacco, M. Riva, M. Cantoni, F. Ciccacci, H. V. Känel, G. J. Norga, Materials Science in Semiconductor Processing **9** (2006) 701-705

[14] K. Prabhakaran, T. Ogino, Surface Science **325** (1995) 263-271

[15] T. Deegan, G. Hughes, Applied Surface Science **123/124** (1998) 66-70

[16] C. J Powell, A Jablonski, *NIST Electron Effective-Attenuation-Length Database* version 1.0 copyright 2001

[17] G.W.C. Kaye, T.H. Laby *Tables of Physical and Chemical Constants* (16th edition) Longman: Harlow (1995)

[18] H. Okumura, T. Akane, S. Matsumoto, Applied Surface Science **125** (1998) 125-128

[19] J. S. Hovis, R. J. Hamers, C. M. Greenlief, Surface Science **440** (1999) L815-819

[20] G. W. Anderson, M. C. Hanf, P. R. Norton, Z. H. Lu, M. J. Graham, Appl. Phys. Lett. **66 (9)** (1995) 1123-1125

[21] K. Choi, J. M. Buriak, Langmuir, **16** (2000) 7737

[22] X. –J. Zhang, G. Xue, A. Agarwal, R. Tsu, M, -A. Hasan, J. E. Greene, A. Rockett, J. Vac. Sci. Technol. A. **11** (1993) 2553

[23] J. F. Moulder, W. F. Stickle, P. E. Sobol, K. D. Bomben, *Handbook of X-ray Photoelectron Spectroscopy* Perkin-Elmer Corporation, Physical Electronics Division (1992)

[24] N. Tabet, M. Faiz, N. M. Hamden, Z. Hussain, Surface Science **523** (2003) 68-72

[25] J. C. Revière. J. A. A. Crossley, B. A. Sexton, J. Appl. Phys. **64(9)** (1988) 4585-4600

[26] A. Ohta, H. Nakagawa, H. Murakami, S. Higashi, S. Miyazaki, e-Journal of Surface Science and Naotechnology, **4** (2006) 174-179

[27] K. Prabhakaran, T. Ogino, Surface Science **325** (1995) 263-271

[28] D.R. Lide, *CRC Handbook of Chemistry and Physics* (88th edition) CRC Pres: Boca Raton, FL, (2000)

[29] G. Margaritondo, F. Gozzo and C. Coluzza, Phys. Rev. B. **47(15)** (1993) 9907-9909

[30] Sivasubramani, P. *Materials Properties and Thermal Stability of Hafnium and Lanthanum Based High-κ Gate Dielectrics for Mosfet Digital Logic* (2006)

8 Conclusions and future work

8.1 Conclusions

In this photoemission study of high-κ/semiconductor interfaces, three different semiconducting substrates were investigated. Whenever possible the experiments were conducted *in-situ* so that any changes in interfacial chemistry could be confidently attributed to processing conditions without the need to consider the effects of ambient exposure. In selected studies, MOS capacitor structures were formed on identical films to those monitored by photoemission so that information gained about the interfacial chemistry could be correlated with the electrical characteristics of these dielectric materials. This section will summarise the key results obtained, for each semiconducting substrate, during the course of this work and the conclusions that can be drawn from them.

8.1.1 Hafnium oxide grown on silicon

Both *in-situ* and *ex-situ* studies were conducted on the HfO_2/Si system. The *in-situ* studies focused primarily on controlling the interfacial oxide formation by using an intentionally grown ultra-thin buffer oxide. The ratio of the integrated intensities of the substrate and oxide photoemission spectra was used to monitor the thickness of the interfacial oxide region while the core-level chemical shift between the silicon substrate and the bulk oxide component was used to monitor the changes in the chemical state of this interfacial region. It was found that while this interfacial oxide grew thicker during the deposition of hafnium oxide, its chemical state changed from silicon dioxide to hafnium silicate. As hafnium oxide was deposited onto the buffer oxide, a new feature emerged in the Si 2p core-level spectra which was assigned to silicon atoms in the sub-interface region without a full arrangement of silicon neighbours. The suggested cause for this disruption of the SiO_2/Si interface was the incorporation of silicon atoms from the substrate into the growing interfacial oxide region. Such disruption could be a direct cause of reduced charge carrier mobility in the channel region.[1]

In-situ high temperature UHV anneals were carried out on $HfO_2/SiO_x/Si$ systems grown at room temperature and 250 °C. The formation of hafnium silicide was noted at 1000 °C for samples grown at room temperature and 700 °C for samples grown at 250 °C. These results have been compared to the results published by other authors[2,3] which suggested that these silicide formation temperatures are typical for systems where HfO_2 is grown on an SiO_2 buffer layer (1000 °C), or directly onto clean silicon (700 °C). Varying the photon energy for analysing the hafnium core-levels confirmed that the silicide formed at 700 °C was localised at the HfO_2/Si interface and extended anneals at 700 °C showed that the formation of hafnium silicide was self limiting. This indicated that the growth of HfO_2 at a substrate temperature of 250 °C allowed for sufficient diffusion of hafnium and hafnium oxide molecules through the monolayer buffer oxide. These hafnium species that were in direct contact with the silicon substrate allowed for the limited growth of hafnium silicide at 700 °C without breaking down the buffer oxide layer. The substrate temperature during the deposition of HfO_2 was shown to have a large effect on the high temperature thermal stability of these systems.

The *ex-situ* grown of HfO_2 by plasma ion assisted e-beam deposition in an oxygen back pressure was found to result in the growth of a 30-40 Å thick SiO_2 interfacial layer. The cause of this excessively thick interfacial oxide growth was identified as the exposure of the hydrogen passivated silicon substrate to an oxygen plasma at a substrate temperature of 150 °C. This oxidation was found to take place even through a 1 nm HfO_2 grown by conventional e-beam deposition. The plasma ion assist was found to cause sufficient structural damage to the silicon surface, in the absence of an oxygen back pressure, to result in electrically leaky HfO_2 dielectric layers that were unusable as gate dielectrics.

8.1.2 High-κ dielectrics on GaAs substrates

Gallium arsenide was chosen as an example of a III-V high electron mobility substrate. The primary goal for this study was to better understand the cause of the frequency dependent dispersion of the maximum capacitance in accumulation phenomenon that is common to many high-κ/nGaAs systems.[4] During the course of

this study, other important results were obtained relating to preparation of GaAs surfaces and to the affects of HfO_2 and Al_2O_3 grown by ALD directly onto GaAs surfaces.

The reduction of the native oxides by chemical and *in-situ* methods was studied and the exposure of the GaAs surface, heated to 430 °C, to atomic hydrogen was found to be the easiest and most repeatable way of achieving oxide free substrates, while NH_4OH was found to result in a thin oxide that could be made gallium oxide rich by *in-situ* high temperature anneals from 300-450 °C in agreement with other studies.[5,6]

Depositions of silicon onto NH_4OH treated GaAs were found to completely remove all arsenic oxides in agreement with other studies.[7-9] It is also found to result in the core-level chemical shift between the gallium bulk core-level and gallium oxide spectral features being reduced and this was explained here by a shifting from As-O-Ga bonds to Si-O-Ga bonds which suggested that silicon replaced arsenic without any significant removal of oxygen.

The atomic layer deposition of Al_2O_3 and HfO_2 using TMA and TEMA-Hf as sources for Al and Hf respectively on untreated and NH_4OH treated GaAs substrates showed that Al_2O_3 preferential reduces the lower coordinated arsenic oxide As_2O_3 and leaves a detectable presence of the higher coordination As_2O_5 while the HfO_2 preferential reduces the higher co-ordination As_2O_5 and leaves a detectable As_2O_3 signal. The removal of the As_2O_5 by NH_4OH prior to Al_2O_3 growth therefore resulted in arsenic oxide free samples. While the preferential removal of As_2O_3 by the deposition of Al_2O_3 is straight forward, the preferential removal of As_2O_5 by the HfO_2 deposition required further explanation. It was suggested here that since the higher coordination Hf atoms in HfO_2 are more stable than lower coordination Hf atoms[10] that it could possibly be energetically more favourable for HfO_2 to preferentially reduce the higher coordination As_2O_5 over the As_2O_3.

The effects of a silicon interlayer, grown *in-situ* prior to Al_2O_3 growth, on the interfacial chemistry were correlated with the electrical characteristics of MOS capacitor structures formed from the same samples. It was found that the absence of

gallium oxides was essential in order to reduce the frequency dependent dispersion of the maximum capacitance in accumulation. It is quite possible that these gallium oxide are the responsible for the disordered low bandgap region which is thought to be the cause of this phenomenon.[4] It has been suggested here that the use of a silicon interlayer grown only on a gallium oxide free surface prevents the formation of a low bandgap disordered region which allows for the tunnelling of interface states into the dielectric and results in the frequency dependant dispersion of maximum capacitance in accumulation.

8.1.3 High-κ dielectrics on germanium substrates

An exploratory photoemission study was conducted on the sample preparation and interfacial layer growth of germanium substrates. Preliminary cleaning studies showed that exposure of the germanium wafer to UV-ozone was required in order to remove carbon contamination from the surface. Post UV-ozone exposure flash cleans at temperatures of 430 °C provided oxide and carbon free surfaces for the growth of interfacial layers. The reason for the use of interfacial layers in high-κ/Ge systems was to prevent the formation of unstable GeO_2 at the interface. Hafnium germanate was grown as the high-κ dielectric onto GeON, GeN and Si. Useful interfacial information about the $HfGeO_x$/GeON/Ge system was difficult to obtain; however it served as a comparison to the $HfGeO_x$/GeN/Ge system by showing the oxidation of the GeN layer by the hafnium germanate was not complete and so the GeN layer could serve as a diffusion barrier to prevent the oxidation of the underlying germanium. In the case of the $HfGeO_x$/Si/Ge system, there was a clear unoxidised silicon signal which showed that silicon served as a diffusion barrier to prevent the oxidation of the underlying germanium.

Post deposition anneals at 400 °C in N_2 were known to be essential in order to obtain a C-V response with capacitor structures formed from these HGO/GeON/Ge systems. XPS showed that such anneals removed the distinction between GeO_x and HfO_2 features in the oxygen 1s core-level spectra resulting in a single O 1s feature corresponding to hafnium germanate.

8.2 Future work

The immediate future of the semiconductor industry appears to involve a shift towards HfO_2. Hafnium has already been successfully integrated into the fabrication process with the current state of the art devices utilising a hafnium silicate gate dielectric. While scaling of the hafnium silicate layer may be possible, an eventual shift to a higher dielectric constant material will be required and using these hafnium silicates as interlayers for HfO_2 to be introduced as a gate dielectric would seem to be the most logical way to achieve this without the introduction of new elements. The use of mid-κ dielectric materials such as Al_2O_3 that can be grown without an SiO_x interfacial layer and are thermodynamically stable at the current process temperatures could be one way of allowing high-κ dielectrics that are currently being studied to be integrated into device processing.[11]

An important finding from this study was the soft-XPS evidence of the disruption of the SiO_2/Si interface. The presence of a silicon core-level feature only after the deposition of a high-κ material and at a binding energy consistent with surface states on atomically Si(111) suggests that silicon atoms that are incorporated into the interfacial oxide region leave behind a disrupted region which could be a direct cause of reduced mobility in the channel region of high-κ gate dielectric MOSFETs. As such, continued experiments should focus on finding materials or depositions techniques that do not degrade the quality of the SiO_2/Si interface.

Indium gallium arsenide (InGaAs) has a higher electron mobility than gallium arsenide (GaAs) and as such is currently under intensive investigation as a potential high mobility substrate material. Studies conducted on GaAs provide an invaluable wealth of information to researchers exploring InGaAs, since many of the same problems such as the frequency dependant dispersion of maximum accumulation capacitance are still present on InGaAs with high gallium contents. Research into higher dielectric constant materials will be required on these substrates with the use of aluminates being the logical research step following the extensive studies of the Al_2O_3/GaAs systems. Further *In-situ* studies on silicon interlayers of different

thicknesses should easily establish a minimum required thickness of silicon to prevent the oxidation of the underlying gallium.

The studies of the germanium substrates in this work were largely exploratory and a wide range of dielectric materials could be utilised as germanium research continues. However, mixing high-κ materials into the well studied and promising GeON/Ge system could serve as a good starting point for the development of a functional high-κ germanium oxynitride dielectric material. This would be analogous to the mixing of high-κ materials with the stable SiO_2/Si system as a way to implement high-κ materials on to silicon, which is the preferred short term option of the semiconductor device industry.

Continued work on these systems would logically involve the addition of nitrogen to the hafnium germanate dielectric as well as continued studies on the effects of various common post deposition anneals on the chemical and electrical properties of these films. The growth of a nitrided hafnium germanate film with an increasing hafnium concentration from the germanium substrate to the metal gate could possibly allow for the films to have a high dielectric constant while maintaining the GeON/Ge interface and removing any effects that could be caused by a high-κ/GeON interface.

8.3 References

[1] J-.P. Locquet, C. Marchiori, M. Sousa, J. Fompeyrine, J. W. Seo, J. Appl. Phys. **100** (2006) 051610

[2] M. C. Zeman, C. C. Fulton, G. Lucovsky, R. J. Nemanich, W.-C. Yang, J. Appl. Phys. **99** (2006) 023519

[3] R. Xu, Z. J. Yan, S. Chen, Y. L. Fan, X. M. Ding, Z. M. Jiang, Z. S. Li, Surface Science 581 (2005) 236-240

[4] H. Hasegawa and T. Sawada, IEEE Trans. Electron Devices **27**, (1980) 1055

[5] K. Tone, M. Yamada, Y. Ide and Y, Katayama, Jpn. J. Appl. Phys. **31** (1992) L721

[6] M. V. Lebedev, D. Ensling, R. Hunger, T. Mayer and W. Jaegermann, Applied Surface Science **229** (2004) 226

[7] I. Jiménez, F. J. Palomaresa and J. L. Sacedón, Phys Rev B **49(16)** (1994) 11117

[8] J. Ivanco, T. Kubota, H. Kobayahsi, J. Appl. Phys. **97** (2005) 073712

[9] I. Jiménez, J. L. Sacedón, JVST B **12(6)** (1994) 3095

[10] G. Jun and K. Cho, Mater. Res. Soc. Symp. Proc. **747** (2003) 5.1.1

[11] G. D. Wilk, R. M. Wallace, J. M. Anthony, J. App. Phys. **89(10)** (2001) 5243-5275